

Tridentate Schiff Bases of some Aroylhydrazides and their Metal Complexes: Spectral and Structural Studies

**Thesis submitted to
Cochin University of Science and Technology**

**In partial fulfillment of the
requirements for the degree of**

DOCTOR OF PHILOSOPHY

Under the Faculty of Science

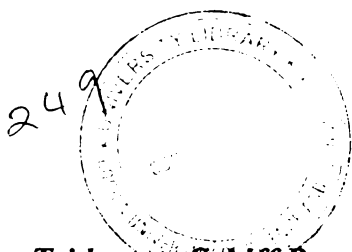
By

Mini Kuriakose



**Department of Applied Chemistry
Cochin University of Science and Technology
Kochi - 682 022**

December 2006



Tridentate Schiff Bases of some Aroylhydrazides and their Metal Complexes: Spectral and Structural Studies
Ph. D. Thesis under the Faculty of Science

Author:

Mini Kuriakose

Research Fellow, Department of Applied Chemistry
Cochin University of Science and Technology
Kochi, India 682 022
E mail: mini_kuriakose@cusat.ac.in

Research Advisor:

Dr. M. R. Prathapachandra Kurup

Professor and Head
Department of Applied Chemistry
Cochin University of Science and Technology
Kochi, India 682 022
Email: mrp@cusat.ac.in

T
U44.142.3
MUN

Department of Applied Chemistry,
Cochin University of Science and Technology
Kochi, India 682 022

December 2006

Front cover: Crystal structure of a polymeric cadmium(II) complex of pyridine-2-carbaldehyde nicotinoylhydrazone.



Phone Off. 0484-2575804
Phone Res. 0484-2576904
Telex: 885-5019 CUIIN
Fax: 0484-2577595
Email: mrp@cusat.ac.in
mrp_k@yahoo.com

DEPARTMENT OF APPLIED CHEMISTRY
COCHIN UNIVERSITY OF SCIENCE AND TECHNOLOGY
KOCHI - 682 022, INDIA

Prof. M.R. Prathapachandra Kurup
Head

20th December 2006

CERTIFICATE

This is to certify that the thesis entitled “**Tridentate Schiff Bases of Some Aroylhydrazides and their Metal Complexes: Spectral and Structural Studies**” submitted by Ms. Mini Kuriakose, in partial fulfillment of the requirements for the degree of Doctor of Philosophy, to the Cochin University of Science and Technology, Kochi-22, is an authentic record of the original research work carried out by her under my guidance and supervision. The results embodied in this thesis, in full or in part, have not been submitted for the award of any other degree.

M. R. Prathapachandra Kurup
(Supervisor)

DECLARATION

I hereby declare that the work presented in this thesis entitled **“Tridentate Schiff Bases of Some Aroylhydrazides and their Metal Complexes: Spectral and Structural Studies”** is entirely original and was carried out independently under the supervision of Professor M. R. Prathapachandra Kurup, Department of Applied Chemistry, Cochin University of Science and Technology and has not been included in any other thesis submitted previously for the award of any other degree.

20-12-06

Kochi-22



Mini Kuriakose

PREFACE

The interaction of transition metal ions with biologically active ligands provides one of the most fascinating areas of coordination chemistry. Metal chelation has spurred a great interest in the present day medicine and chemical investigations.

Recent years witnessed an intensive investigation of the coordination chemistry of Schiff bases due to their interesting coordination properties and diverse applications. The present work deals with the complexation of Schiff bases of aroylhydrazides with various transition metal ions. The hydrazone systems selected for study are capable of forming bridged polymeric structures which is one of the fascinating subjects in the crystal engineering of coordination polymers owing to their attractive new topologies and intriguing structural features. Complexation with metal ions like copper, manganese, vanadium, nickel, palladium, zinc and cadmium are tried. Various spectral techniques are employed for characterization. The structures of some complexes have been well established by single crystal X-ray diffraction studies.

The work is presented in seven chapters and the last section deals with summary and conclusion. The studies reveal that the aroylhydrazone systems vary in their geometrical configuration depending on the substituents. The coordination modes of the ligands also differ upon chelating with metal ions. One of the hydrazone system selected for study proved that it could give rise to polymeric metal complexes.

ACKNOWLEDGEMENT

I am greatly indebted to my supervising guide, Dr. M. R. Prathapachandran Kurup, Professor and Head, for his guidance, valuable suggestions and comments. I am grateful to Dr. Girish Kumar, for his support as my doctoral committee member. I am thankful for the support received from all the teaching and non-teaching staff of the Dept. of Applied Chemistry, CUSAT.

I deeply acknowledge the Council of Scientific and Industrial Research, Cochin University of Science and Technology and Kerala State Council for Science, Technology and Environment, for the financial support offered.

My thanks are due to Dr. E. Suresh, CSMCRI, Gujarat, for single crystal X-ray diffraction studies. I am thankful to the head of the institutions of SAIK Kochi, IISc Bangalore, IIT Roorkee and IIT Bombay for the services rendered in sample analyses.

I acknowledge Dr. A. Sreekanth, Dr. Varughese Philip and Dr. Marthakutty Joseph for their help during the initial stages of my research tenure. I express my sincere gratitude to Dr. Sreeja P. B. for her kind and helping attitude. I owe much to my dearest senior Dr. Suni V. for her sisterly affection, help and valuable suggestions throughout my research work. I always enjoyed the friendly moments spent with Daby and I am thankful to her for helping me in literature collection. I am much obliged to Bessy, as she had been always with me, whenever I needed her help and for making my life in CUSAT memorable. I sincerely appreciate the friendship and encouragement of Roshini and Suja. My friends Mahi, Elsu and Sujith are treasured for their friendship and support. My special thanks are also due to my labmates Raphael Sir, Laby miss, Seena, Manoj, Prem, Sreasha, Leji, Sheeja and Nancy for providing a friendly work atmosphere. I owe much to all my friends especially Ambily, Rekhia, Radhika, Rajesh, John and Arun for their warm support. I cherish the moments I had with Maya and Rani as they were there to share together the tensions of thesis writing.

I express my heartfelt gratitude to my parents and brother for their love, affection and encouragement. I do realize the love, help and support extended to me by my in-laws. Finally I must recognize the patience and understanding of my husband. I would not have been able to complete this work without his wholehearted support and constant encouragement.

Above all my praises are due to The Almighty Lord, for his unlimited blessings throughout my life.

CONTENTS

Page No.

CHAPTER 1

A brief preamble on hydrazones, their bonding aspects and applications

1.1.	Importance of hydrazones	2
1.2.	Applications of hydrazones	7
1.3.	Objectives of the present work	10
1.4.	Physical measurements	11
1.5.	Crystallographic data collection and structure analyses	11
	References	13

CHAPTER 2

Syntheses, spectral characterization and crystal structures of heteroaroylhydrazone ligands from 2-benzoylpyridine and pyridine-2-carbaldehyde

2.1.	Experimental	19
2.2.	Results and discussion	20
2.2.1	Crystal structures of HL ¹ , H ₂ L ² and HL ³ ·2H ₂ O	20
2.2.2	Spectral characteristics	26
2.2.2a	NMR spectral studies	26
2.2.2b	Electronic spectral studies	33
2.2.2c	IR spectral studies	33
	References	38

CHAPTER 3

Syntheses, structural and spectral studies of some Cu(II) complexes of terdentate NNO donor heteroaroylhydrazone ligands

3.1.	Stereochemistry	42
3.2.	Experimental	42
3.3.	Results and discussion	45
3.3.1	Crystal structures of [Cu(L ¹) ₂], [Cu(HL ²) ₂]·H ₂ O·DMF and [Cu(L ³) ₂]·H ₂ O	46
3.3.2	Spectral characteristics of Cu(II) complexes	54
3.3.2a	Electronic spectral studies	54
3.3.2b	EPR spectral studies	58
3.3.2c	IR spectral studies	72

CHAPTER 4**Structural and spectral investigations of Mn(II) complexes of heteroaroylhydrazones of nicotinoylhydrazide**

4.1.	Stereochemistry	88
4.2.	Experimental	88
4.3.	Results and discussion	90
4.3.1	Crystal structure of $[\text{Mn}(\text{L}^1)_2]$	90
4.3.2	Spectral characteristics of Mn(II) complexes	92
4.3.2a	EPR spectral studies	92
4.3.2b	IR spectral studies	97
4.3.2c	Electronic spectral studies	100
	References	105

CHAPTER 5**Vanadium complexes of 2-benzoylpyridine heteroaroylhydrazones: Syntheses, structural and spectral investigations**

5.1.	Stereochemistry	108
5.2.	Experimental	109
5.3.	Results and discussion	110
5.3.1	Crystal structures of $[\text{VO}_2(\text{L}^1)]$ and $[\text{VO}(\text{HL}^2)(\mu_2\text{-O})]_2 \cdot \text{H}_2\text{O}$	110
5.3.2	Spectral characteristics of oxovanadium complexes	114
5.3.2a	Electronic spectral studies	114
5.3.2b	Electron paramagnetic resonance studies	115
5.3.2c	IR spectral studies	117
	References	121

CHAPTER 6**Syntheses, structural and spectral studies of Ni(II) and Pd(II) complexes of heteroaroylhydrazone ligands**

6.1.	Stereochemistry	124
6.2.	Experimental	124
6.3.	Results and discussion	126
6.3.1	Crystal structures of $[\text{Ni}(\text{L}^1)_2]$ and $[\text{Ni}(\text{L}^3)_2] \cdot \text{H}_2\text{O}$	126
6.3.2	Spectral characteristics of nickel complexes	130
6.3.2a	Electronic spectral studies	130

6.3.2b	IR spectral studies	131
6.3.3	Spectral characteristics of palladium complexes	131
6.3.3a	Electronic spectral studies	131
6.3.3b	¹ H NMR spectral studies	131
6.3.3c	IR spectral studies	134
	References	140

CHAPTER 7

Investigations on the structural and spectral aspects of Zn(II) and Cd(II) complexes of nicotinoylhydrazone

7.1.	Stereochemistry	144
7.2.	Experimental	144
7.3.	Results and discussion	146
7.3.1	Crystal structure of [Zn(L ¹) ₂]	147
7.3.2	Spectral characteristics of Zn(II) complexes	148
7.3.2a	¹ H NMR spectral studies	148
7.3.2b	Electronic spectral studies	150
7.3.2c	IR spectral studies	150
7.3.3	Crystal structures of [Cd(L ¹) ₂] and [Cd(L ³)Cl ₂] _n ·nH ₂ O	151
7.3.4	Spectral characteristics of Cd(II) complexes	156
7.3.4a	¹ H NMR spectral studies	156
7.3.4b	Electronic spectral studies	158
7.3.4c	IR spectral studies	158
	References	167
	Summary and conclusion	169

A brief preamble on hydrazones, their bonding aspects and applications

The realm of inorganic chemistry has steadily evolved over the years. In this growth, the field of coordination chemistry has made its own contribution. Twentieth century witnessed the development of Alfred Werner's coordination chemistry as one of the most productive areas of research. It was Tassaert, who first observed the coordination compound formed by the combination of ammonia with cobalt ore. In 1869, Blomstrand first formulated his chain theory to account for the cobalt ammonium chlorides and other series of ammonates. But the theory was unsuccessful in explaining certain facts. Later, Alfred Werner developed the modern theory of coordination compounds in 1892, explaining two types of valencies for the metal. He was awarded the Nobel Prize in chemistry in 1913 for his painstaking findings. Since then the field of coordination chemistry has been widely explored. The number, variety and complexity of coordination compounds still continues to grow.

The importance of coordination complexes in our day to day life is increasing due to their complex structures and interesting magnetic, electronic and optical properties. The diversity in structures exhibited by the coordination complexes of multidentate ligands have led to their usage as sensors, models for enzyme mimetic centers, medicines etc. The ligands chosen are of prime importance in determining the properties of coordination compounds. The presence of nitrogen, oxygen and sulfur atoms attached to the ligands increases their denticity and thereby enhancing the coordinating possibilities. Moreover, the presence of these atoms in the coordination sphere leads to their biological activity.

Hydrazides, RNH-NH_2 belonging to this class are of special mention. They are derived from hydrazines ($\text{NH}_2\text{-NH}_2$) by suitable substitution. Again, attaching groups with potential donor sites increases the denticity of these hydrazides. One such group is the -C=O group which also makes possible an electron delocalization. Thus compounds with R-CO-NH-NH_2 are called acid hydrazides. These substituted hydrazides could condense with aldehydes or ketones with potential donor sites resulting in Schiff bases with an extended conjugation and enhanced activity. The resultant Schiff bases can function as chelating agents complexing with transition or main group metals producing complexes with versatile stereochemistries, applications and with enhanced bioactivity compared to the parental ligands. Moreover, these compounds contain the basic unit of peptide linkage [-C(O)-NH-] group which is a part of primary structure of proteins and is of crucial importance in biological systems. In enzyme systems, metal ions play an important role in terms of both structure and function. These metal cations are not only involved in the structural properties of proteins, but also show catalytic activity. Over the past few decades, metal Schiff-base complexes have been widely investigated with regard to their function as model compounds for biological enzymes [1, 2]. Some N-O containing metal-Schiff base complexes possessing high catalytic activity shows potential application in the field of catalysis [3, 4]. The presently studied coordination compounds consist of NNO donor Schiff bases.

1.1. Importance of hydrazones

Hydrazones are compounds containing the characteristic -N=N- linkage, which are derived by the condensation of substituted hydrazides with carbonyl compounds namely aldehydes and ketones. According to the needs of a polydentate ligand, the group functionalities are increased by condensation and substitution. The general formula for a substituted acid hydrazone is given in Fig. 1.1.

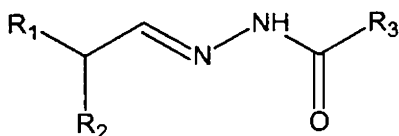


Fig. 1.1. General formula of a substituted acid hydrazone

An attractive aspect of the hydrazones is that they are capable of exhibiting tautomerism (Fig. 1.2). In the solid state, the compound predominantly exists in the keto form, whereas in the solution state the enol form predominates.

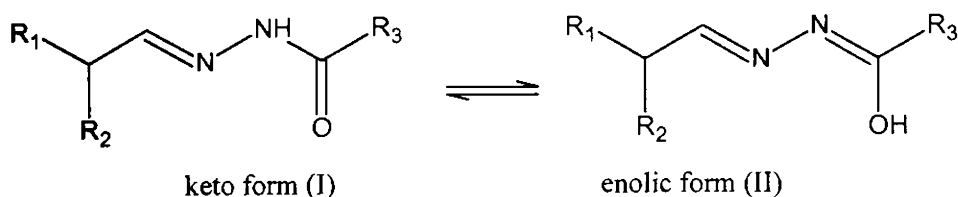


Fig. 1.2. Keto-enol tautomerism of a substituted hydrazone

By attaining the enolic form, the effective conjugation along the hydrazone skeleton is increased thereby giving rise to an efficient electron delocalization. The presence of aromatic substituents on the skeleton can further enhance the delocalization of electron charge density. In the present work, we have chosen 2-benzoylpyridine and pyridine-2-carbaldehyde as the carbonyl components of our ligands.

The reaction of aroylhydrazones with transition metal ions can proceed according to two pathways attaining the ketonic (I) or enolic (II) structure for the hydrazide part of the molecule. Thus coordination compounds with the existence of the ligands in the neutral form and also in the anionic form *via* deprotonation at the enolate oxygen are possible.

The keto form itself exists in *cis* or *trans* form depending on the substituents resulting in a more stable structure (Fig. 1.3). The existence of the ligands in these geometrical forms in the solid state is well established by crystallographic studies. In our study, both *cis* and *trans* forms were observed.

Thus it is well evident that the stereochemistry of the ligand is much decided by the steric effects of the various substituents in the hydrazone moiety and also favored by additional interactions such as intramolecular hydrogen bonding. It is observed that the *cis* nature of the bond usually transforms to *trans* geometry, while coordinating to metal ions. This phenomenon is assumed to be due to chelate effect, which results in an increased stability due to better electron delocalization in chelated ring system consisting of metal ions. The enolic form of the ligand could exist in four possible forms (Fig. 1.4) thus acting as monodentate or bidentate. Upon complexation, the enolic form usually adopts the suitable geometry, with maximum number of coordination sites leading to chelation.

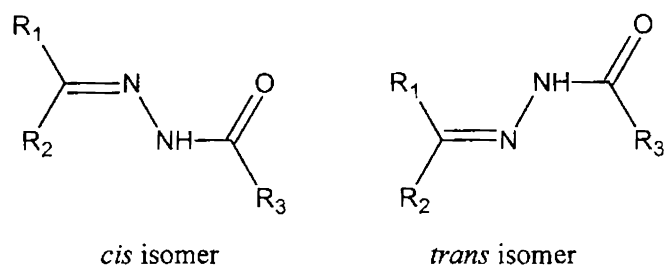


Fig. 1.3. Geometrical isomers of the keto form

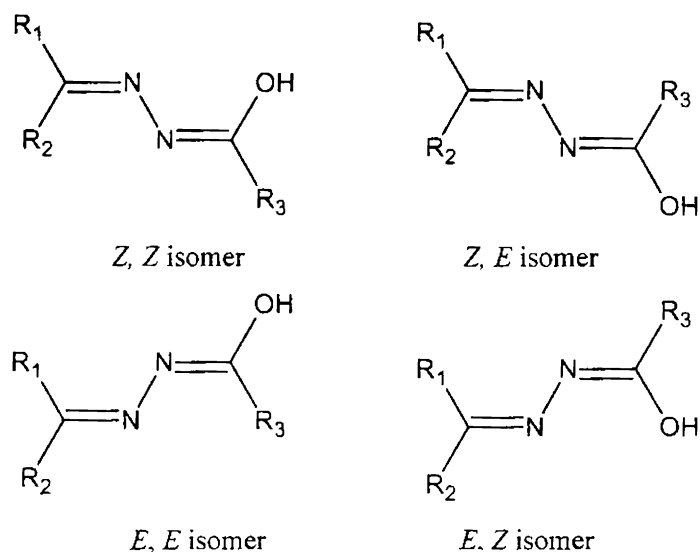
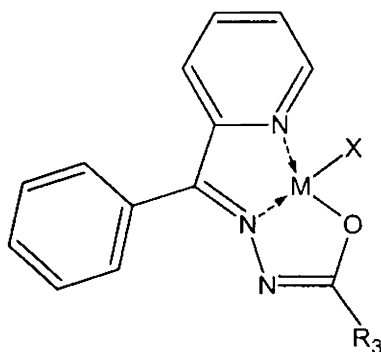


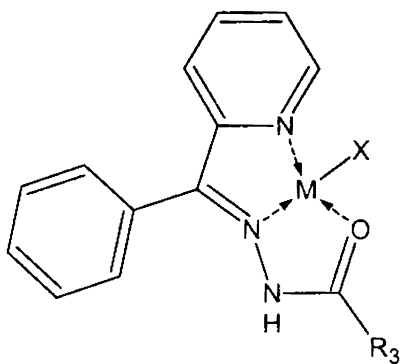
Fig. 1.4. The possible configurations of the enolic form of the ligand

The substituents with potential donor sites increase the denticity of the ligand. Depending on the reaction conditions and the stability of the metal complex formed, the hydrazones show a variety of coordination modes with transition metal, adopting any one of the above four possible forms. The number and type of the substituents influence the coordination mode. The presence of 2-benzoylpyridine and pyridine-2-carbaldehyde as the carbonyl substituents provides one additional nitrogen as a donor. The other two coordinating sites are the azomethine nitrogen and the enolate oxygen. A depiction of a four coordinate metal complex (Structure I) with the tridentate ligand together with the anionic coligand 'X' is given below.

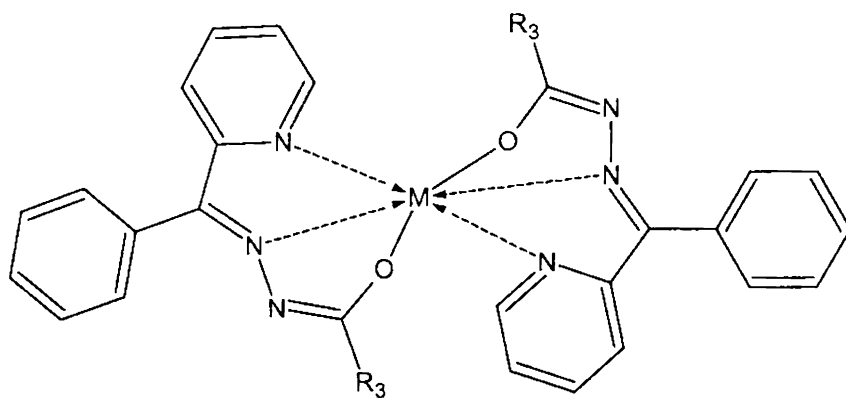


Structure I

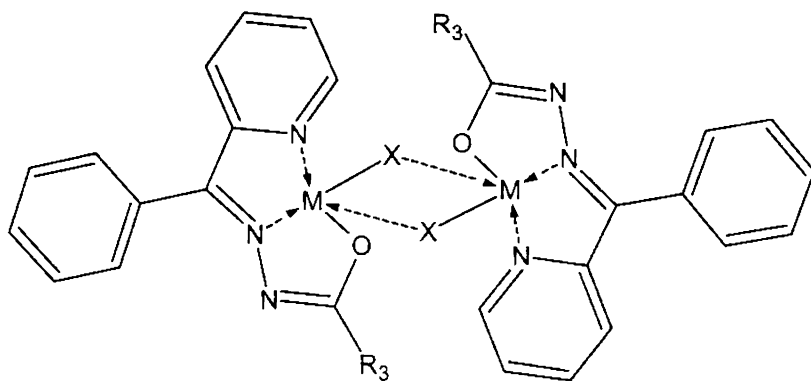
It should be mentioned here that it is not necessary that the ligand should undergo deprotonation and coordinate. Thus the ligand can also coordinate with the metal, in the neutral form. The hydrazide substituents include a nicotinoyl and benzoyl ring. The presence of nitrogen in the nicotinoyl ring at the third position makes it a donor site. But in most cases, the ligand acts as a tridentate ligand without the participation of this donor site in coordination. Though the nitrogen in nicotinoyl ring is not involved in the tridentate coordination of the ligand, it was found that it could form complexes resulting in polymeric structures thereby connecting to an adjacent metal center. Thus in that case the ligand is tetradentate. The various possible coordination modes of the hydrazone ligand under study are shown below (Structures II-V).



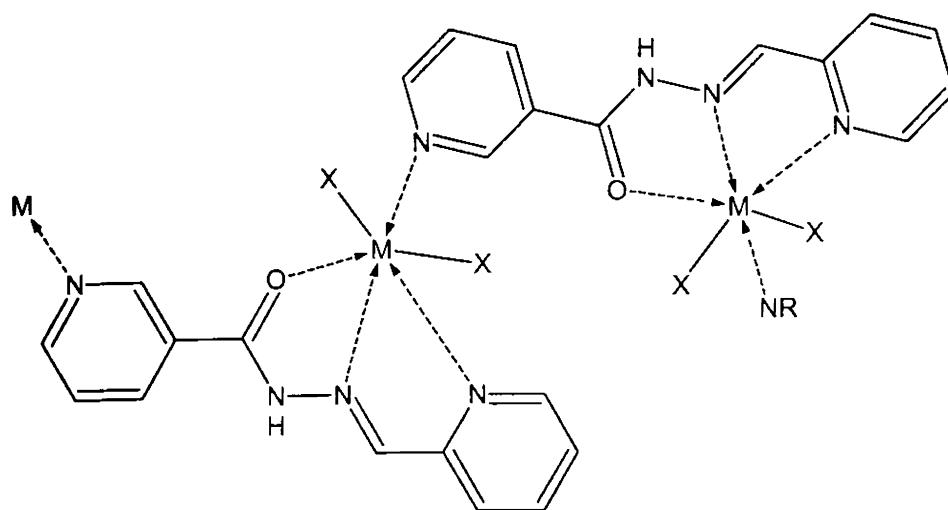
Structure II



Structure III



Structure IV



Structure V

1.2. Applications of hydrazones

Research interests in the field of hydrazones stems from their biological activities. The metal complex is found to be more active than the free ligand and some side effects may decrease upon complexation [5]. The chemical properties of hydrazones have been widely investigated in several research fields because of their chelating capability and their pharmacological applications [6].

The heterocyclic hydrazones constitute an important class of biologically active drug molecules that have attracted attention of medicinal chemists due to their antitubercular activity [7, 8]. Although biological activities of many of these compounds were shown to be related to their metal chelating abilities in the past [9-11], evidence confirming the formation of a lipid soluble copper chelate which facilitates cell internalization has been provided only recently in case of isonicotinoylhydrazide (INH) which is the most effective first-line antitubercular compound used. Patole *et al.* have screened the 2-acetylpyridine benzoylhydrazone and its copper complex for their antitubercular activity [12]. The results were found to be comparable with the drug Ciprofloxacin.

Aroylhydrazones are currently being investigated as orally active iron chelators for the treatment of iron overload, appearing in thalassemia or resulting from repeated blood transfusions [13, 14]. Salicylaldehyde benzoylhydrazone appears to be one of the most promising alternatives to desferrioxamine, the major drug used up to now that demands long and expensive treatment and is not free from side effects. Ponka and his colleagues found that pyridoxal isonicotinoylhydrazone and analogs chelate iron(III) and show promise as orally effective drugs for iron overload diseases [15, 16]. Richardson *et al.* have designed and patented a novel class of ligands based on 2-pyridinecarbaldehyde isonicotinoylhydrazone (HPCIH), that have shown great promise *in vitro*, demonstrating a high iron chelation efficacy [17, 18]. Moreover, these chelators show very low toxicity *in vitro* cultured cells and the compounds are simple and economical to prepare by a Schiff-base condensation reaction.

The discovery that salicylaldehyde benzoylhydrazone inhibits DNA synthesis and cell growth [19, 20] led to the investigation of their metal complexes. Surprisingly, the Cu(II) complex was shown to be significantly more potent than the metal free chelate, leading to the suggestion that the metal complex was the biologically active species. Because of the biological interest in this type of chelate system, several structural studies have been carried out on copper, with this ligand and analogues [21-24]. Acylhydrazones of salicylaldehyde subsequently attracted attention. Salicylaldehyde acetylhydrazone displays radioprotective properties and a range of acylhydrazones has been shown to be cytotoxic, the copper complexes again showing enhanced activity.

The complexes of metal hydrazone continue to attract considerable attention owing to their interesting biological activities and potential applications in industry. The Schiff base hydrazones of pyridoxal phosphate and their analogs have been well studied in order to understand the action mechanism of Vitamin B₆ containing enzymes [25-28]. Coordination complexes of aroylhydrazones act as potential inhibitors for many enzymes [29-33]. N-(Phenyl-pyridin-2-yl-

methylene)-N'-pyridin-2-yl-hydrazine are reported as promising inhibitor of ribonucleotide reductase [34]. Hydrazide and hydrazone derivatives having interesting ligation properties with transition metal ions have potential applications as antineoplastic, antiviral, anti-inflammatory [35-39] and antitumor agents [40]. Radiopharmaceuticals comprised of biomolecules labeled with gamma-ray emitting radionuclides are promising in the noninvasive diagnosis of a variety of diseases such as thromboembolic disease, infection and cancer. Abrams and coworkers have recently described the modification of polyclonal IgG with the 6-hydrazinonicotinyl group (Hynic) for labeling with ^{99m}Tc and subsequent imaging of focal sites of infection [41-42]. Hynic derivatives of somatostatin and monoclonal antibody fragments have shown promise as tumor imaging agents [43-44].

Molecular based second-order nonlinear optical (NLO) chromophores have recently attracted much interest because of their potential applications in emerging optoelectronic technologies. The study of the chemical properties of the metal complexes of suitably substituted aroylhydrazones reveal their NLO activity [45-47].

Hydrazones are used as plasticizers and stabilizers for polymers and as polymerization initiators, antioxidants etc. Aromatic hydrazone molecules dispersed in a binder polymer are used as the main constituent of electrophotographic devices due to their excellent hole-transporting properties and relatively simple synthesis [48]. Other applications of hydrazones include their capability to act as herbicides, insecticides, nematocides, rodenticides and plant-growth regulators.

There are innumerable applications of hydrazones in the field of analytical chemistry. Hydrazones are used in analytical chemistry as metal extracting agents. Biscyclohexanone oxalyldihydrazone is used for the determination of copper in paper pulp products, human serum, steel, plants, non-ferrous metals and alloys. Pyridine-2-aldehyde 2-pyridylhydrazone (PAPH) introduced by Lions and

Chapter 1

Martin [49] has been used for the determination of copper in foodstuffs. The reaction of 2,2'-bipyridyl 2-pyridylhydrazone (BPPH) with Co(II) forming an orange complex is utilized in the spectrophotometric determination of cyanocobalamine and of cobalt in sea water and brine.

Isatin-2-benzothiazolyhydrazone is used for the determination of lead in plastic milk cartons. The most sensitive reagent for the fluorimetric determination of aluminium is salicylaldehyde formylhydrazone.

The complexes of bivalent Cu, Zn, Cd, Fe and Ni with PAPH have been used as acid-base indicators [50] in titration of weak and strong acids and bases. Based on the extraction of their intensely colored deprotonated forms into organic solvents, the Cu, Ni and Fe complexes have been used as extraction indicators in titration of strong acids and bases. Hydrazones are also used as spot test reagents for the detection of metal ions. 2,2'-Bipyridyl-2-quinolyhydrazone and 2,2'-bipyridyl-2-pyrimidylhydrazone are used as spot test reagents for the detection of iron, cobalt and copper. p-Dimethylaminobenzaldehyde isonicotinoylhydrazone forms an intensely orange-yellow precipitate with mercury (I or II) in slightly acidic, neutral or slightly alkaline medium [51]. The complex of Co(III) with pyridine-2-aldehyde 2-pyridylhydrazone (PAPH) has been used in the nephelometric determination [52] of silver and mercury.

1.3. Objectives of the present work

The chemical properties of hydrazones and their complexes are widely explored in recent years, owing to their coordinative capability, pharmacological activity and their use in analytical chemistry as metal extracting agents. In particular the chelating behavior of aroylhydrazones of heteroaromatic aldehydes or ketones is currently being studied in our group [53-58] with the aim of investigating the influence coordination exerts on their conformation and or configuration, in connection with the nature of the metal and of the counter ion. The selection of the nicotinoylhydrazide as the hydrazide part was based on its

capability to form polymeric structures expecting single chain molecular magnets. Only the cadmium metal was found to form such one-dimensional chains with nicotinoylhydrazone. This reveals the nature of the metal and the steric effects imposed by the ligands in deciding the geometry of the coordinated metal complex. Hence it is interesting to explore the coordinating capabilities of these ligands whether in neutral form or anionic form and to study the structural variations occurring in the ligands during complexation such as change in conformation.

So three ligands and their metal complexes are synthesized. They were characterized by various spectroscopic techniques and by crystallographic studies. Magnetic studies were also conducted.

1.4. Physical measurements

Elemental analyses were carried out at the Sophisticated Analytical Instruments Facility, Kochi using VarioEL III CHNS. The magnetic susceptibility measurements were done in the polycrystalline state at room temperature on a Vibrating Sample Magnetometer at the Indian Institute of Technology, Roorkee, India. IR spectral analyses were done using KBr pellets on Thermo Nicolet AVATAR 370 DTGS FT-IR spectrophotometer in the 4000-400 cm^{-1} region. UVD-3500, UV-VIS Double Beam Spectrophotometer was used to record the electronic spectra in the range 200-900 nm. NMR spectra were recorded using Bruker AMX 400 FT-NMR Spectrometer using TMS as the internal standard at the Sophisticated Instruments Facility, Indian Institute of Science, Bangalore, India. EPR spectral measurements were carried out on a Varian E-112 X-band spectrometer using TCNE as standard at the Sophisticated Analytical Instruments Facility, Indian Institute of Technology, Bombay, India.

1.5. Crystallographic data collection and structure analyses

Single crystal X-ray diffraction measurements were carried out on a Bruker Smart Apex CCD diffractometer and on a Nonius MACH3 diffractometer,

both equipped with fine-focused sealed tube at the Analytical Sciences Division, Central Salt & Marine Chemicals Research Institute, Gujarat and at the Indian Institute of Technology, Bombay respectively. The unit cell parameters were determined and the data collections were performed using a graphite-monochromated Mo K α ($\lambda = 0.71073 \text{ \AA}$) radiation. The data collected were reduced using SAINT [59] and MAXUS programs [60] correspondingly for the Bruker Smart Apex CCD and Nonius MACH3 diffractometers. The trial structure was obtained by direct methods [61] using SHELXS-97, which revealed the position of all non-hydrogen atoms and refined by full-matrix least squares on F^2 (SHELXL-97) [62] and the graphics tool used includes DIAMOND version 3.0 [63]. All non-hydrogen atoms are refined anisotropically, while the hydrogen atoms are treated with a mixture of independent and constrained refinements.

References

1. P.Espinet, M. A. Estreuelas, L. A. Oro, J. L. Serrano. E. Sola, *Coord. Chem. Rev.* 117 (1992) 215.
2. A. M. G. Godquin, P. M. Maitlis, *Angew. Chem. Int. Ed. Engl.* 30 (1991) 375.
3. E. N. Jacobsen, W. Zhang, A. R. Muci, J. R. Ecker, L. Deng, *J. Am. Chem. Soc.* 113 (1991) 7063.
4. H. Schmidt, M. Bashirpoor, D. Rehder, *J. Chem. Soc. Dalton Trans.* (1996) 3865.
5. H. Beraldo, D. Gambino, *Mini Rev. Med. Chem.* 4 (2004) 159.
6. L. F. Lindoy, S. E. Livingstone, *Coord. Chem Rev.* 2 (1967) 173.
7. J. R. Dilworth, *Coord. Chem. Rev.* 21 (1976) 29.
8. Q. Albert, *Nature* 9 (1953) 370.
9. N. Nawar, N. M. Hosny. *Trans. Met. Chem.* 25 (2000) 1.
10. E. W. Ainscough, A. M. Brodie, W. A. Denny, G. J. Finlay, S. A. Gothe, J. D. Ranford, *J. Inorg. Biochem.* 77 (1999) 125.
11. B. Swamy, J. R. Swamy, *Trans. Met. Chem.* 16 (1991) 35.
12. J. Patole, U. Sandbhor, S. Padhye, D. N. Deobagkar, C. E. Anson, A. Powell, *Bioorg. Med. Chem. Lett.* 13 (2003) 51.
13. M. L. Vitolo, J. Webb, *J. Inorg. Biochem.* 20 (1984) 255.
14. E. Baker, M. L. Vitolo, J. Webb, *Biochim. Pharmacol.* 34 (1985) 3011.
15. P. Ponka, J. Borova, J. Neuwirt, *Biochem. Biophys. Acta* 586 (1979) 278.
16. P. Ponka, D. R. Richardson, E. Baker, *Biochem. Biophys. Acta* 967 (1988) 122.
17. D. R. Richardson, E. Becker, P. V. Bernhardt, *Acta Cryst. C* 55 (1999) 2102.
18. E. Becker, D. R. Richardson, *J. Lab. Clin. Med.* 134 (1999) 510.
19. D. K. Johnson, T. B. Murphy, N. J. Rose, W. H. Goodwin, L. Pickart, *Inorg. Chim. Acta* 67 (1982) 159.
20. L. Pickart, W. H. Goodwin, W. Burgua, T. B. Murphy, D. K. Johnson, *Biochem. Pharmacol.* 32 (1983) 3868.

21. A. A. Aruffo, T. B. Murphy, D. K. Johnson, N. J. Rose, V. Schomaker. *Acta Cryst. C* 40 (1984) 1164.
22. E. W. Ainscough, A. M. Brodie, A. Dobbs, J. D. Ranford, J. M. Waters, *Inorg. Chim. Acta* 236 (1995) 83.
23. S. C. Chan, L. L. Koh, P. H. Leung, J. D. Ranford, K. Y. Sim, *Inorg. Chim. Acta* 236 (1995) 101.
24. E. W. Ainscough, A. M. Brodie, A. Dobbs, J. D. Ranford, J. M. Waters, *Inorg. Chim. Acta* 267 (1998) 27.
25. H. R. Maghler, E. H. Cordes, *Biological Chemistry*, Harper and Row, New York 1971, 393.
26. H. M. Dawes, J. M. Waters, T. N. Waters, *Inorg. Chim. Acta* 66 (1982) 29.
27. S. P. Rath, S. Mondal, A. Chakravorty, *Inorg. Chim. Acta* 263 (1997) 247.
28. S. P. Rath, K. K. Rajak, S. Mondal, A. Chakravorty, *J. Chem. Soc. Dalton Trans.* (1998) 2097.
29. J. C. Craliz, J. C. Rub, D. Willis, J. Edger, *Nature* 34 (1955) 176.
30. M. F. Iskander, L. Sayed, A. F. M. Hefny, S. E. Zayan, *J. Inorg. Nucl. Chem.* 38 (1976) 2209.
31. G. H. Havnur, V. B. Mahale, *Indian J. Chem.* 26A (1987) 1063.
32. H. Adams, D. E. Fenton, G. Minardi, E. Mura, M. Angelo, *Inorg. Chem. Commun.* 3 (2000) 4.
33. Z. Y. Yang, R. D. Yang, F. S. Li, K. B. Yu, *Polyhedron* 19 (2000) 2599.
34. J. Easmon, G. Heinisch, G. Purstinger, T. Langer, J. K. Osterreicher, H. H. Grunicke, J. Hofmann, *J. Med. Chem.* 40 (1997) 4420 and references cited therein.
35. D. Wester, G. J. Palenik, *J. Am. Chem. Soc.* 95 (1973) 6505.
36. E. C. Constable, J. M. Holmes, *Inorg. Chim. Acta* 126 (1987) 195.
37. T. J. Giordano, G. J. Palenik, R. C. Palenik, D. A. Sullivan, *Inorg. Chem.* 18 (1979) 2445.
38. A. Bino, R. Frim, M. V. Genderen, *Inorg. Chim. Acta* 127 (1987) 95.
39. E. C. Constable, F. K. Khan, J. Lewis, M. C. Liptrot, P. R. Raithby, *J. Chem.*

Soc. Dalton Trans. (1985) 333.

40. B. A. Booth, E. C. Moore, A. C. Sartorelli, *Cancer Res.* 31 (1971) 228.
41. M. J. Abrams, M. Juweid, C. I. Tenkate, D. A. Schwartz, M. M. Hauser, F. E. Gaul, A. J. Fucello, R. H. Rubin, H. W. Strauss, A. J. Fischman, *J. Nucl. Med.* 31 (1990) 2022.
42. D. A. Schwartz, M. J. Abrams, M. M. Hauser, F. E. Gaul, S. K. Larsen, D. Rauh, J. A. Zubieta, *Bioconjugate Chem.* 2 (1991) 333.
43. H. R. Macke, M. Behe, *J. Nucl. Med.* 37 (1996) 29.
44. G. J. Bridger, M. J. Abrams, S. Padmanabhan, F. E. Gaul, S. K. Larsen, G. W. Henson, D. A. Schwartz, C. B. Clongley, C. A. Burton, M. E. Ultee, *Bioconjugate Chem.* 7 (1996) 255.
45. F. Cariati, U. Caruso, R. Centore, W. Marcolli, A. De Maria, B. Panunzi, A. Roviello, A. Tuzi, *Inorg. Chem.* 41 (2002) 6597.
46. P. G. Lacroix, *Eur. J. Inorg. Chem.* (2001) 339.
47. U. Caruso, R. Centore, B. Panunzi, A. Roviello, A. Tuzi, *Eur. J. Inorg. Chem.* (2005) 2747.
48. V. Getautis, M. Daskeviciene, T. Malinauskas, V. Gaidelis, V. Jankauskas, Z. Tokarski, *Synthetic Metals* 155 (2005) 599.
49. F. Lions, K. Martin, *J. Am. Chem. Soc.* 80 (1958) 3858.
50. A. J. Cameron, N. A. Gibson, *Anal. Chim. Acta* 51 (1970) 249.
51. G. S. Vasilikiotis, *Microchem. J.* 13 (1968) 526.
52. C. F. Bell, M. A. Quddus, *Anal. Chim. Acta* 52 (1970) 313.
53. P. B. Sreeja, A. Sreekanth, C. R. Nayar, M. R. P. Kurup, A. Usman, I. A. Razak, S. Chantrapromma, H. -K. Fun, *J. Mol. Stru.* 645 (2003) 221.
54. P. B. Sreeja, M. R. P. Kurup, A. Kishore, C. Jasmin, *Polyhedron* 23 (2004) 575.
55. P. B. Sreeja, M. R. P. Kurup, *Spectrochim. Acta* 61 (2005) 331.
56. M. Kuriakose, M. R. P. Kurup, E. Suresh, *Spectrochim. Acta* (2006) in press.
57. B. N. B. Raj, M. R. P. Kurup, *Spectrochim. Acta* (2006) in press.

Chapter 1

58. B. N. B. Raj, M. R. P. Kurup, E. Suresh, *Struct. Chem.* in press.
59. Siemens, SMART and SAINT, Area Detector Control and Integration Software, Siemens Analytical X-ray Instruments Inc., Madison, Wisconsin, USA, 1996.
60. S. Mackay, C. J. Gilmore, C. Edwards, N. Stewart and K. Shankland, maXus Computer Program for the Solution and Refinement of Crystal Structures. Nonius, The Netherlands, MacScience, Japan and The University of Glasgow, 1999.
61. G. M. Sheldrick, *Acta Crystallogr. A* 46 (1990) 467.
62. G. M. Sheldrick, SHELXS-97 Program for the solution of Crystal Structures, University of Göttingen, Göttingen, Germany, 1997.
63. K. Bradenburg, H. Putz, DIAMOND Version 3.0, Crystal Impact, GbR, Postfach 1251, D-53002 Bonn, Germany, 2004.

Syntheses, spectral characterization and crystal structures of heteroaroylhydrazone ligands from 2-benzoylpyridine and pyridine-2-carbaldehyde

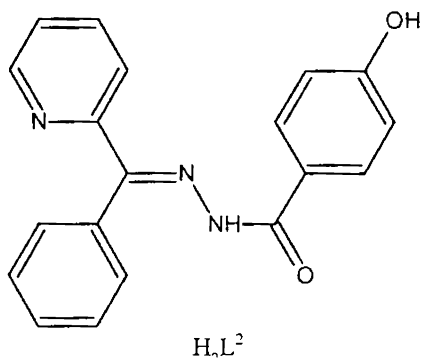
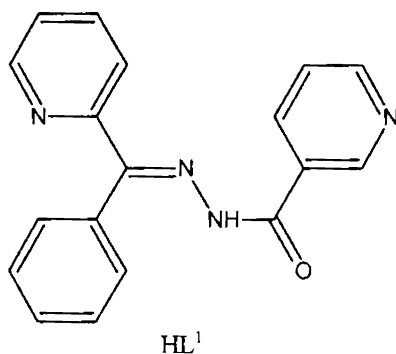
The exceptional qualities of Schiff bases such as facile syntheses, easily tunable steric, electronic properties and good solubility in common solvents have led to their extensive study [1]. Schiff bases display biological activity and play an important role in biological systems [2-6]. Additionally the Schiff bases are found to have wide applications in fields such as antibacterial, antiviral, antifungal agents [7], homogeneous or heterogeneous catalysis [8-12] and magnetism [13]. The hydrazones formed by the condensation of hydrazides with aromatic aldehydes or ketones belong to the general family of Schiff bases. This condensation leads to an extended electron delocalization along the azomethine bond. Hydrazones and their metal complexes are widely studied due to their versatile applications in the field of analytical and medicinal chemistry [14-24]. Compounds containing hydrazide and acylhydrazone moieties and their complexes possess biological activity, especially as potential inhibitors for many enzymes. These ligands due to their facile keto-enol tautomerisation and the availability of several potential donor sites can coordinate with metals. Hydrazone ligands can act as bidentate, tridentate or tetradentate ligands depending on the nature of heterocyclic ring substituents attached to the hydrazone unit. Hydrazides and hydrazones have interesting ligation properties due to presence of several coordination sites. The ligands in the coordination sphere can exist in the neutral or anionic form depending on the reactions conditions employed.

Metal complexes of heteroaroylhydrazone with aldehydes and ketones have been widely reported. But hydrazones with carbonyl compounds such as

2-benzoylpyridine and pyridine-2-carbaldehyde have been less reported [25-30]. Although a variety of aroylhydrazones with isonicotinic acid hydrazide and their transition metal complexes are reported [31-35], systems based on nicotinic acid hydrazones are only few [36-39]. Keeping these in view, we have synthesized three new heteroaroyl hydrazone systems (Fig. 2.1) with nicotinoylhydrazide, 4-hydroxybenzhydrazide, 2-benzoylpyridine and pyridine-2-carbaldehyde. The ligands synthesized are

1. 2-Benzoylpyridine nicotinoylhydrazone (HL^1)
2. 2-Benzoylpyridine-4-hydroxybenzoylhydrazone (H_2L^2)
3. Pyridine-2-carbaldehyde nicotinoylhydrazone (HL^3)

Thus the ligands (HL^1) and (HL^3) are monoprotic whereas H_2L^2 is diprotic. Ligands (HL^1) and (HL^3) coordinate with the metal centre both in keto form as well as in enolate form under neutral conditions. The second ligand (H_2L^2) in spite of two protons remained monoanionic upon coordination. The noninvolvement of the second probable anionic site in complexation is explained by its position far away from the other coordinating centers. The possibility for the formation of a bridged complex, by this site, cannot be neglected. However, such complexes were not found in our study.



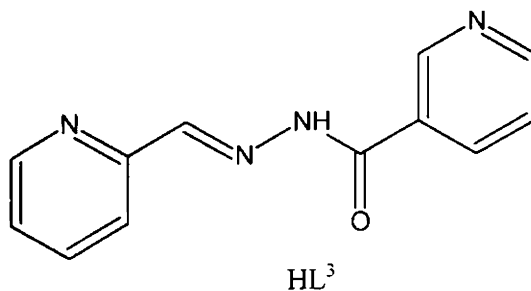


Fig. 2.1. Structures of the three ligands HL¹, H₂L² and HL³

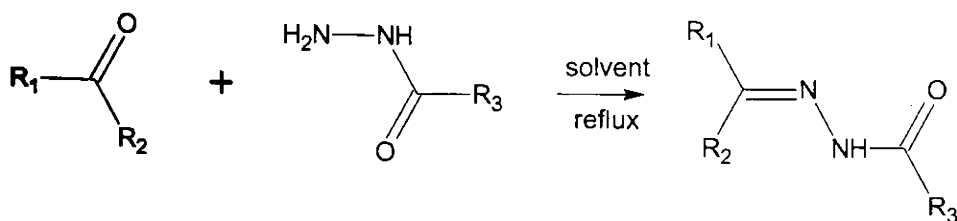
2.1. Experimental

2.1.2 Materials

2-Benzoylpyridine (Sigma Aldrich), pyridine-2-carbaldehyde (Sigma Aldrich), nicotinoylhydrazide (Sigma Aldrich) and 4-hydroxybenzhydrazide (Fluka) were used as received. The solvent used, ethanol was distilled before use.

2.1.3 Synthesis of ligands

A general procedure was adopted for the preparation of the ligands. Equimolar ratios of corresponding hydrazide and carbonyl compound were refluxed for 6 hours in suitable solvent media containing 4-5 drops of glacial acetic acid. The general Scheme 2.1 is given below.



Scheme 2.1.

HL¹: Reagents were 2-benzoylpyridine (0.366 g, 2 mmol) and nicotinoylhydrazide (0.274 g, 2 mmol). The solvent used was ethanol. The

resulting solution after refluxation was poured into ice by stirring. The white precipitate obtained was filtered, washed with water and dried over P_4O_{10} *in vacuo*. The product was recrystallized from ethanol. Yield (0.315 g, 52.2%). Elemental Anal. Found (Calcd.) (%): C, 71.07 (71.51); H, 4.78 (4.67); N, 18.70 (18.53).

H₂L²: Reagents were 2-benzoylpyridine (0.366 g, 2 mmol) and 4-hydroxybenzhydrazide (0.304 g, 2 mmol). DMF and ethanol mixture (1:1 v/v) was chosen as the solvent. The white shining crystalline precipitate obtained on cooling the reaction media was filtered, washed with ethanol and dried over P_4O_{10} *in vacuo*. The product was recrystallized from DMF-ethanol mixture. Yield (0.415 g, 65.5%). Elemental Anal. Found (Calcd.) (%): C, 70.93 (71.91); H, 4.93 (4.76); N, 13.13 (13.24).

HL³: Reagents were pyridine-2-carbaldehyde (0.214 g, 2 mmol) and nicotinoylhydrazide (0.274 g, 2 mmol). Ethanol was used as the solvent. The yellow crystalline precipitate obtained was filtered, washed with ethanol and dried over P_4O_{10} *in vacuo*. The product was recrystallized from ethanol. Yield (0.325 g, 61.9%). Elemental Anal. Found (Calcd.) (%): C, 55.04 (54.96); H, 5.62 (5.38); N, 21.68 (21.36).

2.2. Results and discussion

The ligands were synthesized in a straightforward fashion by refluxing equimolar solutions of the corresponding hydrazides with the ketone or aldehyde.

2.2.1 Crystal structures of HL¹, H₂L² and HL³·2H₂O

HL¹: *The ligand HL¹, crystallizes into a triclinic lattice with $P\bar{1}$ symmetry. Block shaped colorless single crystals suitable for diffraction was grown from a solution of the compound in an ethanol-DMF mixture (1:1 v/v). There are two molecules per unit cell. The crystal data and structural refinement

* Published in Spectrochim Acta Part A (2006) (in press)

parameters are given in Table 2.1. The molecular structure of HL¹ along with the atom numbering scheme is given in Fig. 2.2.

The ketone condenses with the hydrazide producing a new azomethine bond that is the C(6)–N(2) bond whose bond length, 1.2924(15) Å is similar to that of a C=N bond. The selected bond lengths and bond angles are illustrated in Table 2.3. The torsion angle of 1.76° perceived by N(2)–N(3)–C(13)–O(1) confirms the existence of the C(13)–N(3) bond to be *cis* in nature. Similarly, the configuration along the C(6)–N(2) bond is *cis*, as agreed by the N(3)–N(2)–C(6)–C(5) torsion angle value of 2.84°. This arrangement enables the N(3)–H to involve in H-bonding with the N(1) atom of pyridyl ring resulting in a six membered ring in which the N(3)–N(1) distance corresponds to a value of 2.618 Å.

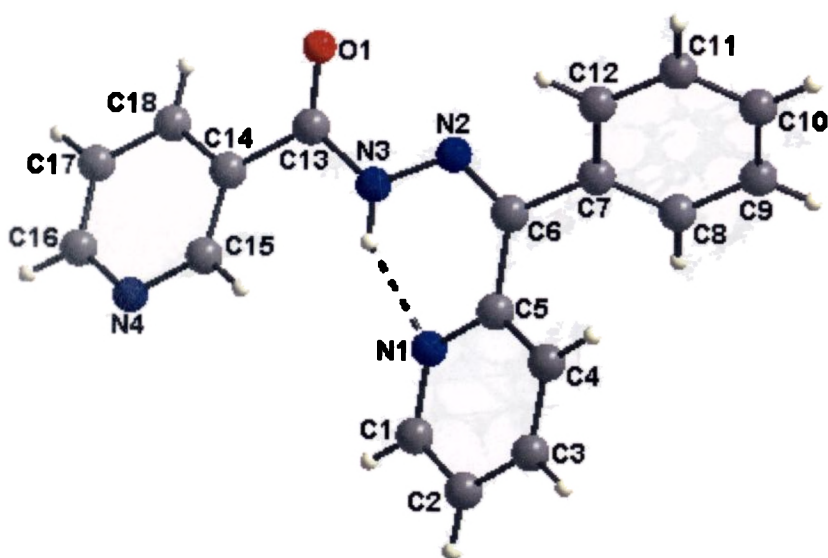


Fig. 2.2. Molecular structure of HL¹, with intramolecular hydrogen bonding, represented as dashed line

The atoms other than the three ring atoms are almost planar with *E* configuration along the N(2)–N(3) bond. The existence of ligand in keto form in the solid state is evident from the the C(13)–O(1) bond length of 1.2158(17) Å. The dihedral

angle of 61.82° suggest that the phenyl ring is tilted from the plane comprising of atoms N(1), C(1), C(2), C(3), C(4) and C(5) due to steric hindrance. The two pyridyl rings exist with a dihedral angle of 12.33° .

The molecules are centrosymmetrically arranged in the unit cell. The packing of the molecule in a unit cell is given in Fig. 2.3. The weak π - π interactions between the planes Cg(1)-[1]...Cg(2)ⁱ [Cg(1): N(1), C(1), C(2), C(3), C(4), C(5); Cg(2): N(4), C(15), C(14), C(18), C(17), C(16); $d_{Cg \dots Cg} = 3.8013 \text{ \AA}$; $i = 1-x, 1-y, -z$] and the C-H... π interaction C(9)-H(9)...Cg(2)ⁱⁱ [$d_{C(9) \dots Cg} = 3.6445 \text{ \AA}$; $ii = x, y, 1+z$] also adds to the well organized arrangement of molecules in the unit cell.

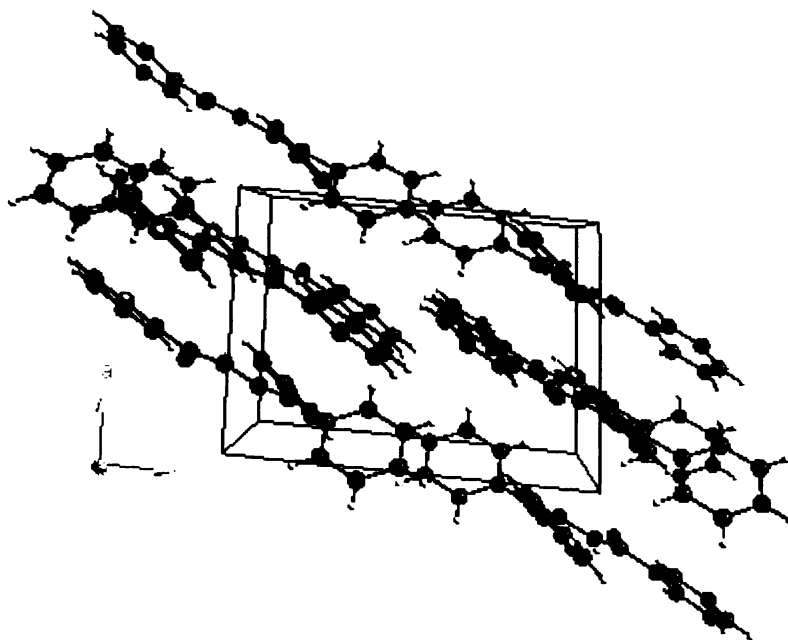


Fig. 2.3. Molecular packing diagram of HL¹

H₂L²: Colorless block shaped crystals were grown from a solution of the ligand in DMF-ethanol mixture (1:1 v/v). The lattice is monoclinic in nature with $P2_1/n$ symmetry. The crystal data and structural refinement parameters are given

in Table 2.1. The configuration along the C(6)–N(2) bond and N(2)–N(3) bond is similar to the ligand HL¹ thereby forming the intramolecular hydrogen bonded molecular structure (Fig. 2.4) given below. The selected bond lengths and bond angles are shown in Table 2.3. The presence of three aromatic rings and the steric requirement for the centroids Cg(1) and Cg(2) defined by atoms, N(1), C(1), C(2), C(3), C(4), C(5) and C(7), C(8), C(9), C(10), C(11), C(12) respectively, makes the molecule nonplanar. The dihedral angle value of 61.22° between these centroids supports this nonplanarity. The centroid Cg(1) makes a dihedral angle separation of 18.71° with the centroid Cg(3) defined by atoms C(14), C(15), C(16), C(17), C(18) and C(19). However, the central core of the molecule constituted by atoms C(6), N(2), N(3) and C(13) is planar as suggested by the torsion angle of –179.05° due to extensive conjugation. The double bonds C(6)–N(2) and C(13)–O(1) are within the usual range of double bonds, augmenting the fact that the molecule exists in keto form. The N(3)–N(2) bond length of 1.3658(14) is similar to the earlier reported benzoylhydrazone ligands [40, 41].

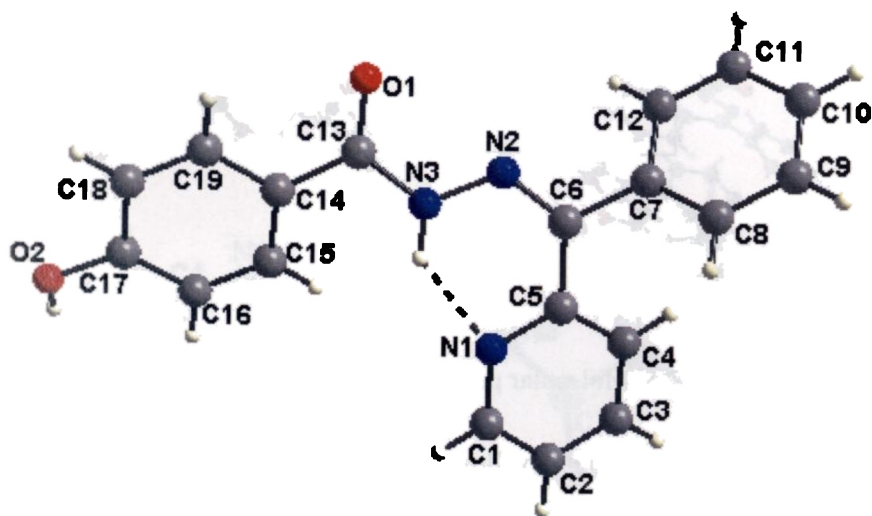


Fig. 2.4. Molecular structure of H₂L² with intramolecular hydrogen bonding interaction

The molecular packing diagram is shown in Fig. 2.5. The unit cell is viewed down the 'a' axis. In the unit cell, sets of two molecules are well arranged in an offset fashion. The molecules are interconnected in the cell through the intermolecular hydrogen bonds *viz.*, O(2)–H---O(1)ⁱ [$d_{\text{O(2)}\cdots\text{O(1)}} = 2.6998(15) \text{ \AA}$; $i = -1/2+x, 3/2-y, -1/2+z$] and C(2)–H(2)---O(1)ⁱⁱ [$d_{\text{C(2)}\cdots\text{O(1)}} = 3.2985(19) \text{ \AA}$; $ii = 1/2+x, 3/2-y, -1/2+z$]. The C–H--- π interaction observed is C(18)–H(18)---Cg(3)ⁱⁱⁱ [Cg(3): C(14), C(15), C(16), C(17), C(18), C(19); $d_{\text{C(18)}\cdots\text{Cg}} = 3.873 \text{ \AA}$; $iii = 1-x, 1-y, -z$]. These intermolecular interactions perceived between the adjacent molecules in two layers leads to the tight packing of molecules in the unit cell.

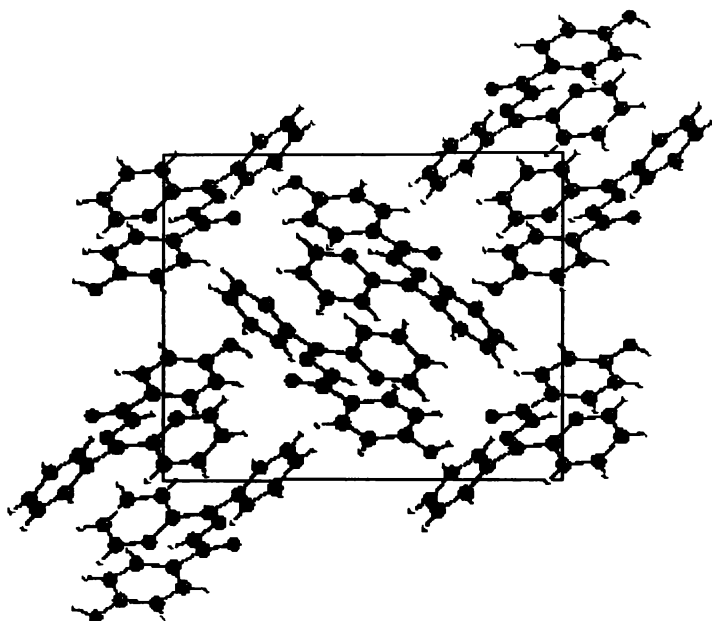


Fig. 2.5. Molecular packing diagram of H_2L^2

$\text{HL}^3 \cdot 2\text{H}_2\text{O}$: The light yellow block shaped crystals suitable for analysis were obtained by the slow evaporation of a DMF-ethanol mixture (1:1 v/v). The geometry of the molecule is similar to the earlier reported pyridine-2-carboxaldehyde picoloylhydrazone [27]. The lattice consists of two molecules of water-of-crystallization. The crystal data and structural refinement parameters are

given in Table 2.2. The molecule as a whole is roughly planar with a maximum dihedral angle separation of 11.70° between the rings formed by the atoms C(1), C(2), C(3), C(4), C(5) and C(8), C(9), N(4), C(10), C(11), C(12) respectively (Fig. 2.6). The ligand exists in keto form with the C(7)–O(3) bond length of 1.2274(17), typical of a carbon oxygen double bond. The selected bond lengths and bond angles are shown in Table 2.3. The C(6)–N(2) bond length of 1.2665(19) Å confirms to the value for a double bond. The torsion angle values, 178.80° and 0.19° attained by N(3), N(2), C(6), C(5) and N(2), N(3), C(7), O(3) confirms the existence of the ligand in *trans* configuration along the C(6)–N(2) bond and in *cis* conformation along the C(7)–N(3) bond. The existence of C(6)–N(2) bond in *trans* configuration, rules out the possibility of intramolecular N(3)–H---N(1) hydrogen bonding, compared to the molecular structures of HL¹ and H₂L². Instead another five membered ring is formed by the involvement of C(9)–H in intramolecular hydrogen bonding with O(3). Also the C(1)–H is intermolecularly hydrogen bonded to O(1). Due to conjugation effects in the molecule, the bond length of C(7)–N(3) is greater than the value for a double bond and less than the value for a single bond.

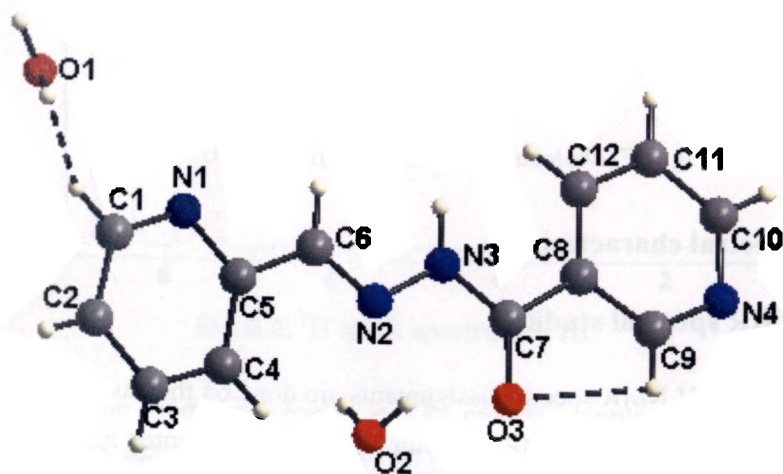


Fig. 2.6. Molecular structure of HL³·2H₂O with hydrogen bonding interaction

The packing of molecules of HL^3 is shown in Fig. 2.7. The basic unit consists of a set of two molecules arranged in a face-to-face manner. Two adjacent sets are then aligned in an offset fashion, which forms the repeating unit. The two water molecules interconnect these adjacent sets. The intermolecular hydrogen bonding interactions observed are *viz.*, $\text{N}(3)\text{--H}\cdots\text{O}(2)^{\text{i}}$ [$d_{\text{N}(3)\cdots\text{O}(2)} = 2.8512(19)$; $i = -1+x, 1+y, z$], $\text{O}(1)\text{--H}\cdots\text{N}(2)^{\text{ii}}$ [$d_{\text{O}(1)\cdots\text{N}(2)} = 3.192(2)$; $ii = 1-x, 1-y, 1-z$], $\text{O}(1)\text{--H}\cdots\text{N}(4)^{\text{iii}}$ [$d_{\text{O}(1)\cdots\text{N}(4)} = 2.947(2)$; $iii = x, -1+y, -1+z$], $\text{O}(2)\text{--H}\cdots\text{O}(3)^{\text{iv}}$ [$d_{\text{O}(2)\cdots\text{O}(3)} = 2.8818(19)$; $iv = x, -1+y, z$] and $\text{O}(2)\text{--H}\cdots\text{N}(1)^{\text{v}}$ [$d_{\text{O}(2)\cdots\text{N}(1)} = 2.9000(2)$; $v = 1-x, 1-y, 1-z$]. The molecules in the adjacent layers are held together by these interactions.

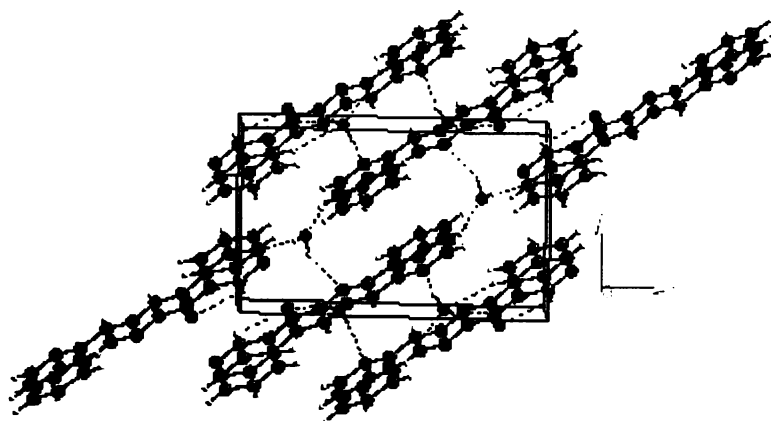


Fig. 2.7. Molecular packing diagram of $\text{HL}^3 \cdot 2\text{H}_2\text{O}$

2.2.2 Spectral characteristics

2.2.2a NMR spectral studies

HL^1 : ^1H NMR spectral assignments are done on the basis of ^{13}C NMR, COSY and HSQC. The ^1H NMR spectrum of HL^1 is represented in Fig. 2.8. The spectral studies reveal that the two pyridyl rings are in different environments. The protons of the *meta*-substituted pyridyl ring are found to be downfield shifted

more than the protons of the other pyridyl ring. This may be due to the presence of $-C=O$ group in the *meta* position. The singlet peak at 9.18 ppm corresponds to H(15) proton which is highly deshielded by the adjacent ring nitrogen and the carbonyl group attached to C(14). From the two dimensional $^1H-^1H$ correlation spectrum (Fig.2.9), it is evident that the H(15) couples neither with H(18) nor with H(16). The two protons near to the ring nitrogen, viz. H(16) and H(1) are observed as doublets at 8.86 and 8.79 ppm due to coupling with H(17) and H(2) observed at 7.43 ppm respectively. This downfield shift occurs as these protons are near to the more electronegative nitrogen atom.

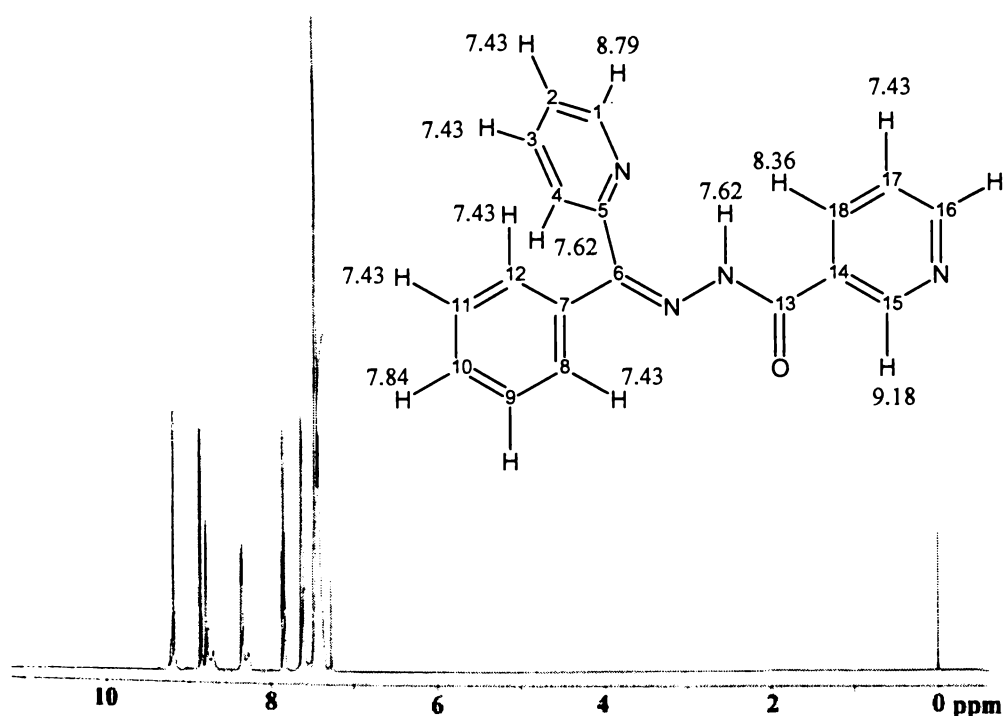


Fig. 2.8. 1H NMR spectrum of HL¹

The H(10) proton produces a triplet at 7.84 ppm by coupling with neighboring H(9) and H(11) protons. The H(18) proton couples with H(17) at 7.43 ppm resulting in a doublet at 8.36 ppm. The phenyl protons except H(10) are assigned to the multiplet found at 7.43 ppm. Though the NH proton lies in a highly

deshielded environment, it was surprising to find that no peaks corresponding to the NH proton was found in the usual range 9.5-13 ppm. The absence of this peak suggests that the intramolecular H-bonding between the NH proton and pyridyl nitrogen found in the solid state is lost in solution medium, i.e. the *cis* nature of the bond may be changed. But the integration pattern of signals reveals 15 protons suggesting the existence of a keto-enol equilibrium in solution. So it is interpreted that the signal observed at 7.62 ppm corresponds to two protons viz. H(4) and NH. The correlation of H(4) proton with H(3) proton in the multiplet (7.43 ppm) is evident from the ^1H - ^1H correlation spectra. The appearance of the NH proton in the range 7.5-8.5 ppm has been reported by Sen *et al.* [42]. The multiplet at 7.43 ppm corresponds to eight protons, which agrees with the existence of OH proton in this region. When strong intramolecular bonding is not involved, the enolic proton absorbs in about the same range as the phenolic proton ($\delta \sim 7.5 - 4.0$) [43].

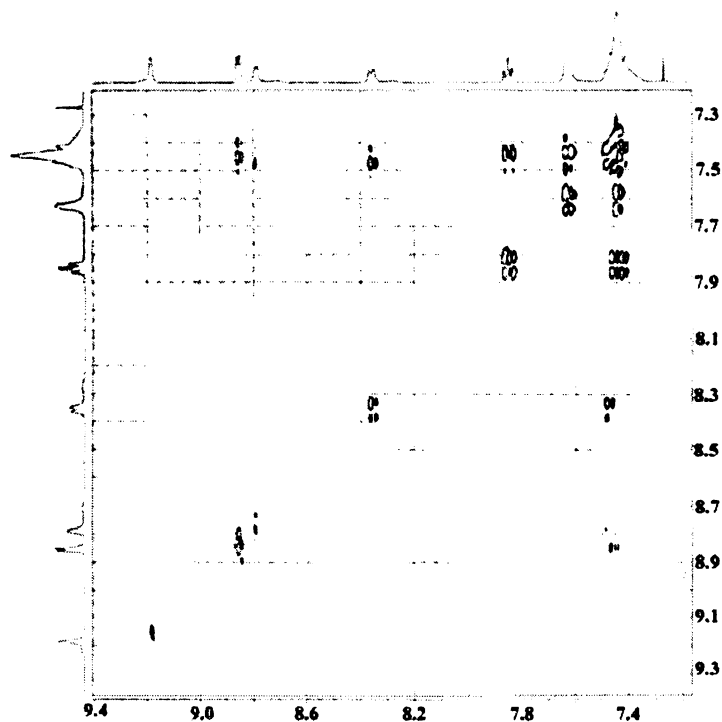


Fig. 2.9. ^1H - ^1H COSY spectrum of HL¹

Heteronuclear chemical shift correlation experiments correlate the chemical shift of one nucleus with the chemical shift of another. HSQC can be performed as either a ^1H - ^{15}N or ^1H - ^{13}C correlation experiment. The carbon skeleton of the molecule was identified by recording ^{13}C NMR and HSQC (Heteronuclear Single Quantum Coherence) ^1H - ^{13}C correlation spectrum (Fig. 2.10). The carbonyl carbon C13 appears at a δ value of 162.478, which indicates the downfield shifting due to conjugative effect of the N2-N3-C13-O1 core in the hydrazone. In both the pyridyl rings, the carbon atoms *viz.* C1, C5, C15, C16 adjacent to the electronegative nitrogen are found to resonate at lower field.

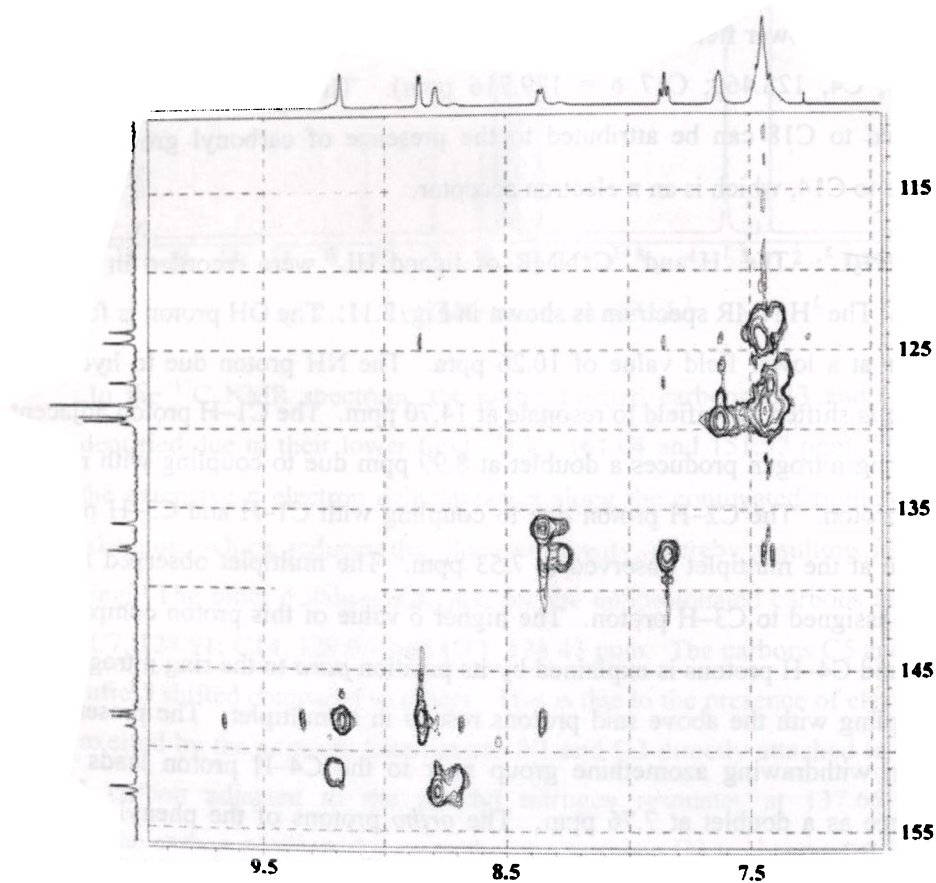


Fig. 2.10. HSQC spectrum of HL¹

Out of these, the protonated carbons, C1, C15 and C16 are found to correlate with the protons directly attached to them in the HSQC spectra. Thus they are assigned respectively at 152.576, 151.592, 148.177 ppm. However the nonprotonated carbon C5 is easily identified due to its lack of correlation and is assigned at 148.793. The lower field value of the nonprotonated carbon atom C6 ($\delta = 153.065$ ppm) is due to the extensive π electron delocalization of the C6=N2 bond. The remaining nonprotonated carbons C7 and C14 are found to resonate at 136.044 and 147.909 respectively. The phenyl resonances are C8, 129.494; C9, 124.507; C10, 137.505; C11, 123.821; C12, 129.284. The carbon atoms positioned *para* to the ring nitrogen of the pyridyl rings (C3, 128.813; C18, 137.760 ppm) are found to resonate at lower field values than the carbon atoms at the *meta* positions (C2, 127.070; C4, 128.460; C17 $\delta = 129.716$ ppm). The higher δ value of C14 compared to C18 can be attributed to the presence of carbonyl group C13=O attached to C14, which is an π electron acceptor.

H₂L²: The ¹H and ¹³C NMR of ligand HL² were recorded in DMSO solvent. The ¹H NMR spectrum is shown in Fig. 2.11. The OH proton is found to resonate at a lower field value of 10.26 ppm. The NH proton due to hydrogen bonding is shifted downfield to resonate at 14.70 ppm. The C1–H proton adjacent to the ring nitrogen produces a doublet at 8.99 ppm due to coupling with nearby C2–H proton. The C2–H proton due to coupling with C1–H and C3–H protons resonate at the multiplet observed at 7.53 ppm. The multiplet observed at 8.03 ppm is assigned to C3–H proton. The higher δ value of this proton compared to C2–H and C4–H protons is explained by its position *para* to the ring nitrogen and its coupling with the above said protons results in a multiplet. The presence of electron withdrawing azomethine group near to the C4–H proton leads to its resonance as a doublet at 7.76 ppm. The *ortho* protons of the phenyl ring *viz.* C8–H and C12–H are observed at 7.36 ppm. The *meta* and *para* positioned protons of the phenyl ring, C9–H, C11–H and C10–H are found to be overlapped with the multiplet observed at 7.53 ppm due to coupling. The protons *ortho* to the hydroxyl carbon of the disubstituted phenyl ring, C16–H and C18–H resonates at

7.63 ppm as a multiplet. The signals corresponding to C15–H and C19–H are observed at 6.92 ppm.

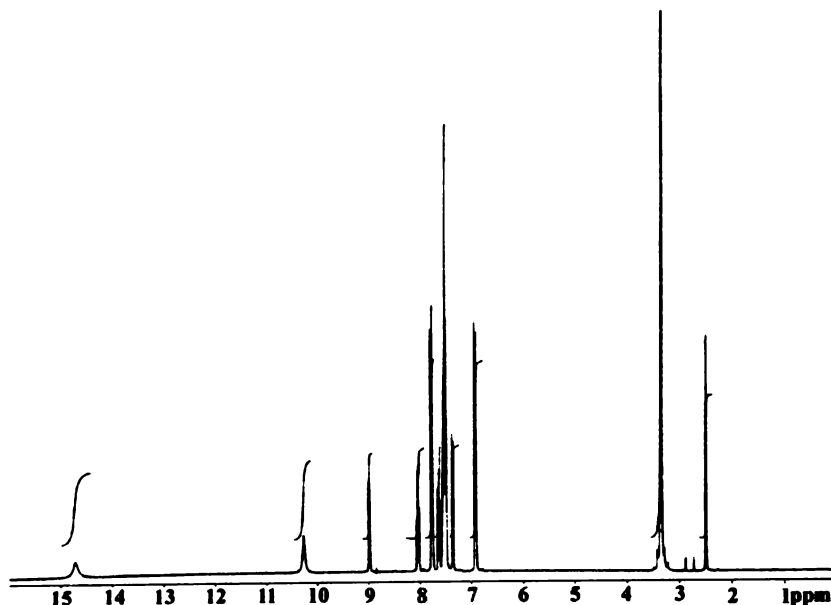


Fig. 2.11. ¹H NMR spectrum of H₂L²

In the ¹³C NMR spectrum, the nonprotonated carbons C13 and C6 are easily identified due to their lower field values 161.04 and 151.97 ppm. This is due to the extensive π electron delocalization along the conjugated frame of the carbon skeleton, which reduces the electron density, thereby resulting in their deshielding. The other δ values assigned for the nonprotonated carbons are C5, 148.70; C7, 128.91; C14, 129.05; and C17, 138.43 ppm. The carbons C5 and C17 are downfield shifted compared to others. This is due to the presence of electronic effects exerted by the adjacent heteroatoms N1 and O2 directly attached to them. The C1 carbon adjacent to the pyridyl nitrogen resonates at 137.66 ppm. Similarly the carbon positioned *para* to the ring nitrogen C3 is observed at higher δ value (129.38 ppm) than the corresponding *meta* positioned carbons, C2, 126.24; C4, 128.42 ppm. The carbons C16 and C18, *ortho* to the hydroxy substituted carbon C17, give signal at 129.8 ppm. The other carbons C15 and C19

are found to resonate at 115.59 ppm. The phenyl resonances observed are: C8 and C12, 123.60; C9 and C11, 128.01; and C10 at 124.86 ppm.

HL³: The ¹H NMR of HL³ was recorded in the solvent DMSO. The N–H peak was highly deshielded and found at 15.5 ppm. The aldehydic proton due to the deshielding effect of C6=N and the adjacent pyridyl ring was found to resonate as a singlet at 11.9 ppm (Fig. 2.12). The C9–H proton with no neighboring protons for coupling is assigned for the singlet at 8.9 ppm. This lower field value is explained by the nearby ring nitrogen and carbonyl group. The other protons adjacent to ring nitrogen, C1–H and C10–H correspond to the doublets observed at 8.01 and 8.53 ppm respectively. The higher δ value of C10–H compared to C1–H is due to the presence of carbonyl substituent (C7=O) attached to C8, which is positioned *para* to the C10 carbon. The assignment of remaining protons was difficult as their resonances overlapped with the multiplet observed at 7.75–7.09 ppm. Coupling of corresponding protons with their neighboring protons lead to this multiplet.

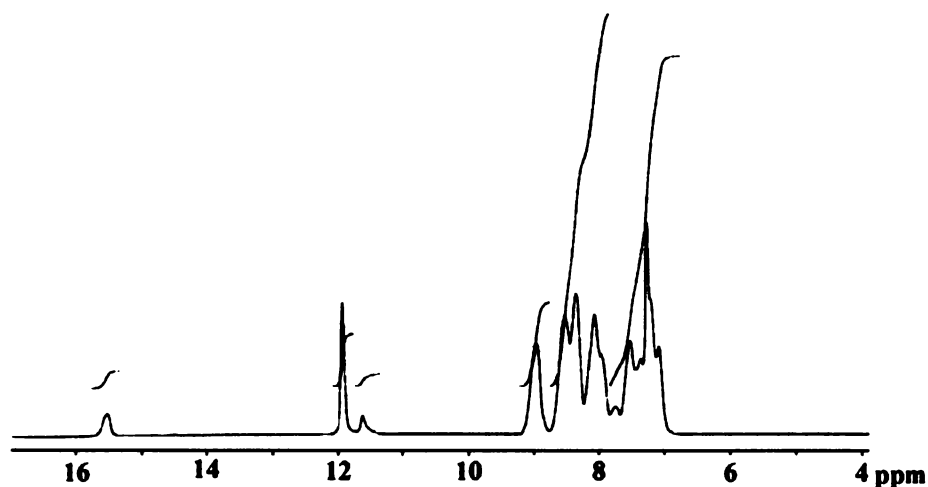


Fig. 2.12. ¹H NMR spectrum of HL³

2.2.2b Electronic spectral studies

HL¹: The electronic spectrum of the ligand (Fig. 2.13) in ethanol solution (10^{-4} M) shows a band at 31340 cm^{-1} , which corresponds to $n \rightarrow \pi^*$ transition of the carbonyl group. The $\pi \rightarrow \pi^*$ transitions observed as a band and as a shoulder at 37040 and 46510 cm^{-1} are assigned for the aromatic rings and azomethine moiety respectively.

H₂L²: The $n \rightarrow \pi^*$ and $\pi \rightarrow \pi^*$ transitions are observed as a band and as a shoulder at 30580 and 35460 cm^{-1} .

HL³: The spectrum recorded for a 10^{-4} M ethanol solution of the ligand consists of a shoulder at 31440 cm^{-1} , which corresponds to the $n \rightarrow \pi^*$ transition. The $\pi \rightarrow \pi^*$ transition was observed at 33780 cm^{-1} .

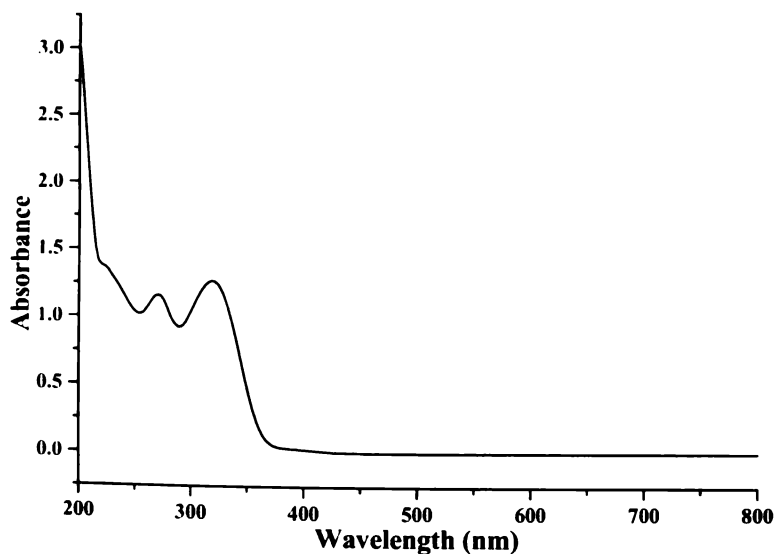


Fig. 2.13 Electronic spectrum of the ligand HL¹

2.2.2c IR spectral studies

HL¹: IR spectral analysis confirms the presence of characteristic groups present in the compound. The band at 1683 cm^{-1} confirms the existence of

carbonyl group in the keto form in solid state. The amide (II) band which occurs due to interaction between the N–H bending and the C–N stretching of the C–N–H group is found at 1537 cm^{-1} [43]. Splittings observed in this band may be due to the ring stretching vibrations. The C=N stretching band appears at 1579 cm^{-1} . The band at 3339 cm^{-1} is assigned for the NH stretching frequency. Aromatic C–H stretching bands occur in the region 3057 cm^{-1} . Carbon to carbon stretching vibrations within the ring occurs at 1463 cm^{-1} .

H₂L²: The bands at 3318 and 3197 cm^{-1} are assigned to O–H and N–H stretching frequencies. The carbonyl and azomethine absorptions are observed at 1620 and 1590 cm^{-1} respectively. The band at 1537 cm^{-1} corresponds to amide II band. The strong peak observed at 1327 cm^{-1} is assigned to phenolic C–O stretch. The bands in the range $1570 - 1325\text{ cm}^{-1}$ are difficult to assign due to crowding of bands.

HL³: In the IR spectrum of the ligand HL³, it is seen that the conjugation of the –C=O group with the adjacent heteroaromatic ring results in its absorption at 1669 cm^{-1} . The azomethine band is assigned at 1595 cm^{-1} . The broad band observed at 2987 cm^{-1} may be due to the aldehydic –C–H stretch, which also consists of a shoulder at 2843 cm^{-1} due to the first overtone of aldehydic –C–H bending. The amide II band is observed at 1565 cm^{-1} . The other bands observed in the range $1466 - 1293\text{ cm}^{-1}$ can be attributed to the heteroaromatic rings, which undergo significant alterations upon complexation.

Table 2.1.
Crystal data and structure refinement for HL¹ and H₂L²

Parameters	HL ¹	H ₂ L ²
Empirical formula	C ₁₈ H ₁₄ N ₄ O	C ₁₉ H ₁₅ N ₃ O ₂
Formula weight	302.33	317.34
Crystal system	Triclinic	Monoclinic
Space group	<i>P</i> $\bar{1}$	<i>P</i> 2 ₁ / <i>n</i>
Unit cell dimensions		
a (Å)	8.4016(10)	9.1294(15)
b (Å)	8.6679(10)	12.081(2)
c (Å)	11.0260(13)	14.760(2)
α (°)	91.531(2)	90.00
β (°)	93.946(2)	99.095(3)
γ (°)	109.135(2)	90.00
Volume V (Å ³), Z	755.76(15), 2	1607.5(5), 4
Calculated density (ρ) (Mg m ⁻³)	1.329	1.311
Absorption coefficient μ (mm ⁻¹)	0.086	0.088
F (000)	316	664
Crystal size (mm)	0.45 x 0.32 x 0.30	0.22 x 0.18 x 0.16
θ range for data collection	1.85 - 28.27	2.19 - 28.21
Index ranges	-11 ≤ h ≤ 11, -11 ≤ k ≤ 11, 14 ≤ l ≤ 14	-11 ≤ h ≤ 11, -13 ≤ k ≤ 15, -19 ≤ l ≤ 14
Reflections collected / unique	6562 / 3419 [R(int) = 0.0154]	9483 / 3731 [R(int) = 0.0148]
Refinement method	Full-matrix least-squares on F^2	Full-matrix least-squares on F^2
Data / restraints / parameters	3419 / 0 / 212	3731 / 0 / 222
Goodness-of-fit on F^2	1.066	1.052
Final R indices [$I > 2\sigma(I)$]	R1 = 0.0460, wR2 = 0.1344	R1 = 0.0428, wR2 = 0.1125
R indices (all data)	R1 = 0.0523, wR2 = 0.1397	R1 = 0.0520, wR2 = 0.1192

Table 2.2.
Crystal data and structure refinement for $\text{HL}^3 \cdot 2\text{H}_2\text{O}$

Parameters	$\text{HL}^3 \cdot 2\text{H}_2\text{O}$
Empirical formula	$\text{C}_{12}\text{H}_{14}\text{N}_4\text{O}_3$
Formula weight	262.27
Crystal system	Triclinic
Space group	$P\bar{1}$
Unit cell dimensions	6.4181(10)
a (Å)	8.0026(12)
b (Å)	12.934(2)
c (Å)	87.708(3)
α (°)	76.433(3)
β (°)	80.705(3)
γ (°)	
Volume V (Å ³), Z	637.31(17), 2
Calculated density (ρ) (Mg m ⁻³)	1.367
Absorption coefficient μ (mm ⁻¹)	0.101
F (000)	276
Crystal size (mm)	0.46 x 0.36 x 0.30
θ range for data collection	3.04 - 28.26
Index ranges	$-8 \leq h \leq 8$, $-10 \leq k \leq 9$, $-15 \leq l \leq 16$
Reflections collected / unique	3723 / 2765 [R(int) = 0.0155]
Refinement method	Full-matrix least-squares on F^2
Data / restraints / parameters	2765 / 0 / 192
Goodness-of-fit on F^2	1.066
Final R indices [$I > 2\sigma(I)$]	R1 = 0.0523, wR2 = 0.1455
R indices (all data)	R1 = 0.0604, wR2 = 0.1611

Table. 2.3

Selected bond lengths (Å) and bond angles (°) of HL¹, H₂L², HL³·2H₂O

Bonds	HL¹	H₂L²	HL³·2H₂O
C6–N2	1.2924(15)	1.2956(15)	1.2665(19)
C13–O1	1.2158(15)	1.2239(15)	-
C7–O3	-	-	1.2274(17)
N2–N3	1.3681(13)	1.3658(14)	1.3805(17)
C13–N3	1.3578(16)	1.3616(15)	-
C7–N3	-	-	1.3484(19)
C5–C6	1.4925(16)	1.4883(17)	1.466(2)
C13–C14	1.5001(16)	1.4777(17)	-
C7–C8	-	-	1.496(2)
Bond angles			
C6–N2–N3	117.55(10)	118.50(10)	115.91(12)
N2–N3–C13	120.71(10)	118.94(10)	-
N2–N3–C7	-	-	118.38(12)
N3–C13–O1	124.55(11)	122.49(12)	-
N3–C7–O3	-	-	122.40(13)
C5–C6–N2	127.49(10)	126.94(11)	121.41(13)
N3–C13–C14	113.60(10)	115.07(10)	-
N3–C7–C8	-	-	116.78(12)

References

1. Q. Shi, L. Xu, J. Ji, Y. Li, R. Wang, Z. Zhou, R. Cao, M. Hong, A. S. C. Chan, *Inorg. Chem. Commun.* 7 (2004) 1254.
2. V. Razakantoanina, P. P. Nguyen Kim, G. Jaureguiberry, *Parasitol Res.* 86 (2000) 665.
3. R. E. Royer, L. M. Deck, T. J. V. Jagt, F. J. Martinez, R. G. Mills, S. Young, A. D. L. V. Jagt, *J. Med. Chem.* 38 (1995) 2427.
4. M. R. Flack, R. G. Pyle, N. Mullen, M. B. Lorenzo, Y. W. Wu, R. A. Knazek, B. C. Nusule, M. M. Reidenberg, *J. Clin. Endocrinol Metab.* 76 (1993) 1019.
5. R. Baumgrass, M. Weiwad, F. Edmann, *J. Biol. Chem.* 276 (2001) 47914.
6. P. J. E. Quintana, A. Peyster de, S. Klatzke, H. Park, *J. Toxicol Lett.* 117 (2000) 85.
7. S. Chandra, X. Sangeetika, *Spectrochim. Acta* 60A (2004) 147.
8. E. Fujita, B. S. Brunshwig, T. Ogata, S. Yanagida, *Coord. Chem. Rev.* 132 (1994) 195.
9. E. Kimura, S. Wada, M. Shiyonoya, Y. Okazaki, *Inorg. Chem.* 33 (1994) 770.
10. B. De Clercq, F. Verpoort, *Macromolecules* 35 (2002) 8943.
11. T. Opstal, F. Verpoort, *Angew. Chem. Int. Ed.* 42 (2003) 2876.
12. B. De Clercq, F. Lefebvre, F. Verpoort, *Appl. Catal. A* 247 (2003) 345.
13. S. L. Lambert, C. L. Spiro, R. R. Gagne, D. N. Hendrickson, *Inorg. Chem.* 21 (1982) 68.
14. M. F. Iskander, L. Sayed, A. F. M. Hefny, S. E. Zayan, *J. Inorg. Nucl. Chem.* 38 (1976) 2209.
15. G. H. Havanur, V. B. Mahale, *Indian J. Chem.* 26A (1987) 1063.
16. H. Adams, D. E. Fenton, G. Minardi, E. Mura, M. Angelo, *Inorg. Chem. Commun.* 3 (2000) 4.
17. Z. Y. Yang, R. D. Yang, F. S. Li, K. B. Yu, *Polyhedron* 19 (2000) 2599.

18. S. S. Katiyar, S. N. Tandon, *Talanta* 11 (1964) 892.
19. G. S. Vasilikiotis, J. A. Tossidis, *J. Microchem.* 14 (1969) 380.
20. M. Gallego, M. G. Vargas, M. Valcarcel, *Analyst* 104 (1979) 613.
21. R. L. Dutta and M. M. Hossain, *J. Sci. Ind. Res.* 44 (1985) 635.
22. M. L. Vitolo, J. Webb, *J. Inorg Biochem.* 20 (1984) 255.
23. E. Baker, M. L. Vitolo, J. Webb, *Biochim. Pharmacol* 34 (1985) 3011.
24. P. Ponka, D. Richardson, E. Baker, H. M. Schulman, J. T. Edward, *Biochim, Biophys. Acta* 967 (1988) 122.
25. E. W. Ainscough, A. M. Brodie, S. L. Ingham and J. M. Waters, *Inorg. Chim. Acta* 249 (1996) 47.
26. D. Demertzi, D. Nicholls, K. Tracey, *Inorg. Chim. Acta* 85 (1984) 143.
27. S. C. Shao, Z. L. You, L. L. Tang, Y. S. Lin, H. L. Zhu, *Acta Cryst. E60* (2004) o2185.
28. J. E. Going, C. Sykora, *Anal. Chim. Acta* 70 (1974) 127.
29. D. Demertzi, D. Nicholls *Inorg. Chim. Acta* 73 (1983) 37.
30. P. Domiano, C. Pellizzi, G. Predieri, *Polyhedron* 3 (1984) 281.
31. M. R. Maurya, S. Khurana, W. Zhang, D. Rehder, *J. Chem. Soc. Dalton Trans.* (2002) 3015.
32. C. M. Armstrong, P. V. Bernhardt, P. Chin, Des R. Richardson, *Eur. J. Inorg. Chem.* (2003) 1145.
33. P. R. Mandik, A. S. Aswar, *Polish J. Chem.* 77 (2003) 129.
34. R. C. Maurya, P. Patel, D. Sutradhar, *Synth. React. Inorg. Met.-Org. Chem* 33 (2003) 1857.
35. D. Sriram, P. Yogeeswari, K. Madhu, *Bioorg. Med. Chem. Lett.* 15 (205) 4502.
36. C. Y. Duan, Z. L. Lu, D. H. Wu, X. Z. You, *Transition Met. Chem.* 23 (1998) 631.
37. Z. H. Chohan, A. Rauf, S. Noreen, A. Scozzafava, C. T. Supuran, *J. Enzy. Inhib. Med. Chem.* 17 (2002) 101.
38. M. R. Maurya, S. Agarwal, C. Bader, M. Ebel, D. Rehder, *J. Chem. Soc.*

- Dalton Trans. (2005) 537.
39. T. D. Harris, M. Sworin, N. Williams, M. Rajopadhye, P. R. Damphousse, D. Glowacka, M. J. Poirier, K. Yu, *Bioconjugate Chem.* 10 (1999) 808.
 40. A. Lyubchova, A. C. Barbi, J. P. Doucet, *Acta Cryst. C*51 (1995) 1893.
 41. S. S. S. Raj, H. -K. Fun, Z. L. Lu, W. Xiao, Y. X. Tong, B. S. Kang, *Acta Cryst. C*55 (1999) 942.
 42. S. Sen, P. Talukder, G. Rosair, S. Mitra, *Struct. Chem.* 16 (2005) 605.
 43. R. M. Silverstein, G. C. Bassler, T. C. Morrill, *Spectrometric Identification of Organic Compounds*, fourth ed., Wiley, New York, 1981.

Syntheses, structural and spectral studies of some Cu(II) complexes of terdentate NNO donor heteroaroylhydrazone ligands

Copper is a bioelement and an active site in several metalloenzymes and proteins [1-4]. The most important contribution to copper chemistry must be the role that biological copper [5-8] has played in stimulating research in the inorganic chemistry of copper, not only in the chemistry of copper proteins, for which Cu(I), Cu(II) and Cu(III) species are relevant, but also in systems where more than one type of Cu is considered present. The blue copper proteins have received considerable interest because of their unusual spectral and structural properties. The geometry around copper in blue copper proteins is intermediate between tetrahedral and square planar. Several model systems, including those with bidentate Schiff base ligands, have been reported correlating the molecular structure with the electronic ground state of those complexes [9-11]. The Cu atom switches between the Cu(I) and Cu(II) states [12, 13] in redox reactions involving copper containing enzymes. This is an essential factor for many of the properties of these enzymes.

Another interesting aspect of copper(II) coordination complexes is their biological activity, which is of interest in pharmacology. Schiff base Cu(II) complexes especially of thiosemicarbazones present a great variety of biological activity ranging from antitumoral [14, 15], fungicide [16], bactericide [17] and anti-inflammatory [18]. Coming to aroylhydrazones, the discovery that salicylaldehyde benzoylhydrazone inhibits DNA synthesis and cell growth [19, 20] led to their investigation of metal complexes. Surprisingly the Cu(II) complex was shown to be significantly more potent than the metal free chelate, leading to

the suggestion that the metal complex was the biologically active species. Because of the biological interest in this type of chelate system, several structural studies have been carried out on copper with this ligand and analogues [21-25]. Acylhydrazones of salicylaldehyde subsequently attracted attention. Salicylaldehyde acetylhydrazone displays radioprotective properties, and a range of acylhydrazones has been shown to be cytotoxic, the Cu complexes again showing enhanced activity.

3.1. Stereochemistry

The Cu(II) ion with $3d^9$ outer electron configuration lacks cubic symmetry and hence exhibits distorted forms of the basic stereochemistries such as tetrahedral, square planar, square pyramidal and octahedral [26]. Coordination numbers of four, five and six predominate, but variations of each structure occur through bond length or bond angle distortions. Jahn Teller effect plays a major role in deciding the distortion effect of stereochemistries of Cu(II) complexes. The typical distortion involved in octahedral geometry is elongated structures with the odd electron residing in the $d_{x^2-y^2}$ orbital resulting in four short Cu-L bonds and two trans long bonds, which are usually more energetically favorable than the compressed structures, consistent with their more frequent occurrence.

3.2. Experimental

3.2.1 Materials

Nicotinoylhydrazide (Sigma Aldrich), 4-hydroxybenzhydrazide (Fluka), 2-benzoylpyridine (Sigma Aldrich), pyridine-2-carbaldehyde (Sigma Aldrich), $\text{Cu}(\text{OAc})_2 \cdot \text{H}_2\text{O}$ (Qualigens), $\text{CuSO}_4 \cdot 5\text{H}_2\text{O}$ (Merck), CuBr_2 (Merck), $\text{CuCl}_2 \cdot 2\text{H}_2\text{O}$ (Merck), NaN_3 (Reidel-De Haen), 2,2'-bipyridyl (CDH) and DMF (S.D. Fine) were used as received. When ethyl alcohol was used as the solvent repeated distillation was carried out before use.

3.2.2 Syntheses of ligands

Preparation of the ligands HL¹, H₂L² and HL³ were done as described previously in Chapter 2.

3.2.3 Preparation of copper(II) complexes

[Cu(HL¹)Cl₂]₂·6H₂O (1): To an ethanolic solution of HL¹ (0.302 g, 1 mmol), CuCl₂·2H₂O (0.170 g, 1 mmol) dissolved in ethanol was added. The resulting green colored solution was stirred for 3 hours. The green product obtained was filtered, washed with ethanol followed by ether and dried over P₄O₁₀ *in vacuo*. Yield: 0.305 g (62.1%). Elemental Anal. Found (Calcd.) (%): C, 43.81 (44.05); H, 3.42 (4.11); N, 11.58 (11.41). $\mu = 1.97$ BM.

[Cu(L¹)₂] (2): Cu(OAc)₂·H₂O (0.199 g, 1 mmol) dissolved in ethanol was added to an ethanolic solution of HL¹ (0.302 g, 1 mmol) and stirred for 10 min. Then 2,2'-bipyridyl (0.156 g, 1 mmol) dissolved in ethanol was added and further stirred for 5-6 hours. The resulting deep green solution was then concentrated on a water bath and cooled at room temperature, filtered and kept overnight. Black shining crystals separated out, which were filtered, washed with ether and dried over P₄O₁₀ *in vacuo*. Yield: 0.355 g (53.2%). Elemental Anal. Found (Calcd.) (%): C, 64.40(64.90); H, 3.53 (3.93); N, 16.56 (16.82). $\mu = 1.77$ BM.

[Cu(HL²)Cl] (3): Solutions of H₂L² (0.317 g, 1 mmol) in DMF and CuCl₂·2H₂O (0.170 g, 1 mmol) in ethanol were mixed to obtain a dark brown solution. After 3 hours of stirring, the green product separated out was filtered, washed with ethanol followed by ether and dried over P₄O₁₀ *in vacuo*. Yield: 0.281 g (67.6%). Elemental Anal. Found (Calcd.) (%): C, 55.75 (54.94); H, 3.49 (3.40); N, 10.37 (10.12). $\mu = 1.69$ BM.

[Cu(HL²)N₃] (4): Cu(OAc)₂·H₂O (0.199 g, 1 mmol) dissolved in ethanol was added to a solution of H₂L² (0.317 g, 1 mmol) in DMF and stirred for 10 min. Aqueous solution of NaN₃ (0.0651 g, 1 mmol) was then added to the solution

followed by a further stirring of 3-4 hours. The green product formed was separated, washed with ethanol followed by ether and dried over P_4O_{10} *in vacuo*. Yield: 0.279 g (66.2%). Elemental Anal. Found (Calcd.) (%): C, 53.60 (54.09); H, 3.34 (3.39); N, 19.51 (19.92). $\mu = 1.75$ BM.

[Cu(HL²)₂] (5): To a solution of H_2L^2 (0.317 g, 1 mmol) in DMF, $CuSO_4 \cdot 5H_2O$ (0.249 g, 1 mmol) in water was added and stirred for 5-6 hours. The dark brown solution was left overnight. The black product separated out was collected, washed with ethanol followed by ether and dried over P_4O_{10} *in vacuo*. Yield: 0.034 g, (49.2%). Elemental Anal. Found (Calcd.) (%): C, 65.20 (65.56); H, 4.01 (4.05); N, 12.50 (12.07). $\mu = 1.94$ BM.

[Cu(L³)Cl] (6): $CuCl_2 \cdot 2H_2O$ (0.170 g, 1 mmol) in ethanol was added to HL^3 (0.262 g, 1 mmol), dissolved in ethanol by stirring. Formation of green precipitate was spontaneous, so stirring continued only for 2 hours. The product was filtered, washed with ethanol followed by ether and dried over P_4O_{10} *in vacuo*. Yield: 0.453 g (67.9%). Elemental Anal. Found (Calcd.) (%): C, 42.91 (43.25); H, 2.76 (3.02); N, 16.72 (16.81). $\mu = 1.86$ BM.

[Cu(HL³)Br]Br (7): HL^3 (0.262 g, 1 mmol) was dissolved in ethanol and stirred with a solution of $CuBr_2$ (0.223 g, 1 mmol) in ethanol for 2 hours. The green product immediately formed was separated, washed with ethanol followed by ether and dried over P_4O_{10} *in vacuo*. Yield: 0.294 g (65.4%). Elemental Anal. Found (Calcd.) (%): C, 32.73 (32.06); H, 2.14 (2.24); N, 12.60 (12.46). $\mu = 1.58$ BM.

[Cu(L³)₂]·H₂O (8): $Cu(OAc)_2 \cdot H_2O$ (0.199 g, 1 mmol) dissolved in ethanol was added to an ethanolic solution of HL^3 (0.262 g, 1 mmol) and stirred for 10 min. Then 2,2'-bipyridyl (0.156 g, 1 mmol) dissolved in ethanol was added and further stirred for 4-5 hours. The resulting dark brown solution was then concentrated on a water bath and then cooled. The solution was then cooled at room temperature, filtered and kept overnight. Dark brown shining crystals

separated out, which were filtered, washed with ether and dried over P_4O_{10} *in vacuo*. Yield: 0.273 g (51.3%). Elemental Anal. Found (Calcd.) (%): C, 54.34 (54.18); H, 3.61 (3.79); N, 20.78 (21.06). $\mu = 1.84$ BM.

Caution! Azide salts of metal complexes with organic ligands are potentially explosive. So they should be prepared and handled carefully.

3.3. Results and discussion

Reaction of equimolar ratios of corresponding ligands and metal salts yielded the metal complexes under neutral conditions. However, the reactions done with the addition of heterocyclic bases so as to incorporate them resulted in metal complexes with ligand to metal ratio 2:1. Such attempts to incorporate heterocyclic bases are reported earlier [23, 27-32] in case of 2-hydroxyl substituted ligands, yielding successfully monomeric coordination compounds with and without heterocyclic bases as donors and also dimeric metal complexes with oxo bridging. In the present case, absence of hydroxyl group in the ligands may be a reason for the lack of such compounds and also the presence of an effective chelating species with more potential sites than the base led to the formation of $M(L)_2$ complexes under conditions in which the reactants are chosen in ratio of 1:1:1. Thus the monobasic ligands are deprotonated under neutral conditions itself, coordinating through enolic oxygen except in some cases. That may be due to the peculiarity of the metal salt chosen, with two anions of the metal salt satisfying the copper(II) valency. In such cases, the carbonyl oxygen may coordinate or not, it depends. Though attempts to prepare heterocyclic base adducts of the complex were unsuccessful, metathetical displacement of anions of the metal salt was possible by replacing them with azide anion.

The complexes prepared were either green or dark brown in color. All the complexes were found to be soluble in DMF and DMSO, but only partially soluble in other organic solvents such as $CHCl_3$, ethanol, methanol etc. The magnetic susceptibility measurements obtained in the range of 1.5 – 1.9 BM were in accordance with the presence of an unpaired electron.

3.3.1 Crystal structures of $[\text{Cu}(\text{L}^1)_2]$, $[\text{Cu}(\text{HL}^2)_2]\cdot\text{H}_2\text{O}\cdot\text{DMF}$ and $[\text{Cu}(\text{L}^3)_2]\cdot\text{H}_2\text{O}$

$[\text{Cu}(\text{L}^1)_2]$: The structure of $[\text{Cu}(\text{L}^1)_2]$ (Fig. 3.1) consists of two trifunctional Schiff base ligands, in which the Cu(II) ion is located on the pseudo twofold symmetry axis. The structural refinement parameters are given in Table 3.1 and the selected bond distances and bond angles are given in Tables 3.3 and 3.4. Two molecules of the terdentate ligand bind to the Cu(II) ion to form four five-membered chelate rings [1. Cu–N(1)–C(5)–C(6)–N(2), 2. Cu–N(2)–N(3)–C(13)–O(1), 3. Cu–N(5)–C(23)–C(24)–N(6), 4. Cu–N(6)–N(7)–C(31)–O(2)]. Due to Jahn-Teller effect and also due to non-equivalent nature of the donor atoms, there are considerable variations in bond lengths. So the plane defined by the two azomethine nitrogens, one pyridine ring nitrogen and by the enolate oxygen is chosen as the basal plane of the Cu(II) distorted octahedron. The remaining pyridine ring nitrogen and the enolate oxygen of the second ligand occupy the apical positions.

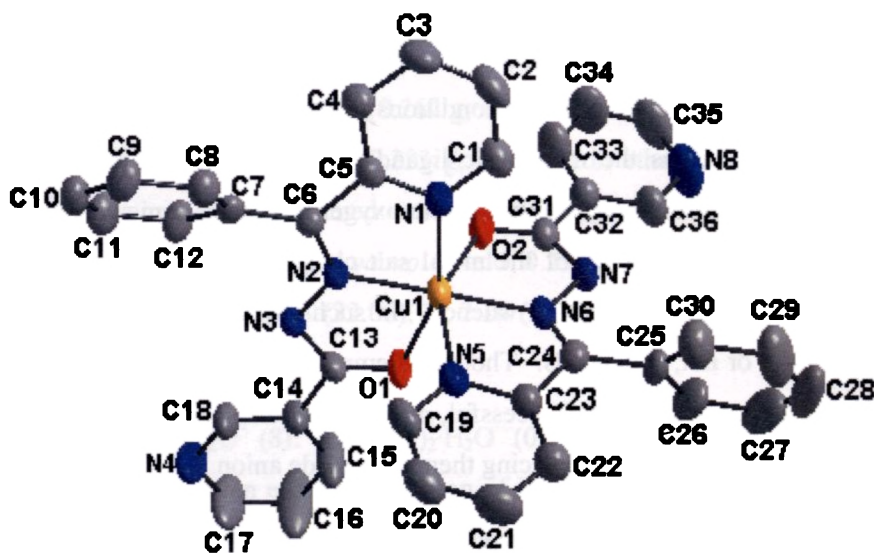


Fig. 3.1. Molecular structure of $[\text{Cu}(\text{L}^1)_2]$. Hydrogen atoms are omitted for clarity

The binding angles (Table 3.4) at the Cu(II) centre show large deviations from the ideal octahedral values of 90° and 180° . The mean deviation of plane N(2)–O(1)–N(6)–N(1) from the least square plane is 0.0719 \AA , with the Cu(II) ion dispositioned from the plane by 0.0163 \AA . The dihedral angle separation of 2.88° between the chelate rings 1 and 2 and 2.13° for rings 3 and 4 suggest that the ligating centers of the ligand are almost planar.

It is well clear from the figure that, the configuration along the C6–N2 bond is *trans*, suggesting that the ligand has undergone a rotation along this bond so has to make an effective coordination through the three donor atoms N, N, and O. The torsion angle N(3)–N(2)–C(6)–C(5) $-177.8(5)$ observed, evidences this rotation. The average bond distances for each of Cu–O and Cu–N in this coordination geometry are 2.14 and 2.07 respectively. The observed distances of $2.067(5) \text{ \AA}$ and $2.305(5) \text{ \AA}$ corresponding to Cu–N(1) and Cu–N(5) are slightly longer than $1.952(4) \text{ \AA}$, $1.983(4) \text{ \AA}$ of Cu–N(2) and Cu–N(6) bonds, which can be related to greater *trans* influence of the oxo group on the each Cu–N(1) and Cu–N(5) bonds. The relatively short C(13)–N(3) and C(31)–N(7) bond distances of $1.323(6) \text{ \AA}$ and $1.348(7) \text{ \AA}$ (normal single bond is 1.52 \AA) [33], coupled with the lengthened C(13)–O(1) and C(31)–O(2) distances of $1.272(6) \text{ \AA}$ and $1.245(6) \text{ \AA}$ (ketonic linkage 1.23 \AA) [25], indicate that the ligands bind in the enolate form.

The packing diagram of the compound is given in Fig. 3.2. The repeating unit consists of a set of two molecules aligned in a zig-zag manner to the neighboring set. Although some π – π interactions are found, they are observed at distances greater than 3.8 \AA . So the main interaction among the molecules may be the weak van der Waals forces. Some of the weak C–H--- π interactions worth quoting are the following: C(1)–(H)---Cg(2)ⁱ [Cg(2): Cu(1), O(2), C(31), N(7), N(6); $d_{C(1)\text{---}Cg} = 3.1175 \text{ \AA}$; $i = x, y, z$]; C(9)–H(9)---Cg(1)ⁱⁱ [Cg(1): Cu(1), O(1), C(13), N(3), N(2); $d_{C(9)\text{---}Cg} = 3.5815 \text{ \AA}$; $ii = 1-x, 1/2+y, 1-z$].

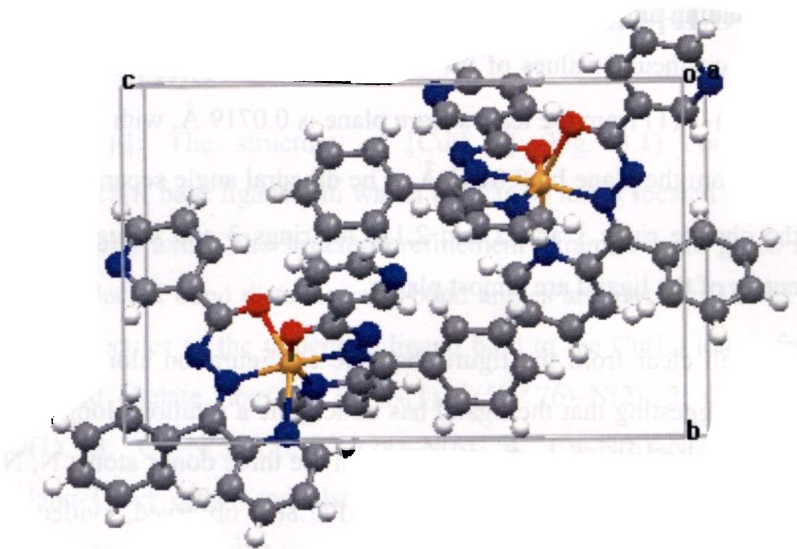


Fig. 3.2. Packing diagram of $[\text{Cu}(\text{L}^1)_2]$

$[\text{Cu}(\text{HL}^2)_2] \cdot \text{H}_2\text{O} \cdot \text{DMF}$: Wine red colored plate shaped crystals of the compound suitable for analysis were grown from a solution of the compound dissolved in a mixture of ethanol and DMF (1:1 v/v). The structural refinement parameters are given in Table 3.1 and the selected bond distances and bond angles are given in Tables 3.3 and 3.4. The molecular structure (Fig. 3.3) found is similar to that of the $[\text{Cu}(\text{L}^1)_2]$ discussed above. Comparing with the above-discussed crystal, the present compound also crystallized into monoclinic lattice, but with $P2_1/n$ space group. The compound crystallized with two solvent molecules, one each of water and DMF. The basic skeleton of the complex is mononuclear, consisting of two equivalents of the tridentate ligand. The coordination geometry of the central copper(II) ion can be described as distorted octahedral. The N_3O core constructs the square plane and the O(1) and N(1) atoms of the ligand occupy the axial positions. The bond distances suggest a Jahn-Teller elongation of the molecule, resulting in two long bonds and four short bonds.

Only the *trans* angle created by the azomethine nitrogens, N(5)–Cu(1)–N(2), $175.59(12)^\circ$ approach that of a regular octahedron. The other *trans* angles

O(3)–Cu(1)–N(4), 158.34(11)°, O(1)–Cu(1)–N(1), 149.37(10)° and the remaining bite angles indicate that the molecule considerably deviates from the regular octahedral bond angles of 180° and 90°. The copper atom is displaced from the square plane constituted by the atoms N(2), N(4), N(5), O(3) by 0.0053 Å. Though the ligands are similar, the binding of the donor atoms to the central Cu(II) ion is different, while taking into consideration the dihedral angle separation of the chelate rings formed by the two ligands. The dihedral angle separation of chelate rings [1. Cu(1)–N(1)–C(5)–C(6)–N(2), 2. Cu(1)–N(2)–N(3)–C(13)–O(1) 3. Cu(1)–N(4)–C(24)–C(25)–N(5) and 4. Cu(1)–N(5)–N(6)–C(32)–O(3)] 8.36° (rings 1 and 2) and 1.87° (rings 3 and 4) indicate that the donor atoms of the second ligand are nearly planar compared to that of the first ligand resulting in a meridional coordination around the copper atom. The lengthening of the C(13)–O(1) bond as a result of coordination is lesser in the present compound, compared to the [Cu(L¹)₂] crystal.

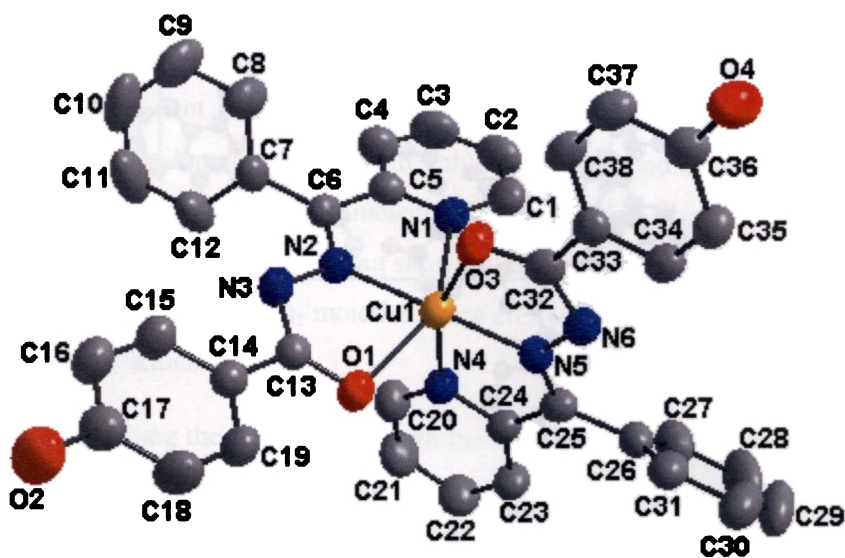


Fig. 3.3. Molecular structure of [Cu(HL²)₂]·H₂O·DMF. The ellipsoids are drawn at 50% probability. Hydrogen atoms and solvent molecules are omitted for clarity

The partial packing diagram of the compound is given in Fig. 3.4. Though π - π interactions exist in the lattice, they are observed at distances greater than 4.0 Å. Hence they contribute little towards the effective packing of the molecules in the lattice. However, some C-H \cdots π interactions, which are rather short are observed. They are C(23)-H(23) \cdots Cg(5)ⁱ [Cg(5): N(1), C(1), C(2), C(3), C(4), C(5); $d_{\text{C(23)}-\text{Cg}} = 3.4341$ Å; $i = 1/2+x, 1/2-y, 1/2+z$] and C(39)-H(39B) \cdots Cg(8)ⁱ [Cg(8): C(14), C(15), C(16), C(17), C(18), C(19); $d_{\text{C(39)}-\text{Cg}} = 3.6854$ Å; $i = 1/2-x, 1/2+y, 1/2-z$]. The presence of the water molecule and the DMF molecule leads to an extensive packing interconnecting the adjacent layers. The intramolecular and intermolecular hydrogen bonding interactions found are listed in Table 3.6.

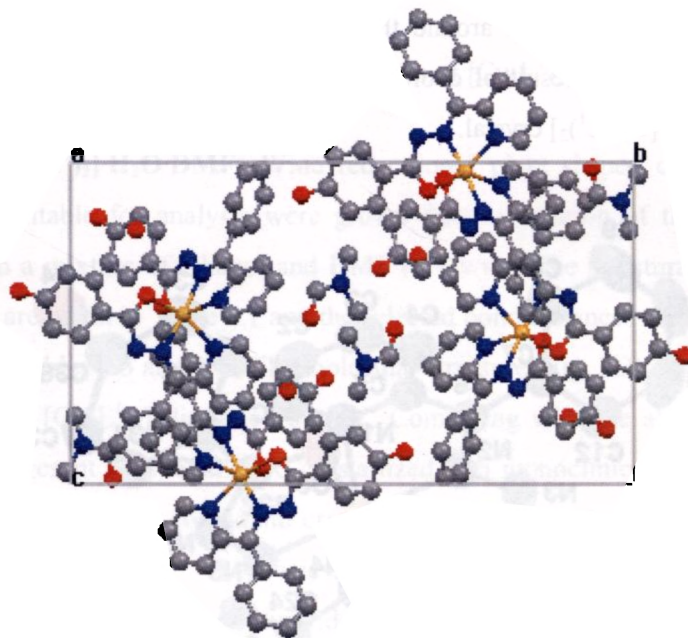


Fig. 3.4. Packing diagram of $[\text{Cu}(\text{HL}^2)]_2 \cdot \text{H}_2\text{O} \cdot \text{DMF}$

[Cu(L³)₂].H₂O: Block shaped black colored single crystals suitable for X-ray diffraction of the compound Cu(L³)₂ were grown by room temperature slow evaporation of a 1:1 solution of the complex in ethanol and DMF (1:1 v/v) mixture. There are two crystallographically independent molecules in the

asymmetric unit of $[\text{Cu}(\text{L}^3)_2]\cdot\text{H}_2\text{O}$ (Fig. 3.5) arranged in an offset fashion. The lattice nature is triclinic with $P\bar{1}$ symmetry. There are four molecules per unit cell and the compound crystallized with one water molecule.

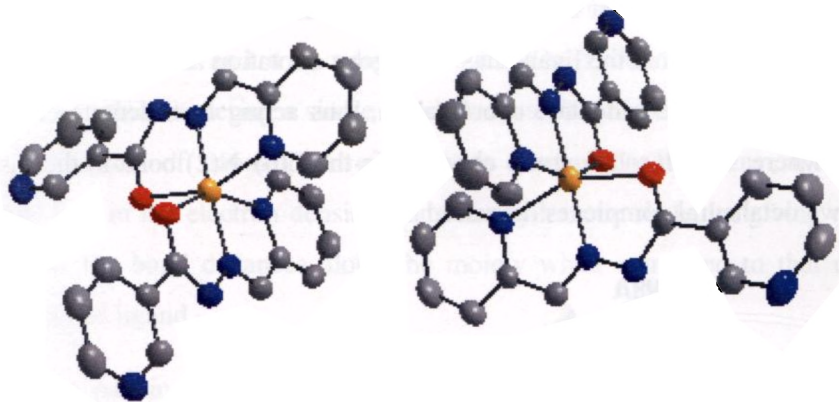


Fig. 3.5. Molecular structure of the compound $[\text{Cu}(\text{L}^3)_2]\cdot\text{H}_2\text{O}$. Hydrogen atoms and water molecules are omitted for clarity

The molecule with the atom numbering scheme is given in Fig. 3.6. The structural refinement parameters are given in Table 3.2 and the selected bond distances and bond angles are given in Table 3.5. The bonding parameters in the crystallographically independent molecules in the asymmetric lattice show only minor variations in bond lengths, but shows considerable variation in bond angles. In addition to the two $\text{Cu}(\text{L}^3)_2$ moieties, there are two solvent molecules, two each of water in the lattice.

Comparing the bond lengths with the other two crystals, it is of interest to note that the present Cu(II) ion has undergone a slight compression. Thus a tetragonally compressed distorted octahedral geometry is observed around each metal center with atoms N(1), O(1), N(5) and O(2) constituting the equatorial plane while the atoms N(2) and N(6) occupying the axial position. The coordination occurs through the azomethine nitrogen, pyridyl nitrogen and enolate oxygen of two ligand moieties and hence a six coordinate environment is present

about the metal center. The central hydrazone core in the present Cu(II) complex, shows an *EZ* conformation about the C(6)–N(2) and C(7)–N(3) bonds, similar to that of the free ligand, which reveals that no rotation has occurred about the azomethine bond for coordination. The O(1)–C(7)–N(3)–N(2) torsion angle value of 3.21° also evidences that the O(1) atom is positioned *cis* to the N(2) atom. But it should be noticed that the ligand has undergone a rotation around the C(5)–C(6) bond for an effective tridentate coordination, thus acting as tridentate chelating species whereas, such rotation was observed in the C(6)–N(2) bond in the case of other two octahedral complexes discussed above.

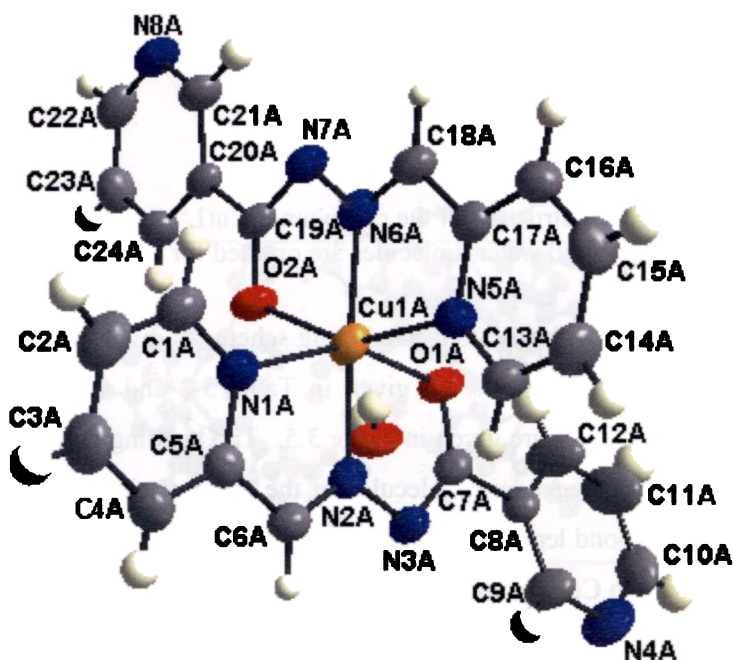


Fig. 3.6. Molecular structure of one independent molecule $[\text{Cu}(\text{L}^3)_2]\cdot\text{H}_2\text{O}$ in the asymmetric unit with the atom numbering scheme.

The molecule consists of two main fragments, viz., two hydrazone ligand moieties. They bind the central Cu(II) atom in such a way that they are almost perpendicular to each other, as revealed from the dihedral angle value of 86.35° of the plane defined by atoms C(6), N(2), N(3), C(7), C(8) and O(1) with the

corresponding plane of C(18), N(6), N(7), C(19), C(20) and O(2). The bite angles N(2)–Cu(1)–O(1) 76.17(7)°, N(5)–Cu(1)–O(1) 95.81(6)°, N(6)–Cu(1)–N(5) 78.04(7)°, N(6)–Cu(1)–O(2) 75.99(6)°, O(2)–Cu(1)–N(1) 92.25(6)°, N(1)–Cu(1)–N(2) 77.58(7)° reveal the distorted octahedral geometry. The C(7)–O(1) bond, lengthens by 0.036 Å upon coordination to the Cu(II) atom. The free ligand exists as the keto tautomer and it coordinates to the Cu(II) ion in the deprotonated enolate form, thus rendering a single bond character for the C–O bond. Similarly the coordination of azomethine nitrogen to central Cu(II) ion results in a redistribution in the electron density along the hydrazone skeleton, giving rise to changes in the bond distances along the moiety when compared to that of the uncoordinated ligand.

The packing of molecules of the compound is shown in Fig. 3.7. The basic unit of crystal packing consists of six molecules, which are three sets, each consisting of two individual molecules arranged in an offset fashion in the asymmetric unit. This whole unit repeats one dimensionally in the lattice. The repeating unit in the crystal lattice is shown in Fig. 3.8. The presence of water molecules in the crystal lattice leads to an extensive hydrogen bonding interaction that plays a pivotal role in the effective crystal packing. A list of hydrogen bonding interactions is listed in Table 3.6.

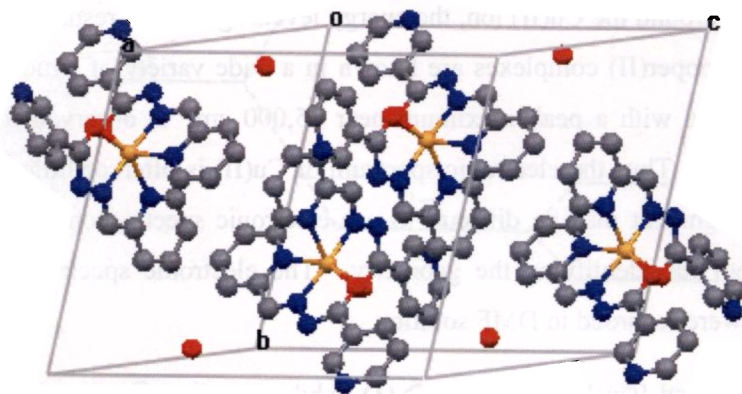


Fig. 3.7. Packing diagram of $[\text{Cu}(\text{L}^3)_2]\cdot\text{H}_2\text{O}$

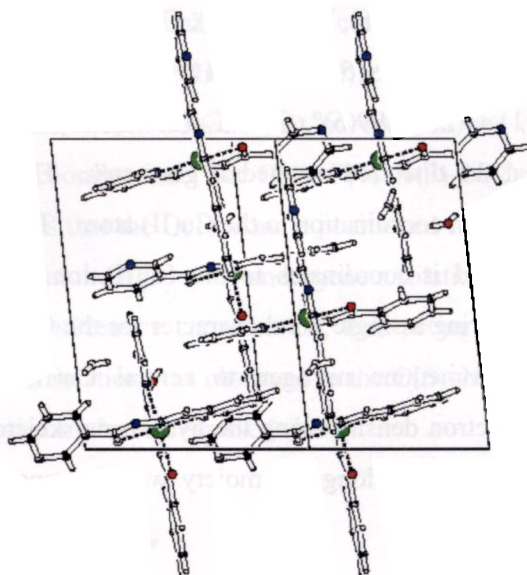


Fig. 3.8. The repeating unit in the lattice of $[\text{Cu}(\text{L}^3)_2]\cdot\text{H}_2\text{O}$

3.3.2 Spectral characteristics of Cu(II) complexes

3.3.2a Electronic spectral studies

The d^9 Cu^{2+} ion with a 2D ground state free ion term has an electron vacancy or hole in its d level and can be regarded as the inverse of a d^1 arrangement. So in an octahedral field, the ground state will be split into a lower 2E_g and upper $^2T_{2g}$ level [34]. But usually due to the lower symmetry of environments around the Cu(II) ion, the energy levels again split resulting in more transitions. Copper(II) complexes are known in a wide variety of structures. A very broad band with a peak maximum near $15,000\text{ cm}^{-1}$ is observed for most geometries [35]. Thus the electronic spectrum of Cu(II) is often of little value in structural assignment making difficult to use electronic spectroscopy alone as a definitive tool for identifying the geometry. The electronic spectra of all the compounds were recorded in DMF solution.

Compound $[\text{Cu}(\text{HL}^1)\text{Cl}_2]\cdot 6\text{H}_2\text{O}$ (**1**) exhibited a broad peak in the range $16000 - 12500\text{ cm}^{-1}$ characteristic of Cu^{2+} complex with a 2B_1 ground state [36]. So the transition is characteristic of a Cu(II) ion with the single electron residing

in the $d_{x^2-y^2}$ orbital. Due to broadness of the band, other two d-d transitions could not be assigned. The intense charge transfer band occurs at 24750 cm^{-1} . The complex has a shoulder at 33300 cm^{-1} corresponding to $n \rightarrow \pi^*$ transition. The $\pi \rightarrow \pi^*$ transitions are observed at 38170 and 40980 (sh) cm^{-1} .

Tetragonal distortion is usually assumed to be the most common example of Cu^{2+} coordination. The energy levels of an axially elongated octahedron are shown in Fig. 3.9. The ground state of $\text{Cu}(\text{II})$ ion in an elongated tetragonally distorted octahedral crystal field of D_{4h} symmetry may be described as a single electron in $d_{x^2-y^2}$ (b_{1g}) orbital, or a ${}^2B_{1g}$ state. In a tetragonal field, transitions expected are ${}^2B_{1g} \rightarrow {}^2A_{1g}$, ${}^2B_{1g} \rightarrow {}^2B_{2g}$ and ${}^2B_{1g} \rightarrow {}^2E_g$ and they occur in the range $12000 - 17000$, $15500 - 18000$ and $17000 - 20000\text{ cm}^{-1}$ respectively. Due to Jahn-Teller distortion, the axial ligands of the octahedron are farther away from the metal ion than the equatorial ligands. The absorption spectra of Cu^{2+} complexes broadened by geometrical distortion from octahedral symmetry may be further broadened by spin-orbit coupling.

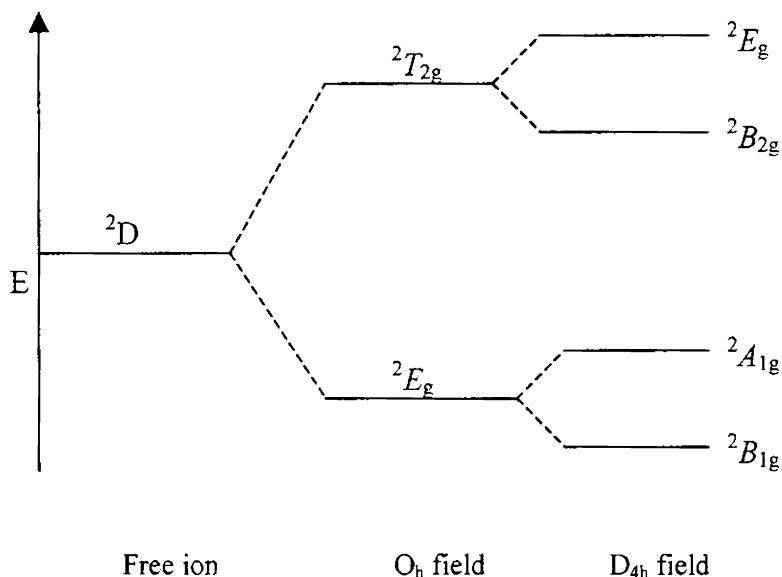
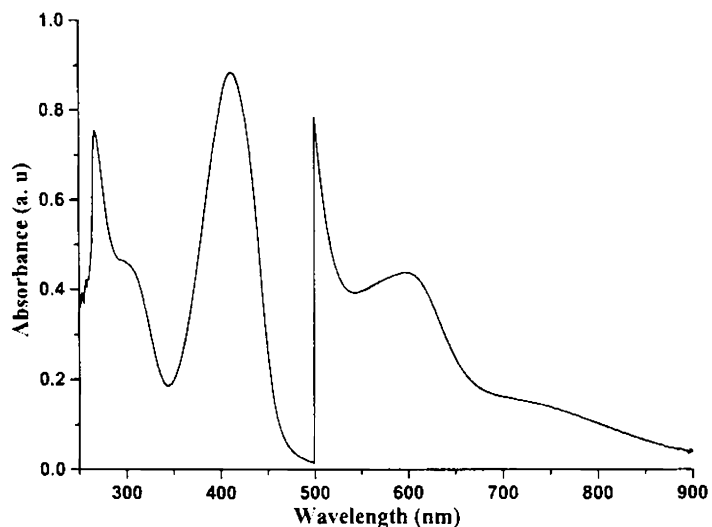


Fig. 3.9. Energy levels for axially elongated octahedral $\text{Cu}(\text{II})$ complexes

For the distorted octahedral compound $[\text{Cu}(\text{L}^1)_2]$ (**2**), the d-d band is observed at 14430 cm^{-1} . Due to the broadness of the band only one transition could be distinguished. The band at 25380 cm^{-1} corresponds to the charge transfer transition. The $n \rightarrow \pi^*$ and $\pi \rightarrow \pi^*$ transitions due to the ligand are viewed at 32470 (sh) and 38760 cm^{-1} respectively.

In the case of square planar complexes also three allowed d-d transitions are expected in the visible region as in the case of octahedral complexes, but often these theoretical expectations are unseen in practice and these bands usually appear overlapped due to the very small energy difference between the d levels. Compound $[\text{Cu}(\text{HL}^2)\text{Cl}]$ (**3**) exhibits (Fig. 3.10) bands at 13240 (sh) and 16640 cm^{-1} , similar to those reported for a copper(II) ion in square planar environments [37, 38]. The ligand to metal charge transfer band appeared at 24330 cm^{-1} . The ligand transitions in the complex are viewed at 32360 and 37310 cm^{-1} where as the free ligand exhibits these bands at 30581 and 35460 cm^{-1} .



*Fig. 3.10. Electronic spectrum of compound $[\text{Cu}(\text{HL}^2)\text{Cl}]$ (**3**)

* The spectrum showed is a combined one, recorded in two different concentrations

The d-d transition for $[\text{Cu}(\text{HL}^2)\text{N}_3]$ (4) is observed as a broad band at 15460 cm^{-1} . The charge transfer band was assigned at 24330 cm^{-1} and the ligand transitions at 32150 and 37450 cm^{-1} . In compound $[\text{Cu}(\text{HL}^2)_2]$ (5), d-d transitions are observed as weak shoulders at 14530 and 19760 cm^{-1} . Ligand to metal charge transfer band appeared at 22730 cm^{-1} and the ligand transitions at 31050 and 36630 cm^{-1} .

The four coordinated complex $[\text{Cu}(\text{L}^3)\text{Cl}]$ (6), exhibits the d-d transition as a broad band at 13480 cm^{-1} . Due to the broadness of the band, the other expected transitions in this range could not be assigned. The charge transfer band is observed in the visible range $23810 - 26950\text{ cm}^{-1}$. The ligand transitions are found in the range of $29410 - 34380\text{ cm}^{-1}$. The d-d electronic transition for the single electron in Cu^{2+} in compound $[\text{Cu}(\text{HL}^3)\text{Br}]\text{Br}$ (7) was observed as a broad band at 13300 cm^{-1} (Fig. 3.11). The charge transfer band consisted of a high intense peak at 26040 cm^{-1} with a shoulder at 24630 cm^{-1} . The ligand transitions are viewed at 34965 (sh) and 36900 cm^{-1} .

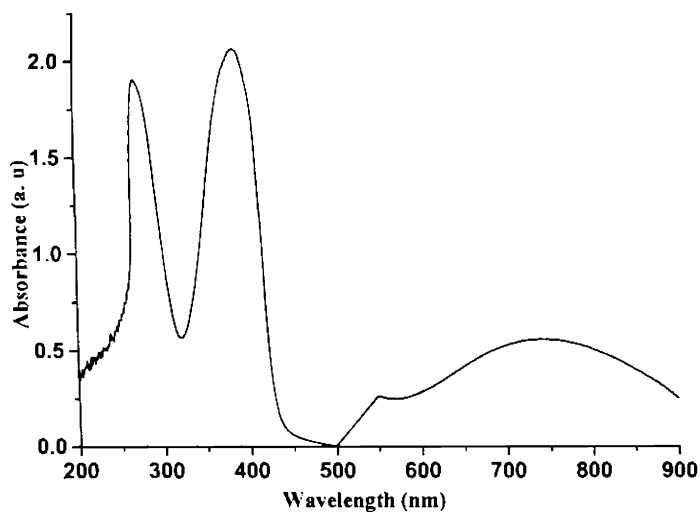


*Fig. 3.11. Electronic spectrum of compound $[\text{Cu}(\text{HL}^3)\text{Br}]\text{Br}$ (7)

* The spectrum showed is a combined one, recorded in two different concentrations

Compound $[\text{Cu}(\text{L}^3)_2]\cdot\text{H}_2\text{O}$ (**8**) also exhibited a broad band in the region $12500 - 125870 \text{ cm}^{-1}$ instead of three peaks expected for an octahedral complex. The charge transfer and the ligand transitions were found in the same region as observed in other complexes.

3.3.2b EPR spectral studies

EPR spectroscopy has been widely used in the study of complexes formed between metal ions and various ligands, both in frozen solution and liquid states, as it offers the potential to define local structure as well as provide information on the chemical reactions. The paramagnetism of the Cu(II) cation and the sensitivity of the spectral parameters to the stereochemistry of the surrounding ligands make EPR the most prolific spectroscopic technique for its study. Thus EPR spectroscopy has played a significant role in identifying the existence or otherwise of the compressed tetragonal or rhombic octahedral stereochemistry for the Cu(II) ion in its six coordinate complexes [39, 40].

The effective spin of the electron $s = 1/2$, associated with a spin angular momentum $m_s = +1/2$ leads to a doubly degenerate spin state for the d^9 Cu(II) ion, in the absence of magnetic field. In the presence of a magnetic field, this degeneracy is lifted resulting in an energy difference between these two states given as

$$E = h\nu = g\beta H$$

where h is Planck's constant, ν is the frequency, g is the Lande splitting factor, β is the electron Bohr magneton and H is the magnetic field. The factors that determine the type of ESR spectrum are:

- a) the nature of the electronic ground state
- b) the symmetry of the effective ligand-field about the copper(II) ion
- c) the mutual orientations of the local molecular axes of the separate copper(II) chromophores in the unit cell

The factors a and b deal with the mode of splitting of the five-fold degenerate 3d orbitals by crystal fields of octahedral and tetrahedral symmetries which are inverse of each other. The orbital sequences of the various stereochemistries determine their ground states. The vast majority of Cu(II) complexes give rise to orbitally non-degenerate ground states involving a static form of distortion and a $d_{x^2-y^2}$ ground state; a substantial number of complexes have a d_{z^2} ground state and a few have a d_{xy} ground state. It depends on the nature of the ligands regarding their π bonding potential. The third factor c, determines the amount of exchange coupling present, which is the major factor in reducing the amount of stereochemical information available from the EPR spectra [41].

The EPR spectra of the compounds **1-8** were recorded in the X-band frequency. The various magnetic interaction parameters are summarized in Table 3.7 for compounds **1-8**. Compound $[\text{Cu}(\text{HL}^1)\text{Cl}_2]_2 \cdot 6\text{H}_2\text{O}$ (**1**) in polycrystalline state at 298 K displayed a reverse axial spectrum with g_{\parallel} 1.99 and g_{\perp} 2.14. However, the frozen solution EPR spectrum (Fig. 3.12) of the compound in DMF at 77 K revealed a dimeric structure with $d_{x^2-y^2}$ ground state. At 77 K, the signal appears more resolved with $g_{\parallel} = 2.34$ and $g_{\perp} = 2.09$, corresponding to the pattern of Cu(II) ion in an elongated geometry, $g_{\parallel} > g_{\perp} > 2.0$ with the $d_{x^2-y^2}$ ground state. For Cu(II) complexes, the g values may display evidence for copper nuclear hyperfine splitting, $2I+1$, for ^{63}Cu , $I = 3/2$ and each g value is split into four lines, separated by the nuclear hyperfine splitting constant A . A_{\parallel} and A_{\perp} values of the present compound are found to be 152.9 and $52.08 \times 10^{-4} \text{ cm}^{-1}$ respectively. It should be mentioned here that the splittings observed in the perpendicular region were not well resolved, so the copper hyperfine splitting constant A_{\perp} was calculated by taking one third of the line widths at half maximum [42, 43].

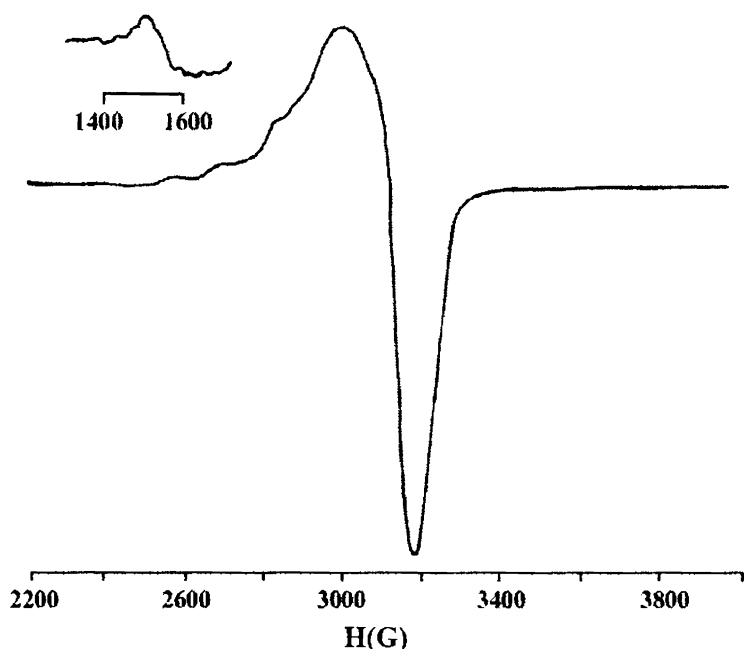


Fig. 3.12. EPR spectrum of compound $[\text{Cu}(\text{HL}^1)\text{Cl}_2]_2 \cdot 6\text{H}_2\text{O}$ at 77 K in DMF

In polynuclear copper(II) complexes, due to Cu–Cu dipolar interaction, the zero field splitting parameter, D gives rise to transitions corresponding to $\Delta M_s = \pm 2$. In the X-band spectra, $\Delta M_s = \pm 1$ transitions are associated with fields of *ca.* 3000 Gauss, while the $\Delta M_s = \pm 2$ transition generate an absorption at the half field value of *ca.* 1500 gauss and the presence of this half field band is a useful criterion for dipolar interaction from the presence of some dinuclear (or polynuclear) complex formation. The solution EPR spectrum of compound $[\text{Cu}(\text{HL}^1)\text{Cl}_2]_2 \cdot 6\text{H}_2\text{O}$ (**1**) at 77 K, exhibited a half field signal at approximately 1550 G, which indicate that indeed a weak interaction between two Cu(II) ions within this compound is present. Moreover, the broad signal in the low field region indicates that spin exchange interactions exist between the Cu(II) ions [41, 44, 45]. The exchange interaction parameter G [$G = (g_{\parallel} - 2)/(g_{\perp} - 2)$] is found to be less than 4.0, suggesting considerable exchange coupling interactions [46, 47] in the octahedral dimeric complex.

The distorted octahedral compound $[\text{Cu}(\text{L}^1)_2]$ (**2**) exhibited an axial spectrum in polycrystalline state at 298 K (Fig. 3.13) with hyperfine splittings in the g_{\parallel} region. The solution EPR spectrum of the compound in DMF at 77 K (Fig. 3.14) displayed rhombic features with three g values. The values of the g factor are in accordance with an $d_{x^2-y^2}$ as ground state. Only the signal in the low field region (g_{\parallel}) exhibited hyperfine splittings due to Cu(II) nucleus.

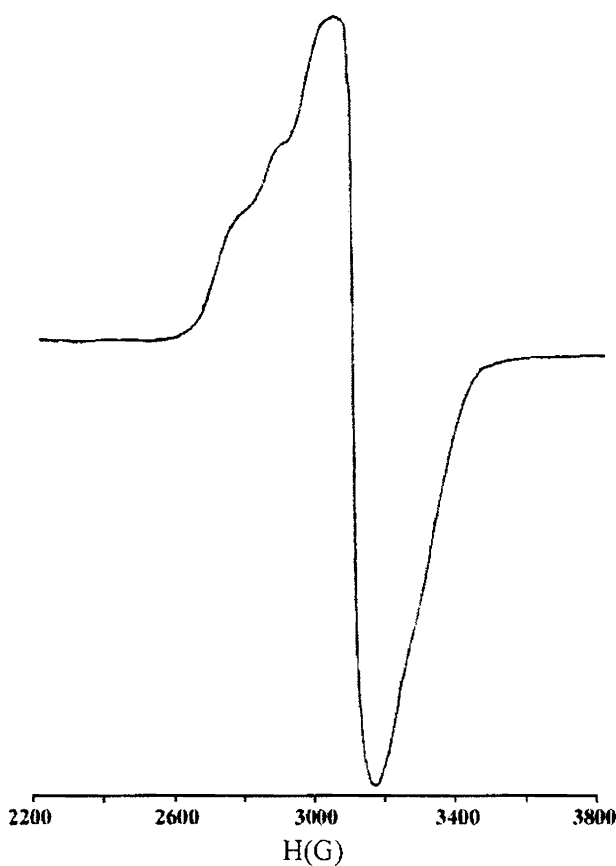


Fig. 3.13. EPR spectrum of compound $[\text{Cu}(\text{L}^1)_2]$ (**2**) in powder at 298 K

The g_{\parallel} values provide information regarding the nature of metal-ligand bond. Values of g_{\parallel} equal to or larger than 2.3 are for ionic and less than 2.3 are

for covalent environments. The g_{\parallel} values obtained for the present complexes indicate a significant degree of covalency in the metal-ligand bonds. The A_{\parallel} and A_{\perp} values are well within the range expected for tetragonally distorted copper(II) complexes.

The values of magnetic parameters and the energies of the electronic d-d transitions have been used for estimating the nature of the chemical bonding between the copper and donor atoms of the ligand. The fraction of unpaired electron density located on the copper ion i.e. the value of in-plane sigma bonding parameter α^2 was estimated from the expression [48-49]

$$\alpha^2 = -\frac{A_{\parallel}}{0.036} + (g_{\parallel} - 2.0023) + \frac{3(g_{\perp} - 2.0023)}{7} + 0.04$$

where A_{\parallel} is the parallel coupling constant. The value of α^2 indicates that the copper(II) complex is fairly covalent. The orbital reduction factors K_{\parallel} and K_{\perp} are calculated using expressions:

$$K_{\parallel}^2 = (g_{\parallel} - 2.0023) \frac{\Delta E(d_{xy} \rightarrow d_{x^2-y^2})}{8\lambda_0}$$

$$K_{\perp}^2 = (g_{\perp} - 2.0023) \frac{\Delta E(d_{xz}, d_{yz} \rightarrow d_{x^2-y^2})}{2\lambda_0}$$

$$K_{\parallel} = \alpha^2 \beta^2$$

$$K_{\perp} = \alpha^2 \gamma^2$$

where λ_0 is the spin-orbit coupling constant and has a value -828 cm^{-1} for Cu(II) d^9 system, α^2 is the in-plane σ -bonding, β^2 the in-plane π -bonding and γ^2 , the out-of-plane π -bonding. The value of α^2 indicates the extent of covalent nature,

where the value of 1.0 corresponds to a purely ionic nature. The covalency of the metal-ligand bond points toward a α^2 value less than 1.0. Hathaway proposed that, for pure σ bonding, $K_{\parallel} \sim K_{\perp} \sim 0.77$; for in-plane π -bonding, $K_{\parallel} < K_{\perp}$ and for out-of-plane π -bonding, $K_{\perp} < K_{\parallel}$. The fact that the K_{\parallel} and K_{\perp} values calculated for our copper complexes showed the trend $K_{\parallel} < K_{\perp}$ suggesting stronger in-plane π -bonding.

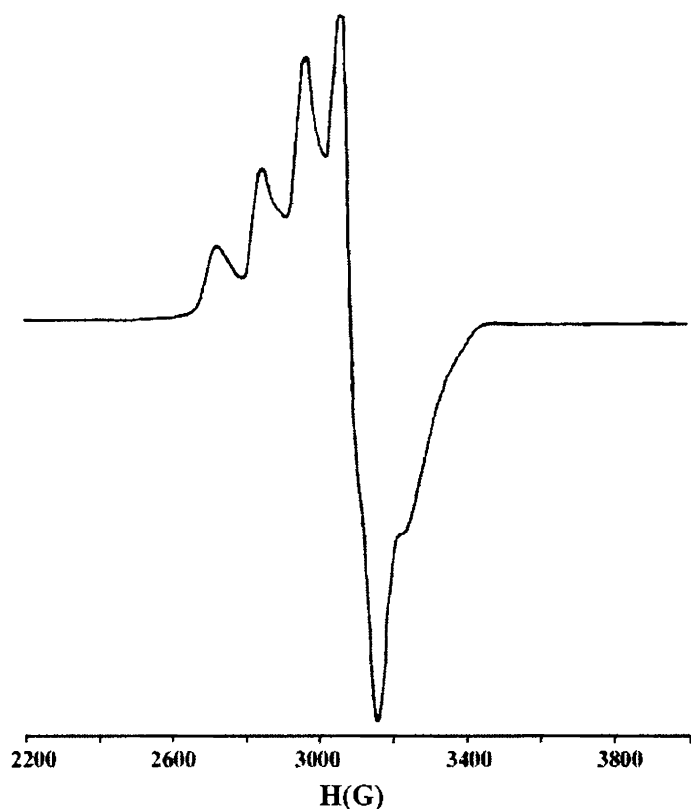


Fig. 3.14. EPR spectrum of compound $[\text{Cu}(\text{L}^1)_2]$ (2) at 77 K in DMF

The EPR spectra of the compound $[\text{Cu}(\text{HL}^2)\text{Cl}]$ (3) recorded in solid at 298 K and in solution in DMF at 77 K (Fig. 3.15) exhibited axial features. The absence of hyperfine interactions at room temperature, can be attributed to strong dipolar and exchange interactions between the Cu(II) ions in the unit cell.

However, the hyperfine splittings were well resolved only in the frozen solution state.

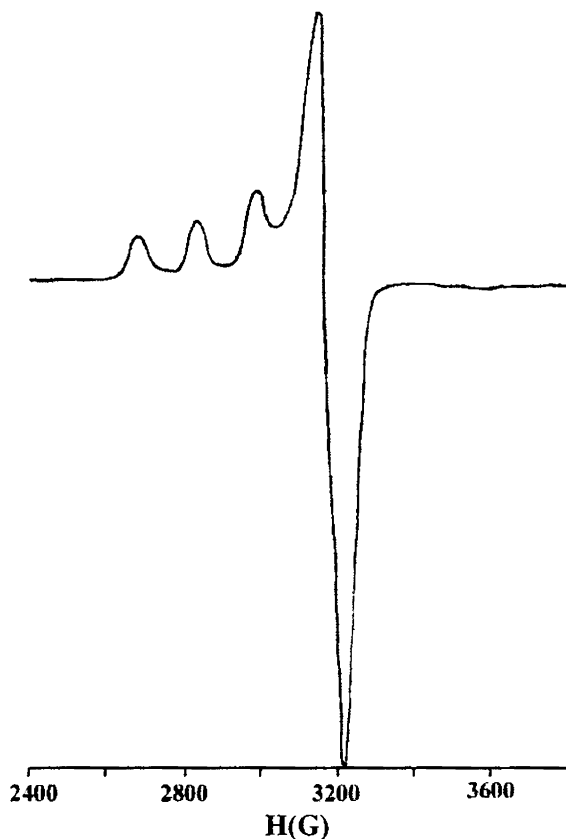


Fig. 3.15. EPR spectrum of compound $[\text{Cu}(\text{HL}^2)\text{Cl}]$ (**3**) at 77 K in DMF

The exchange parameter G calculated for the spectrum at 298 K revealed some magnetic exchange interactions present showing a value less than 4.0. But in solution this value was found to be greater than 4.0. Using the energy of the electronic d-d transitions various magnetic parameters were calculated using the equations given above. The values obtained convince the covalent nature of the metal-ligand bonds. The parameter $f(g_{\parallel}/A_{\parallel})$ is used as an index to express the range of tetrahedral distortion. The value may vary from 105 to 135 for small to extreme distortion. The present compound displays a value of about 119 cm, indicating some amount of distortion.

For the azido compound $[\text{Cu}(\text{HL}^2)\text{N}_3]$ (**4**), the spectrum at 298 K (polycrystalline) exhibited rhombic features with three g values $g_1 = 1.979$, $g_2 = 2.040$, $g_3 = 2.148$. The hyperfine splittings were not found. The solution spectrum in DMF at 77 K (Fig. 3.16), reveals more prominent features near $g \approx 2$ region indicating the characteristic axial spectrum ($g_{\parallel} = 2.194$, $A_{\parallel} = 186.0 \times 10^{-4} \text{ cm}^{-1}$, $g_{\perp} = 2.053$, $A_{\perp} = 12.77 \times 10^{-4} \text{ cm}^{-1}$) of a mononuclear square planar copper(II) species.

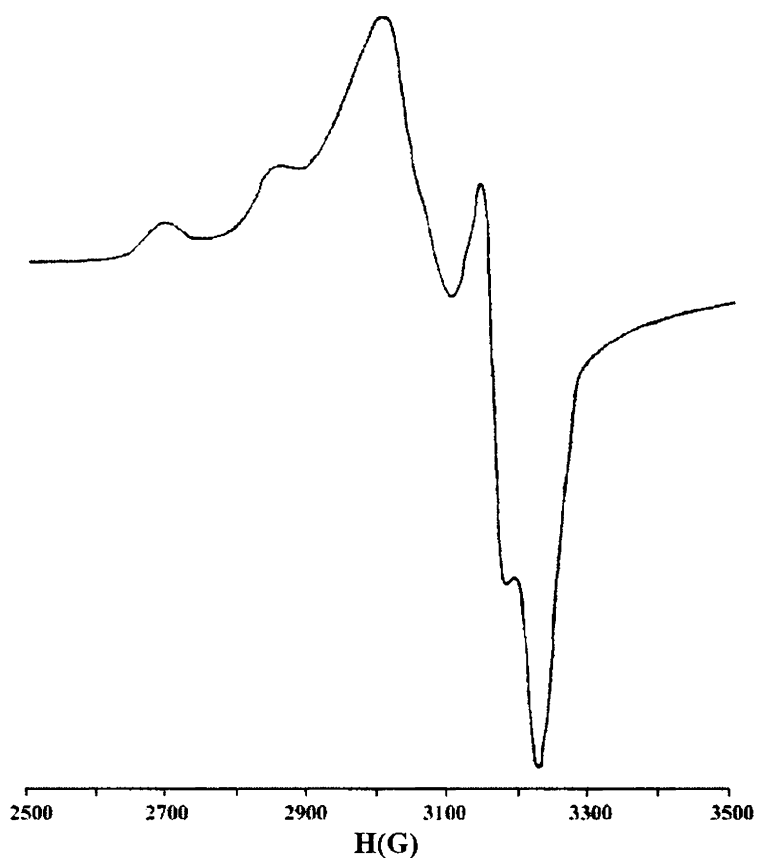


Fig. 3.16. EPR spectrum of compound $[\text{Cu}(\text{HL}^2)\text{N}_3]$ (**4**) at 77 K in DMF

The contribution of the s electrons to the hyperfine interaction can be estimated by the value of Fermi contact hyperfine interaction term (K_0) using the equation:

$$K_0 = A_{\text{iso}} / P\beta^2 + (g_{\text{av}} - 2.0023) / \beta^2$$

where P is taken as 0.036 cm^{-1} , A_{iso} as $1/3(A_{\parallel} + 2A_{\perp})$ and g_{av} as $1/3(g_{\parallel} + 2g_{\perp})$. K_0 is a dimensionless quantity and is generally found to have a value of 0.3. The values calculated for our systems are in the range of 0.3-0.6. The distortion factor f is found to be 117.95 cm, which denotes some amount of distortion from regular geometry.

Compound $[\text{Cu}(\text{HL}^2)_2]$ (**5**), revealed axial features in concordance with an elongated axial geometry both at 298 K (powder) (Fig. 3.17) and at 77 K (DMF) (Fig. 3.18). Hexacoordinated Cu(II) complexes due to Jahn Teller effect exhibits a tetragonal distortion which reduces its symmetry from O_h to D_{4h} [50, 51] This results in an anisotropy of the g -tensor. As the coordinated groups are not equivalent, only static distortion can occur [44, 52]. As $g_{\parallel} > g_{\perp}$, a tetragonal distortion is suggested, corresponding to an elongation along the four-fold symmetry Z-axis. The unpaired electron still remains in $d_{x^2-y^2}$ orbital; in the distorted octahedral structure because the Jahn Teller induced distortion generally favours $d_{x^2-y^2}$ while d_{z^2} configuration are rare. As the g values are less than 2.3 and the calculated α^2 , β^2 and γ^2 values are less than 1.0, it means that considerable covalent character is imparted to the metal-ligand bonds.

The EPR spectrum of compound $[\text{Cu}(\text{L}^3)\text{Cl}]$ (**6**) was much less informative in interpreting the geometry as the broad spectrum revealed isotropic feature at 298 K (powder), g_{iso} 2.120. This may be due to strong dipolar and exchange interactions between the Cu(II) ions in the unit cell. Even the frozen solution spectrum at 77 K (Fig. 3.19) is isotropic in nature (g_{iso} 2.134) with no hyperfine splittings. This may be due to the poor glass formation. Ideally, in the dissolved state at 77 K in a suitable solvent, the intermolecular interactions are reduced, and the EPR spectrum should be well resolved. Such isotropic nature are

observed when, the complex contains grossly misaligned tetragonal axes. The EPR study of the compound thus returned poor results.

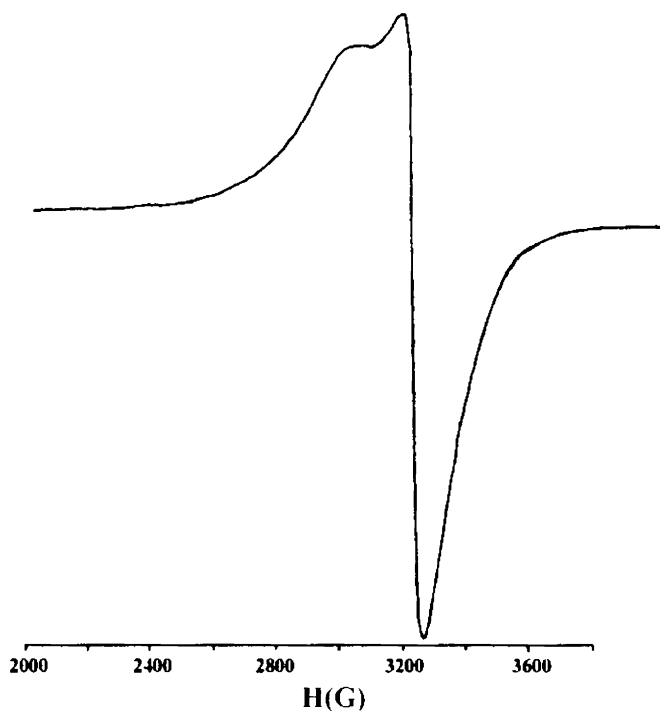


Fig. 3.17. EPR spectrum of compound $[\text{Cu}(\text{HL}^2)_2]$ (5) at 298 K

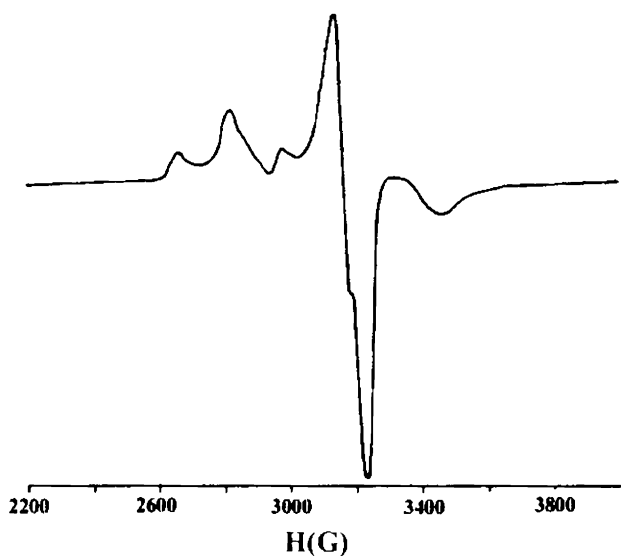


Fig. 3.18. EPR spectrum of compound $[\text{Cu}(\text{HL}^2)_2]$ (5) at 77 K in DMF

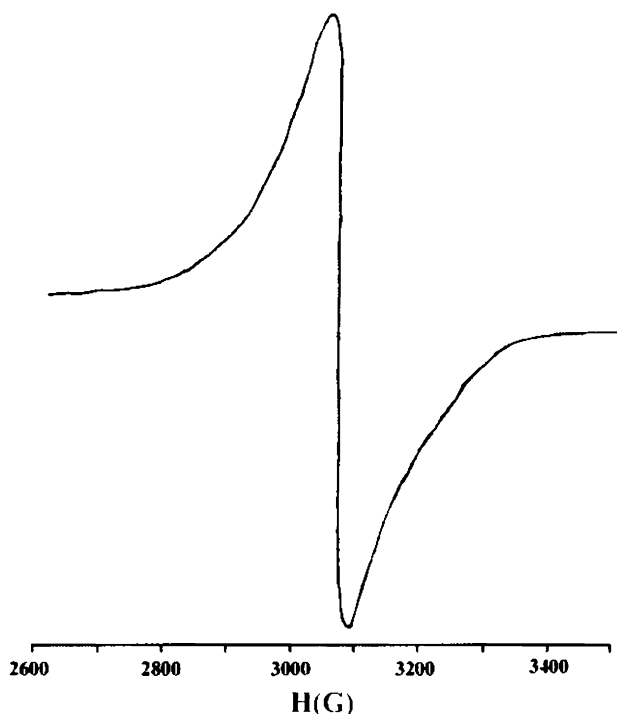


Fig. 3.19. EPR spectrum of compound $[\text{Cu}(\text{L}^3)\text{Cl}]$ (**6**) at 77 K in DMF

Three signals observed for the compound $[\text{Cu}(\text{HL}^3)\text{Br}]\text{Br}$ (**7**) are in complete agreement with the rhombic distortion of the coordination sphere around the Cu(II) ion both in powder at 298 K (Fig. 3.20) and in solution at 77 K (Fig. 3.21). The g values calculated are found to be $g_1=2.050$; $g_2=2.079$; $g_3=2.240$ and $g_1=2.053$; $g_2=2.133$; $g_3=2.243$ respectively.

At room temperature, the EPR spectrum shows relatively lesser g -tensor anisotropy presumably due to larger spin-lattice relaxation time and smaller spin-orbit coupling interactions. The lowest g value is greater than 2.04, which points towards a $d_{x^2-y^2}$ ground state. The anisotropic rhombic g -tensors with $G < 4.0$ [$G = (g_3 - 2.0023)/(g_- - 2.0023)$; $g_1 = (g_1 + g_2) / 2$; $G = 3.67$ at 298 and 2.58 at 77 K] suggest exchange coupling interactions in the complex. The absence of hyperfine splittings restricted the calculation of other magnetic parameters.

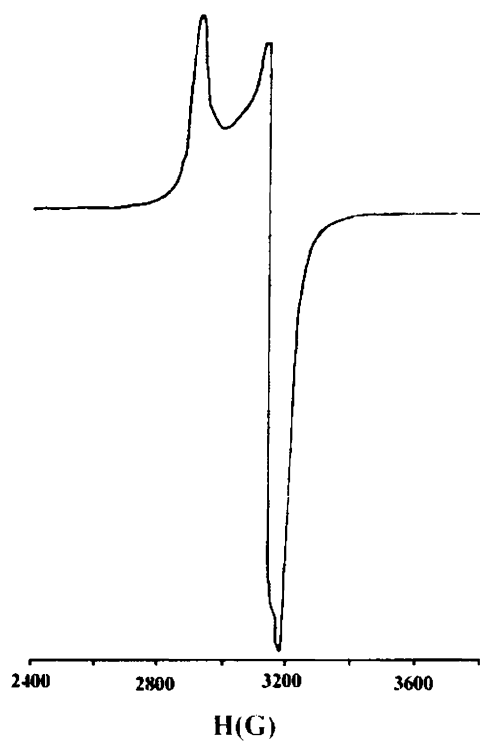


Fig. 3.20. EPR spectrum of compound $[\text{Cu}(\text{HL}^3)\text{Br}]\text{Br}$ (7) at 298 K

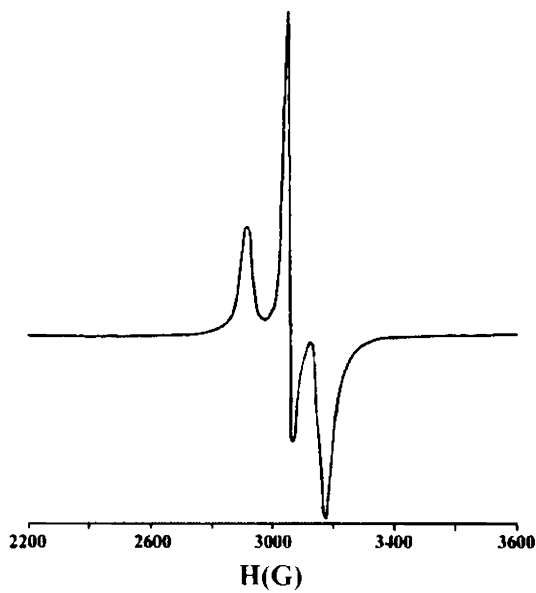


Fig. 3.21. EPR spectrum of compound $[\text{Cu}(\text{HL}^3)\text{Br}]\text{Br}$ (7) in DMF at 77 K

An interesting aspect of the spectrum of compound $[\text{Cu}(\text{L}^3)_2]\cdot\text{H}_2\text{O}$ (**8**), compared to other six-coordinate complexes was that, it displayed reverse axial feature at 298 K which are found to be rare (Fig. 3.22) with g (2.169) greater than g (2.027). Such spectra with g_{min} less than 2.03 can be observed for a Cu(II) ion in an axial symmetry with all the principal axes aligned parallel, and would be consistent with compressed tetragonal-octahedral stereochemistry [41]. The single crystal X-ray analysis of the compound also supports this geometry.

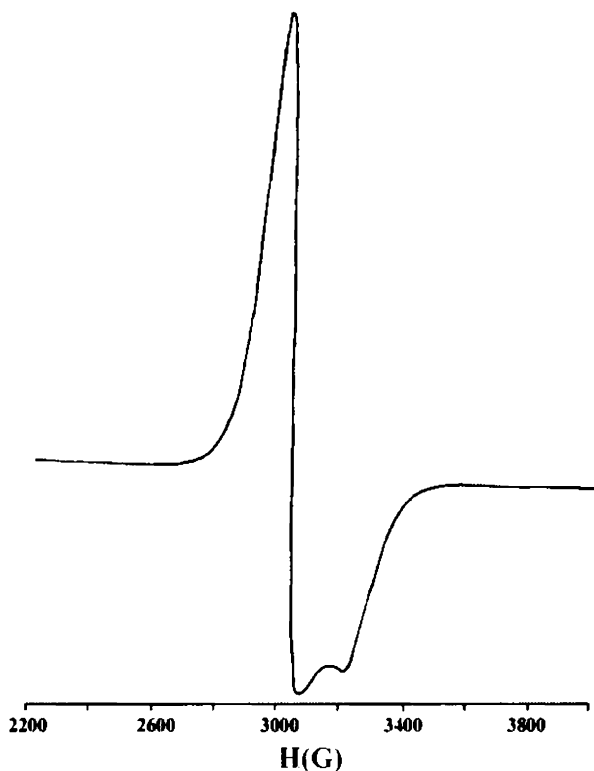


Fig. 3.22. EPR spectrum of compound $[\text{Cu}(\text{L}^3)_2]\cdot\text{H}_2\text{O}$ (**8**) at 298 K

In this compressed stereochemistry, the value of G has no significance. Usually complexes that are susceptible to Jahn-Teller distortion have octahedral configurations that involve asymmetric electron occupation of either the e_g or t_{2g} orbitals. As the e_g orbitals are more involved in σ bonding than the t_{2g} orbitals, the former leads to more pronounced distortions than does the latter.

This distortion takes place either by elongation or by compression leading to some stability. This depends on whether the odd electron resides in the $d_{x^2-y^2}$ or d_{z^2} orbital respectively. Detailed calculations [53] have shown that the elongated structures are usually more energetically favorable than the compressed structures, consistent with their more frequent occurrence. So it is not uncommon for this complex to have bond length differences with two short bonds and four long bonds.

The frozen solution EPR spectrum of the compound also displayed the reverse axial spectrum, thus consistent with axially compressed octahedral geometry. The geometry of the compound was maintained in solution state also. In this state, the hyperfine splittings in the perpendicular region was well evident with A_{\perp} 196.66 G. The g factor values (g_{\parallel} 2.089, g_{\perp} 2.166) calculated from the spectrum of compound $[\text{Cu}(\text{L}^3)_2]\cdot\text{H}_2\text{O}$ (**8**) at 77 K (Fig. 3.23) are in accordance with an axial symmetry with d_{z^2} as ground state.

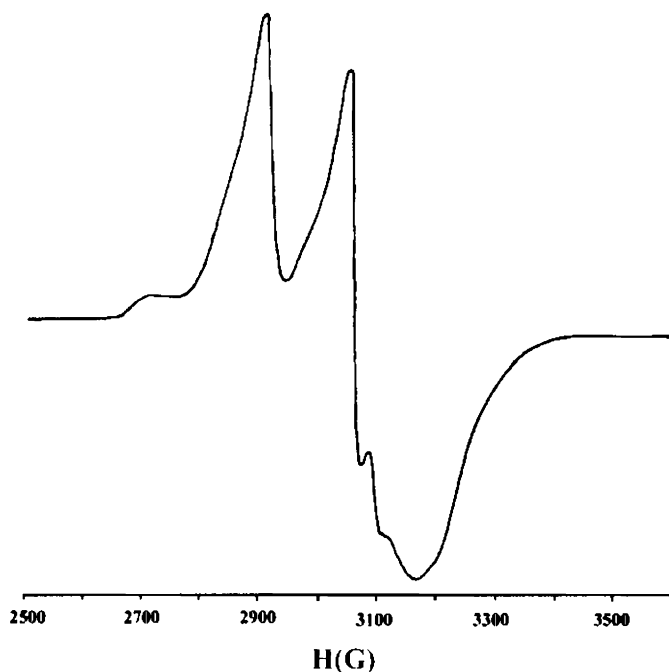


Fig. 3.23. EPR spectrum of compound $[\text{Cu}(\text{L}^3)_2]\cdot\text{H}_2\text{O}$ (**8**) at 77 K in DMF

3.3.2c IR spectral studies

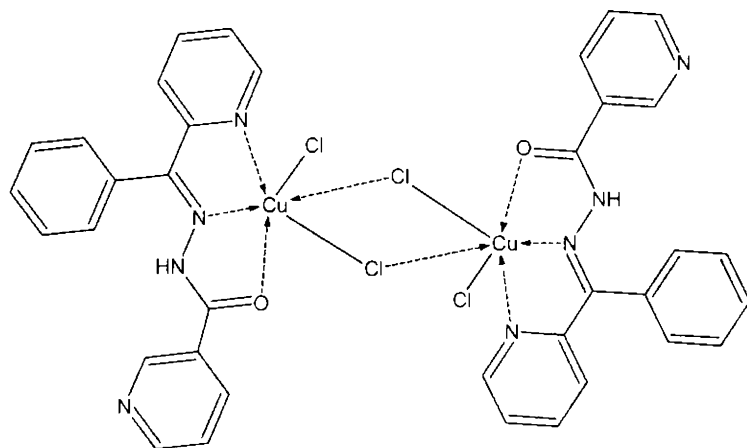
A comparison of the IR spectra of ligands and the metal complexes shows that significant variations have occurred in the characteristic frequencies upon complexation. The IR spectrum of compound $[\text{Cu}(\text{HL}^1)\text{Cl}_2]_2 \cdot 6\text{H}_2\text{O}$ (**1**) reveals a broad band around 3430 cm^{-1} and a medium band at 3067 cm^{-1} , which correspond to the lattice water content and the N–H vibrations respectively. This explains that the ligand is not deprotonated for coordination and the Cu(II) valency is satisfied by the two coordinated chloride anions. However, the negative shift of carbonyl moiety, to 1629 cm^{-1} suggests its coordination. The azomethine band showed a positive shift at 1594 cm^{-1} . Such shifts to higher frequencies have been reported earlier. The sharp bands observed at $1502\text{--}1450$ and 1375 cm^{-1} are assigned to ring vibrations and amide III band respectively. Coming to the far IR region, the Cu–N_{py} vibration frequency was observed at 280 cm^{-1} . The peaks observed at 302 and 227 cm^{-1} , evidenced the presence of terminal chlorine as well as bridging chlorine.

The azomethine band of the six coordinated Cu(II) compound $[\text{Cu}(\text{L}^1)_2]$ (**2**), suffered a negative shift, revealing a band at 1526 cm^{-1} . The band observed at 1581 cm^{-1} , was assigned to the –C=N–N=C– moiety. The amide III band was observed at 1360 cm^{-1} . Compound $[\text{Cu}(\text{HL}^2)\text{Cl}]$ (**3**), with the terminal chlorine in the coordination sphere, exhibited the Cu–Cl band at 303 cm^{-1} in the far IR region. Coordination of pyridyl nitrogen to Cu(II) ion resulted in bands found at 276 and 241 cm^{-1} . The shifted azomethine band was observed at 1562 cm^{-1} . The –C=N–N=C– moiety formed due to deprotonation was viewed at 1596 cm^{-1} . The amide III band was observed as a sharp band at 1376 cm^{-1} . The IR spectrum also reveals the C–N ring stretching (skeletal bands) vibrations of the aromatic rings in the region $1486\text{--}1414\text{ cm}^{-1}$. A comparatively broad band observed at 3391 cm^{-1} corresponds to the –OH vibrations of the hydroxyl group attached to the benzoyl ring. The azido compound $[\text{Cu}(\text{HL}^3)\text{N}_3]$ (**4**), exhibited the antisymmetric $\nu(\text{NNN})$ vibration as a sharp band observed at 2070 cm^{-1} . The far IR spectrum supported

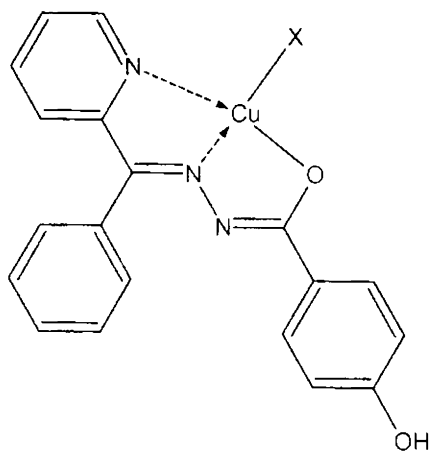
this assignment as the $\nu(\text{M-N})$ vibration of the Cu-azide bond produced a band at 397 cm^{-1} . The other characteristic vibrations were found to be in the usual range. The octahedral compound $[\text{Cu}(\text{HL}^2)_2]$ (**5**), exhibited the $-\text{OH}$ vibration as a broad band at 3428 cm^{-1} . The amide III band was viewed at 1372 cm^{-1} and the coordinated azomethine band at 1552 cm^{-1} . The $-\text{C}=\text{N}-\text{N}-\text{C}-$ vibration is observed as a strong combination band at 1591 cm^{-1} . The $\nu(\text{C}=\text{N})$ ring vibrations may be contributing to this combination band.

The absence of the band corresponding to $-\text{N}-\text{H}$ vibration in the expected region of compound $[\text{Cu}(\text{L}^3)\text{Cl}]$ (**6**), confirmed the deprotonation of the ligand, together with the amide III band observed at 1374 cm^{-1} . The sharp band observed at 1604 cm^{-1} was assigned to the $-\text{C}=\text{N}-\text{N}=\text{C}-$ vibration. The bands in the region $1564-1458\text{ cm}^{-1}$, was so crowded, that accurate assignment of the vibration corresponding to the coordinated azomethine bond was difficult. The terminal Cu-Cl band was observed at 309 cm^{-1} . The IR spectrum of the bromo complex $[\text{Cu}(\text{HL}^3)\text{Br}]\text{Br}$ (**7**), of the same ligand, exhibited interesting features compared to the chloro compound. The elemental analyses suggested the presence of two bromide ions, however the conductivity measurements suggested a nearly 1:1 electrolyte, which means one of the bromide ion is out of the coordination sphere. But the band corresponding to the carbonyl group is shifted to 1600 cm^{-1} suggesting its coordination. The azomethine band is shifted to 1540 cm^{-1} . The N-H band is observed at 3410 cm^{-1} . A sharp band viewed at 1501 cm^{-1} corresponds to the pyridyl ring vibrations. The compound $[\text{Cu}(\text{L}^3)_2]\cdot\text{H}_2\text{O}$ (**8**), produced a broad band around 1642 cm^{-1} , due to the $-\text{C}=\text{N}-\text{N}=\text{C}-$ moieties. The azomethine band was observed at 1582 cm^{-1} . The amide III band was seen at 1359 cm^{-1} . The presence of lattice water was confirmed by the appearance of a broad band at 3432 cm^{-1} .

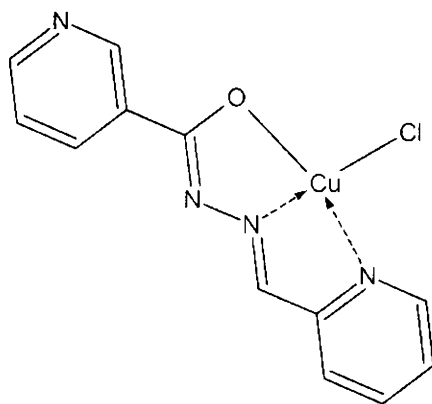
Based on the elemental analyses and spectral investigations, following tentative structures were assigned for the complexes for which, single crystals suitable for crystallographic studies could not be isolated.



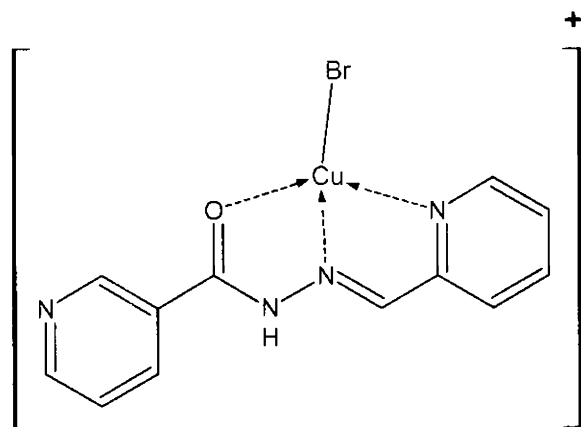
Compound 1



Compounds 3 and 4 (X = Cl, N₃)



Compound 6



Compound 7

Table 3.1
Crystal data and structure refinement of $[\text{Cu}(\text{L}^1)_2]$ and $[\text{Cu}(\text{HL}^2)_2] \cdot \text{H}_2\text{O} \cdot \text{DMF}$

Parameters	$[\text{Cu}(\text{L}^1)_2]$	$[\text{Cu}(\text{HL}^2)_2] \cdot \text{H}_2\text{O} \cdot \text{DMF}$
Empirical formula	$\text{C}_{36}\text{H}_{26}\text{CuN}_7\text{O}_2$	$\text{C}_{41}\text{H}_{35}\text{CuN}_7\text{O}_6$
Formula weight	666.19	785.30
Crystal system	Monoclinic	Monoclinic
Space group	$P2_1$	$P2_1/n$
Unit cell dimensions		
a (Å)	9.2248(9)	11.8506(9)
b (Å)	10.5037(6)	24.0267(17)
c (Å)	16.9037(15)	13.6490(9)
α (°)	90.00	90.00
β (°)	102.789(8)	94.192(2)
γ (°)	90.00	90.00
Volume V (Å ³), Z	1597.2(2), 2	3875.9(5), 4
Calculated density (ρ) (Mg m ⁻³)	1.385	1.346
Absorption coefficient μ (mm ⁻¹)	0.730	0.620
F (000)	686	1628
Crystal size (mm)	0.25 x 0.25 x 0.20	0.20 x 0.14 x 0.08
θ range for data collection	1.24 - 24.97	1.70 - 25.00
Index ranges	$0 \leq h \leq 10, 0 \leq k \leq 12,$ $-20 \leq l \leq 19$	$-10 \leq h \leq 14, -25 \leq k \leq 28,$ $-16 \leq l \leq 14$
Reflections collected / unique	3157 / 2960 [R(int) = 0.0231]	19252 / 6821 [R(int) = 0.0500]
Refinement method	Full-matrix least-squares on F^2	Full-matrix least-squares on F^2
Data / restraints / parameters	2960 / 1 / 424	6821 / 0 / 500
Goodness-of-fit on F^2	1.054	1.020
Final R indices [$I > 2\sigma(I)$]	R1 = 0.0397, wR2 = 0.0941	R1 = 0.0608, wR2 = 0.1519
R indices (all data)	R1 = 0.0776, wR2 = 0.1059	R1 = 0.0935, wR2 = 0.1694

Table 3.2
Crystal data and structure refinement of $[\text{Cu}(\text{L}^3)_2]\cdot\text{H}_2\text{O}$

Parameters	$[\text{Cu}(\text{L}^3)_2]\cdot\text{H}_2\text{O}$
Empirical formula	$\text{C}_{48}\text{H}_{40}\text{Cu}_2\text{N}_{16}\text{O}_6$
Formula weight	1064.04
Crystal system	Triclinic
Space group	$P\bar{1}$
Unit cell dimensions	
a (Å)	12.146(4)
b (Å)	13.355(4)
c (Å)	16.008(5)
α (°)	110.208(5)
β (°)	103.995(5)
γ (°)	94.074(5)
Volume V (Å ³), Z	2330.2(13), 4
Calculated density (ρ) (Mg m ⁻³)	1.517
Absorption coefficient μ (mm ⁻¹)	0.982
F (000)	1092
Crystal size (mm)	0.30 x 0.25 x 0.16
θ range for data collection	1.41 - 28.36
Index ranges	$-16 \leq h \leq 15$, $-17 \leq k \leq 17$, $-21 \leq l \leq 21$
Reflections collected / unique	19542 / 10354 [R(int) = 0.0209]
Refinement method	Full-matrix least-squares on F^2
Data / restraints / parameters	10354 / 0 / 809
Goodness-of-fit on F^2	0.979
Final R indices [$I > 2\sigma(I)$]	R1 = 0.0429, wR2 = 0.1127
R indices (all data)	R1 = 0.0606, wR2 = 0.1246

Table. 3.3
Selected bond lengths (Å) of [Cu(L¹)₂] and [Cu(HL²)₂]·H₂O·DMF

	[Cu(L ¹) ₂]	[Cu(HL ²) ₂]·H ₂ O·DMF
Cu1–N2	1.952(4)	1.975(3)
Cu1–N6	1.983(4)	-
Cu1–N4	-	2.087(3)
Cu1–O1	2.033(4)	2.303(3)
Cu1–N1	2.067(5)	2.318(3)
Cu1–O2	2.247(4)	-
Cu1–O3	-	2.042(3)
Cu1–N5	2.305(5)	1.926(3)
C6–N2	1.293(6)	1.292(5)
C13–O1	1.272(6)	1.266(4)
N2–N3	1.370(6)	1.383(4)
C13–N3	1.323(6)	1.339(5)
C5–C6	1.490(7)	1.487(5)
C13–C14	1.505(8)	1.501(5)

Table. 3.4
 Selected bond angles (°) of $[\text{Cu}(\text{L}^1)_2]$ and $[\text{Cu}(\text{HL}^2)_2]\cdot\text{H}_2\text{O}\cdot\text{DMF}$

	$[\text{Cu}(\text{L}^1)_2]$	$[\text{Cu}(\text{HL}^2)_2]\cdot\text{H}_2\text{O}\cdot\text{DMF}$
N2–Cu1–N6	174.9(2)	-
N2–Cu1–N4	-	104.07(12)
N2–Cu1–O1	78.80(16)	73.99(11)
N6–Cu1–O1	103.85(16)	-
N4–Cu1–O1	-	91.36(12)
N2–Cu1–N1	78.96(17)	76.01(12)
N6–Cu1–N1	98.59(17)	-
N4–Cu1–N1	-	89.96(12)
O1–Cu1–N1	157.49(15)	149.37(10)
N2–Cu1–O2	109.18(16)	-
N2–Cu1–O3	-	97.52(11)
N6–Cu1–O2	75.09(17)	-
N5–Cu1–O3	-	79.27(11)
O1–Cu1–O2	95.28(18)	-
O1–Cu1–O3	-	96.33(11)
N1–Cu1–O2	88.77(18)	-
N1–Cu1–O3	-	93.56(11)
N2–Cu1–N5	99.83(16)	175.59(12)
N6–Cu1–N5	75.94(18)	-
N4–Cu1–N5	-	79.27(12)
O1–Cu1–N5	90.10(19)	103.22(11)
N1–Cu1–N5	97.05(19)	107.08(12)
O2–Cu1–N5	150.99(15)	-
O3–Cu1–N4	-	158.34(11)
C6–N2–N3	122.2(4)	117.3(3)
N2–N3–C13	108.3(4)	110.9(3)
N3–C13–O1	126.7(5)	125.8(3)
C5–C6–N2	111.9(4)	116.5(3)
N3–C13–C14	115.5(4)	114.0(3)

Table. 3.5
Selected bond lengths (Å) and bond angles of [Cu(L³)₂]-H₂O

Bonds			
Cu1A–N2A	1.9615(17)	Cu2B–N2B	1.9703(17)
Cu1A–N6A	1.9558(18)	Cu2B–N6B	1.9508(17)
Cu1A–O1A	2.1560(15)	Cu2B–O1B	2.2745(17)
Cu1A–N1A	2.2187(17)	Cu2B–N1B	2.2433(18)
Cu1A–O2A	2.1862(16)	Cu2B–O2B	2.1074(15)
Cu1A–N5A	2.1845(18)	Cu2B–N5B	2.1443(15)
C6A–N2A	1.280(3)	C6B–N2B	1.286(3)
C7A–O1A	1.263(2)	C7B–O1B	1.252(2)
N2A–N3A	1.376(2)	N2B–N3B	1.369(2)
C7A–N3A	1.332(3)	C7B–N3B	1.340(3)
C5A–C6A	1.465(3)	C5B–C6B	1.469(3)
C7A–C8A	1.497(3)	C7B–C8B	1.502(3)
Bond angles			
N2A–Cu1A–N6A	175.88(7)	N2B–Cu2B–N6B	172.51(7)
N2A–Cu1A–O1A	76.17(7)	N2B–Cu2B–O1B	74.38(6)
N6A–Cu1A–O1A	104.21(7)	N6B–Cu2B–O1B	113.11(6)
N2A–Cu1A–N1A	77.58(7)	N2B–Cu2B–N1B	77.39(7)
N6A–Cu1A–N1A	102.23(7)	N6B–Cu2B–N1B	95.13(6)
O1A–Cu1A–N1A	153.51(6)	O1B–Cu2B–N1B	151.74(6)
N2A–Cu1A–O2A	108.12(6)	N2B–Cu2B–O2B	103.52(7)
N6A–Cu1A–O2A	75.99(6)	N6B–Cu2B–O2B	77.06(7)
O1A–Cu1A–O2A	92.49(6)	O1B–Cu2B–O2B	92.92(6)
N1A–Cu1A–O2A	92.25(6)	N1B–Cu2B–O2B	94.80(6)
N2A–Cu1A–N5A	97.85(6)	N2B–Cu2B–N5B	101.44(7)
N6A–Cu1A–N5A	78.04(7)	N6B–Cu2B–N5B	78.35(7)
O1A–Cu1A–N5A	95.81(6)	O1B–Cu2B–N5B	92.66(6)
N1A–Cu1A–N5A	91.24(6)	N1B–Cu2B–N5B	91.71(6)
O2A–Cu1A–N5A	153.95(6)	O2B–Cu2B–N5B	155.02(6)
C6A–N2A–N3A	120.46(17)	C6B–N2B–N3B	118.61(17)
N2A–N3A–C7A	108.94(16)	N2B–N3B–C7B	110.12(16)
N3A–C7A–O1A	126.37(18)	N3B–C7B–O1B	126.84(19)
C5A–C6A–N2A	117.41(18)	C5B–C6B–N2B	118.23(19)
N3A–C7A–C8A	115.60(17)	N3B–C7B–C8B	113.71(17)

Table 3.6
H-bonding interaction parameters of $[\text{Cu}(\text{HL}^2)_2]$ and $[\text{Cu}(\text{L}^3)_2] \cdot \text{H}_2\text{O}$

Donor---H---A	D-H (Å)	H---A (Å)	D---A (Å)	D-H---A (°)
$[\text{Cu}(\text{HL}^2)_2]$				
O2-H-O6	0.820	1.858	2.675	173.90
O4-H-O1	0.820	1.903	2.720	174.44
C11-H-N6	0.930	2.400	3.299	162.48
C15-H-N3	0.930	2.442	2.771	100.79
C31-H-N6	0.930	2.575	2.931	103.17
C34-H-N6	0.930	2.426	2.755	100.72
$[\text{Cu}(\text{L}^3)_2] \cdot \text{H}_2\text{O}$				
O5-HA-N12	0.88	2.010	2.818	152.04
O5-HB-N16	0.757	2.191	2.945	174.01
O6-HA-N8	0.865	2.054	2.888	161.91
O6-HA-O5	0.739	2.246	2.882	144.72
C9-H-N3	0.871	2.534	2.826	100.54
C18-H-O6	0.995	2.415	3.272	143.86
C21-H-N7	1.046	2.378	2.775	101.02
C22-H-O4	0.937	2.569	3.384	145.63
C24-H-O2	0.809	2.557	2.828	101.23
C30-H-O5	0.967	2.467	3.319	146.86
C34-H-O1	0.953	2.554	3.423	151.67
C35-H-O1	0.880	2.593	3.280	135.63
C36-H-O3	0.810	2.575	2.835	100.31
C39-H-O6	0.929	2.564	3.427	154.69
C42-H-O3	0.931	2.538	3.241	132.66

Table 3.7

Magnetic parameters from the EPR spectra of complexes 1 - 4

Compounds	State	g	g_{av}	$A / 10^4 \text{ cm}^{-1}$	K	α^2	β^2	γ^2
[Cu(HL ¹)Cl ₂] ₂ ·6H ₂ O (1)	Solid (298 K)	g_{\parallel} 1.990	2.095					
		g_{\perp} 2.148						
	DMF (77 K)	g_{\parallel} 2.340	2.174	A_{\parallel} 152.9	K_{\parallel} 0.812	0.840	0.966	0.995
		g_{\perp} 2.092		A_{\perp} 52.08	K_{\perp} 0.836			
[Cu(L ¹) ₂] (2)	Solid (298 K)	g_{\parallel} 2.155	2.118	A_{\parallel} 181.1	K_{\parallel} 0.577	0.737	0.782	1.246
		g_{\perp} 2.099						
		g_1 2.053						
DMF (77 K)	g_2 2.113	A 169.38						
	g_3 2.177							
[Cu(HL ²)Cl] (3)	Solid (298 K)	g_{\parallel} 2.134	2.071		K_{\parallel} 0.513			
		g_{\perp} 2.071						
	DMF (77 K)	g_{\parallel} 2.223		A_{\parallel} 159.0	K_{\parallel} 0.663	0.713	0.929	0.746
		g_{\perp} 2.031						
[Cu(HL ²)N ₃] (4)	Solid (298 K)	g_1 1.979						
		g_2 2.040						
		g_3 2.148						

Table 3.7 contd.

[Cu(HL ²)N ₃] (4)	DMF (77 K)	g_{\parallel} 2.194	2.100	A_{\parallel} 186.0	K_{\parallel} 0.668	0.769	0.868	0.893
		g_{\perp} 2.053		A_{\perp} 12.77	K_{\perp} 0.687			
[Cu(HL ³) ₂] (5)	Solid (298 K)	g_{\parallel} 2.170	2.066					
		g_{\perp} 2.015						
[Cu(L ³)Cl] (6)	DMF (77 K)	g_{\parallel} 2.120		A_{\parallel} 263.8	K_{\parallel} 0.507	0.903	0.561	0.632
		g_{\perp} 2.040	2.066	A_{\perp} 25.33	K_{\perp} 0.571			
	Solid (298 K)	g_{iso} 2.120						
	DMF (77 K)	g_{iso} 2.134						
[Cu(HL ³)Br]Br (7)		g_1 2.050						
	Solid (298 K)	g_2 2.079						
		g_3 2.240						
[Cu(L ³) ₂]·H ₂ O (8)	DMF (77 K)	g_1 2.053						
		g_2 2.133						
		g_3 2.243						
[Cu(L ³) ₂]·H ₂ O (8)	Solid (298 K)	g_{\parallel} 2.027	2.122					
		g_{\perp} 2.169						
[Cu(L ³) ₂]·H ₂ O (8)	DMF (77 K)	g_{\parallel} 2.089		A_{\parallel} 22.75				
		g_{\perp} 2.166	2.140	A_{\perp} 198.8				

References

1. K. W. Penfield, R. R. Gay, R. S. Himmelwright, N. C. Eickman, V. A. Norris, H. C. Freeman, E. I. Solomon, *J. Am. Chem. Soc.* 103 (1981) 4382.
2. E. I. Solomon, K. W. Penfield, D. E. Wilcox, *Struct. Bonding* 53 (1983) 1.
3. B. Abolmaali, H. V. Taylor, U. Weser, *Struct. Bonding* 91 (1998) 91.
4. A. Messerschmidt, *Struct. Bonding* 90 (1998) 37.
5. R. Osterberg, *Coord. Chem. Rev.* 12 (1974) 309.
6. J. A. Fee, *Struct. Bonding* 23 (1975) 1.
7. H. Beinert, *Coord. Chem. Rev.* 23 (1977) 119.
8. E. L. Ulrich, J. L. Markey, *Coord. Chem. Rev.* 27 (1978) 109.
9. I. Bertini, G. Canti, R. Grassi, *Inorg. Chem.* 19 (1980) 2198.
10. H. Yokoi, A. Addison, *Inorg. Chem.* 16 (1977) 1341.
11. H. Yokoi, *Bull. Chem. Soc. Jpn.* 47 (1974) 3037.
12. I. Solomon, L. B. La Croix, D. W. Randall, *Pure Appl. Chem.* 70 (1998) 799.
13. K. Pierloot, J. O. A. De Kerpel, U. Ryde, M. H. M. Olsson, B. O. Roos, *J. Am. Chem. Soc.* 120 (1998) 13156.
14. I. H. Hall, K. G. Rajendran, D. X. West, A. E. Liberta, *Anticancer Drugs* 4 (1993) 231.
15. D. X. West, A. E. Liberta, K. G. Rajendran, I. H. Hall, *Anticancer Drugs* 4 (1993) 241.
16. S. P. Mittal, R. K. Sharma, R. V. Singh, J. P. Tandon, *Curr. Sci.* 50 (1981) 483.
17. A. S. Dobeck, D. I. Klayman, E. J. Dickson, J. P. Scovill, E. C. Tramont, *Antimicrob. Agents Chemother.* 18 (1980) 27.
18. K. Raman, H. K. Singh, S. K. Salman, S. S. Parmar, *J. Pharm. Sci.* 82 (1993) 167.
19. D. K. Johnson, T. B. Murphy, N. J. Rose, W. H. Goodwin, L. Pickart, *Inorg. Chim. Acta* 67 (1982) 159.

20. L. Pickart, W. H. Goodwin, W. Burgua, T. B. Murphy, D. K. Johnson, *Biochem. Pharmacol.* 32 (1983) 3868.
21. A. A. Aruffo, T. B. Murphy, D. K. Johnson, N. J. Rose, V. Schomaker, *Acta Cryst. C* 40 (1984) 1164.
22. E. W. Ainscough, A. M. Brodie, A. Dobbs, J. D. Ranford, J. M. Waters, *Inorg. Chim. Acta* 236 (1995) 83.
23. S. C. Chan, L. L. Koh, P. H. Leung, J. D. Ranford, K. Y. Sim, *Inorg. Chim. Acta* 236 (1995) 101.
24. E. W. Ainscough, A. M. Brodie, A. Dobbs, J. D. Ranford, J. M. Waters, *Inorg. Chim. Acta* 267 (1998) 27.
25. J. Patole, U. Sandbhor, S. Padhye, D. N. Deobagkar, C. E. Anson, A. Powell, *Bioorg. Med. Chem. Lett.* 13 (2003) 51.
26. B. J. Hathaway, G. Wilkinson, R. D. Gillard, J. A. McCleverty, In *Comprehensive Coordination Chemistry* 5 (1987) 558.
27. N. Nawar, N. H. Hosny, *Chem. Pharm. Bull.* 47 (1999) 944.
28. R. Gup, B. Kirkan, *Spectrochim. Acta* 62A (2005) 1188.
29. M. F. Iskander, T. E. Khalil, R. Werner, W. Haase, I. Svoboda, H. Fuess, *Polyhedron* 19 (2000) 1181.
30. J. D. Ranford, J. J. Vittal, Y. M. Wang, *Inorg. Chem.* 37 (1998) 1226.
31. A. Syamal, K. S. Kale, *Indian J. Chem.* 16A (1978) 46.
32. P. B. Sreeja, M. R. P. Kurup, A. Kishore, C. Jasmin, *Polyhedron* 23 (2004) 575.
33. S. Dutta, P. Basy, A. Chakravorty, *Inorg. Chem.* 30 (1991) 4031.
34. J. E. Huheey, E. A. Keiter, R. L. Keiter, *Inorganic Chemistry, Principles of Structure and Reactivity*, 4th ed., Harper Collins College Publishers, New York, 1993.
35. D. N. Sathyanarayana, *Electronic Absorption Spectroscopy and Related Techniques*, Universities Press Publishers, India, 2001.
36. M. F. El. Shazly, L. S. Refaat, *Transition Met. Chem.* 6 (1981) 8.
37. A. B. P. Lever, *Inorganic Electronic Spectroscopy*, Elsevier, Amsterdam

- 1968.
38. L. Sacconi, M. Ciampolini, *J. Chem. Soc.* (1964) 276.
 39. B. J. Hathaway, A. A. G. Tomlinson, *Coord. Chem. Rev.* 5 (1970) 1.
 40. I. Bertini, D. Gattesem, A. Scozzafava, *Coord. Chem. Rev.* 29 (1979) 67.
 41. B. J. Hathaway, D. E. Billing, *Coord. Chem. Rev.* 5 (1970) 143.
 42. P. S. Zacharias, J. M. Elizabathe, A. Ramachandraiah, *Indian J. Chem.* 23A (1984) 26.
 43. B. Swamy, J. R. Swamy, *Transition Met. Chem.* 16 (1991) 35.
 44. J. C. Einstein, *J. Chem. Phys.* 28 (1958) 323.
 45. M. Maajan, K. N. Saxena, C. P. Saxena, *J. Inorg. Nucl. Chem.* 43 (1981) 2148.
 46. I. M. Procter, B. J. Hathaway, P. Nicholls, *J. Chem. Soc.* (1968) 1678.
 47. J. F. Villa, W. E. Hatfield, *Inorg. Chem.* 11 (1972) 1331.
 48. D. Kivelson, R. Neiman, *J. Chem. Phys.* 35 (1961) 149.
 49. A. H. Maki, B. R. McGarvey, *J. Chem. Phys.* 29 (1958) 35.
 50. A. Hudson, *J. Mol. Phys.* 10 (1966) 575.
 51. I. B. Bersuker, *Coord. Chem. Rev.* 14 (1975) 357.
 52. K. K. Sharma, S. Chandra, *Transition Met. Chem.* 9 (1984) 401.
 53. M. H. L. Pryce, K. P. Sinha, Y. Tanabe, *Mol. Phys.* 9 (1965) 164.

Structural and spectral investigations of Mn(II) complexes of heteroaroylhydrazones of nicotinoylhydrazide

The element manganese is relatively abundant, constituting about 0.085% of the earth's crust. Over 90% of all the manganese ores produced are used in steel manufacture, mostly in the form of ferromanganese. Although the primary use of manganese is in the production of steel it also finds widespread and important uses in non-metallurgical industries. The largest non-metallurgical use of manganese is in the manufacture of dry-cell batteries in the form of MnO_2 . Metal complexes of manganese play important roles ranging from bioinorganic chemistry to solid-state physics. Low nuclearity species have been studied extensively as models for the water-oxidizing complex in photosystem II, whereas nanometer-size clusters with high spin ground states are being investigated as single molecule magnets [1-3]. The chemistry of manganese, in various oxidation states of the metal and in various combinations of nitrogen and oxygen donor environment, is presently witnessing intense activity [4-7]. This is because manganese plays a major key role in many biological redox processes, including water oxidation complex in photosystem II [8, 9], decomposition of $O_2^{\cdot -}$ radicals catalysed by superoxide dismutases (SOD's) and disproportionation of hydrogen peroxide (catalase activity) in microorganisms, a reaction which is important for cell detoxification. In all these diverse biologically important roles of manganese, it is present either as mononuclear (SOD, manganese dioxygenase) or polynuclear species (WOC, tetranuclear), catalase and ribonucleotide reductase (binuclear). The coordination environment of the manganese atoms in biological systems is made up of N and O atoms, with more of the latter. There are a quite few reports

on Mn(II) complexes of NNO donor Schiff bases of aroylhydrazides in literature [10-19].

4.1. Stereochemistry

Manganese shows a wide range of oxidation states ranging from (-III) to (+VII). The divalent state is the most common and most stable oxidation state. The majority of Mn(II) complexes are high spin. The usually exhibited geometry is octahedral. However, the present compounds under study exhibits octahedral as well as tetrahedral stereochemistry.

4.2. Experimental

4.2.1 Materials

Nicotinoylhydrazide (Sigma Aldrich), 2-benzoylpyridine (Sigma Aldrich), pyridine-2-carbaldehyde (Sigma Aldrich), Mn(OAc)₂ (Merck), NaN₃ (Reidel-De Haen) and KSCN (BDH) were used as received. The solvent ethyl alcohol used was repeatedly distilled before use.

4.2.2 Syntheses of ligands

The ligands HL¹ and HL³ were prepared as described previously in Chapter 2.

4.2.3 Preparation of manganese(II) complexes

[Mn(L¹)(N₃)]·H₂O (9): To a solution of the ligand (0.302 g, 1 mmol) in ethanol, Mn(II) acetate (0.245 g, 1 mmol) dissolved in ethanol was added and stirred followed by addition of aqueous solution of NaN₃ (0.65 g, 1 mmol). The resulting solution was further stirred for 3 hours to obtain a pale yellow precipitate. It was then separated, washed with water, ethanol followed by ether and dried over P₄O₁₀ *in vacuo*. Yield: 0.243 g (58.3%). Elemental Anal. Found (Calcd.) (%): C, 51.49 (51.93); H, 3.75 (3.63); N, 23.41 (23.55).

[Mn(L¹)NCS]·1.5H₂O (10): Mn(II) acetate (0.245 g, 1 mmol) dissolved in ethanol was added to a solution of the ligand (0.302 g, 1 mmol) in ethanol, and stirred for 10 min. To this solution, KSCN (0.097 g, 1 mmol) was added and further stirred for 6 hours. The resulting solution was then concentrated on a water bath, cooled at room temperature and kept overnight. The pale brown solid formed was separated which was filtered, washed with ether and dried over P₄O₁₀ *in vacuo*. Yield: 0.245 g (55.5%). Elemental Anal. Found (Calcd.) (%): C, 51.70 (51.70); H, 3.69 (3.65); N, 15.30 (15.87).

[Mn(L¹)₂]·H₂O (11): Ethanolic solutions of the ligand (0.604 g, 2 mmol) and Mn(II) acetate (0.245 g, 1 mmol) in 2:1 ratio was refluxed for 3-4 hours. The reddish brown crystalline product obtained was filtered, washed with ethanol followed by ether and dried over P₄O₁₀ *in vacuo*. Yield: 0.364 g (53.9%). Elemental Anal. Found (Calcd.) (%): C, 64.18 (64.00); H, 4.34 (4.18); N, 16.84 (16.59).

[Mn(L³)N₃]·H₂O (12): The ligand (0.262 g, 1 mmol) was dissolved in ethanol. To this solution, Mn(II) acetate (0.245 g, 1 mmol) dissolved in ethanol was added by stirring. NaN₃ (0.650 g, 1 mmol) in aqueous media was added after 10 min. The resulting solution was stirred for 5 hours, and then concentrated on a water bath, cooled at room temperature and kept overnight. The yellowish brown solid formed was separated which was filtered, washed with ether and dried over P₄O₁₀ *in vacuo*. Yield: 0.171 g (50.2%). Elemental Anal. Found (Calcd.) (%): C, 42.17 (42.37); H, 2.94 (3.26); N, 28.33 (28.82).

[Mn(L³)NCS]·H₂O (13): Mn(II) acetate (0.245 g, 1 mmol) dissolved in ethanol was added to a solution of the ligand (0.262 g, 1 mmol) in ethanol, and stirred for 10 min. To this solution, KSCN (0.097 g, 1 mmol) was added by stirring to obtain a yellow solid, stirring was continued for 3 hours. The product was filtered, washed with ethanol followed by ether and dried over P₄O₁₀ *in vacuo*. Yield: 0.226 g (63.5%). Elemental Anal. Found (Calcd.) (%): C, 43.72 (43.83); H, 3.13 (3.11); N, 19.03 (19.66).

[Mn(L³)₂] (14): To a solution of the ligand (0.524 g, 2 mmol) in ethanol, Mn(II) acetate (0.245 g, 1 mmol) dissolved in ethanol was added and refluxed for 3-4 hours. The reddish brown crystalline product obtained was filtered, washed with ethanol followed by ether and dried over P₄O₁₀ *in vacuo*. Yield: 0.343 g (67.9%). Elemental Anal. Found (Calcd.) (%): C, 56.71 (57.04); H, 3.57 (3.59); N, 22.19 (22.17).

4.3. Results and discussion

Equimolar ratios of the ligand, metal salt and the additional anions resulted in complexes of stoichiometry, Mn(L)X, whereas reaction of ligand and metal salt in ratio 2:1 yielded metal complexes of formula Mn(L)₂. The colour of the compounds were found to be pale yellow and reddish brown respectively for Mn(L)X and Mn(L)₂ compounds. Magnetic susceptibility measurements of the compounds showed values in the range 5.6 – 6.2 B.M., which are indicative of a high spin *d⁵* system. All the complexes were found to be soluble in DMF and DMSO, but only partially soluble in other organic solvents such as CHCl₃, ethanol, methanol etc.

4.3.1 Crystal structure of [Mn(L¹)₂]

[Mn(L¹)₂]: The wine red colored diamond shaped crystals suitable for single crystal X-ray analysis was obtained from a solution of the compound in ethanol and DMF (1:1 v/v) mixture. The crystal is monoclinic in nature with P2₁ symmetry and stoichiometry Mn(L¹)₂ (Fig. 4.1). A summary of the key crystallographic information is given in Table 4.1. Selected bond lengths and bond angles are listed in Table 4.2. The environment around the Mn(II) ion is distorted octahedral which is evident from the bond angles, N(2)–Mn(1)–N(6) 165.21(8), O(2)–Mn(1)–O(1) 103.76(9), N(6)–Mn(1)–N(5) 70.61(8) revealing the departures from the ideal octahedral values. The two terdentate ligands chelate the central Mn(II) ion in the monoanionic form through the pyridine nitrogen, azomethine nitrogen and the enolate oxygen. The coordination mode of the

ligands around the central Mn(II) ion is meridional. The increase in bond length of C(13)–O(1) by 0.0512 Å, confirms the coordination of the ligand in the enolate form. The perpendicular existence of the two ligands is well established by the dihedral angle of 84.61° between the planes defined by the atoms Mn(1), N(1), C(5), C(6), N(2), N(3), C(13), O(1) and Mn(1), N(5), C(23), C(24), N(6), N(7), C(31), O(2). The Mn(II) ion is found to be displaced by 0.0153 Å from the plane constituted by the atoms N(1), N(5), O(1), O(2) with the maximum least square plane deviation at O(1) by 0.7329 Å. There are considerable differences in the dihedral angle separation between the aromatic rings of the ketone part in the two-ligand moieties. It is of value 66.25 and 55.43° correspondingly in the first and second ligand. The phenyl rings of the two ligands exist with a dihedral angle of 8.29°.

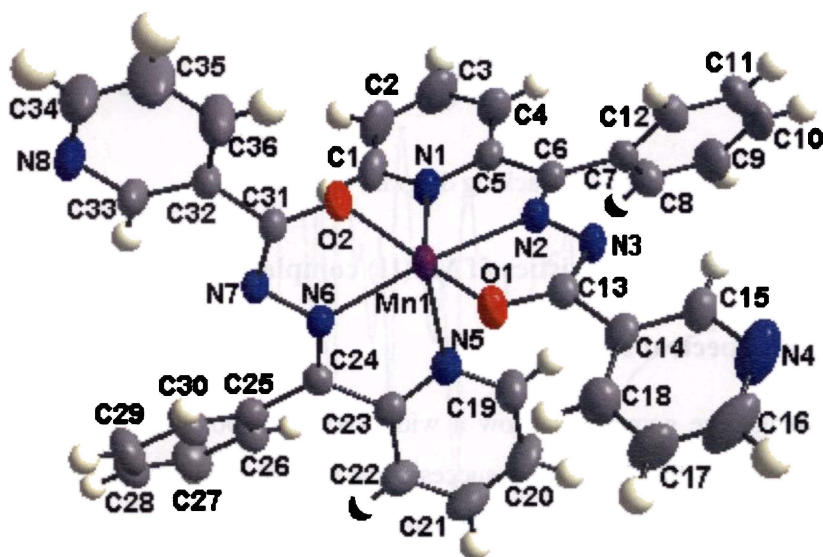


Fig. 4.1. Molecular structure of [Mn(L¹)₂]

The packing in the crystal lattice (Fig. 4.2) consists of sets of two molecules arranged in a regular fashion, which when repeated, one dimensionally forms a layer that is in an offset fashion to the adjacent layer. The π – π interactions and

hydrogen bonding interactions observed are rather weak. A list of C–H--- π interactions is listed in Table 4.3.

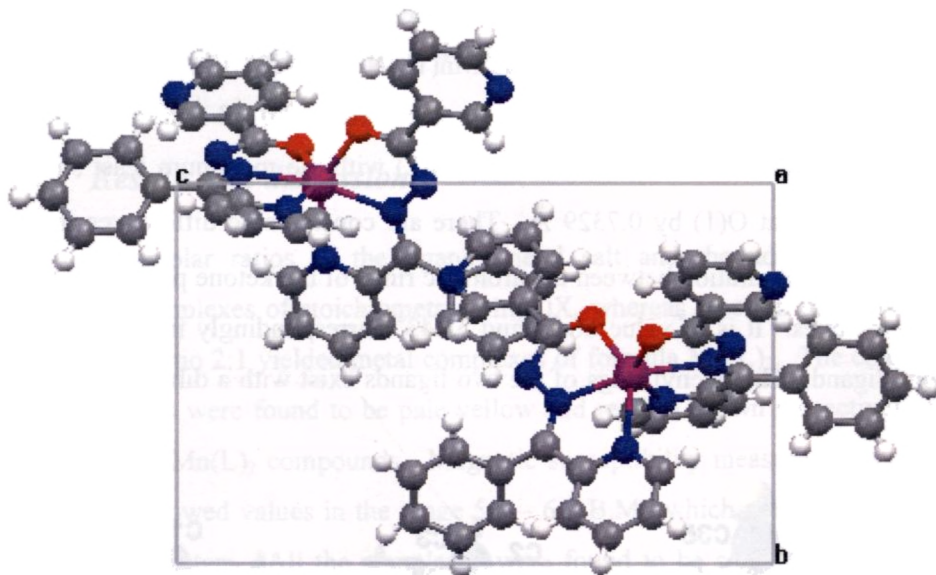


Fig. 4.2. Packing diagram of $[\text{Mn}(\text{L}^1)_2]$

4.3.2 Spectral characteristics of Mn(II) complexes

4.3.2a EPR spectral studies

Manganese complexes show a wide variety of bonding geometries and EPR spectroscopy has been used successfully to probe the structures of these compounds [20, 21]. The spin Hamiltonian for Mn(II) may be described as

$$\hat{H} = g\beta H_s + D[S_z^2 - S(S+1)/3] + E(S_x^2 - S_y^2) \quad (4.1)$$

where H is the magnetic field vector, D is the axial zero field splitting term, E is the rhombic zero field splitting parameter. If D and E are very small compared to $g\beta H_s$, five EPR transitions corresponding to $\Delta m_s = \pm 1$ are expected with a g value of 2.0. However, for the case where D or E is very large, the lowest doublet has

effective g values of $g_{\parallel} = 2$, $g_{\perp} = 6$ for $D \neq 0$ and $E = 0$ but for $D = 0$ and $E \neq 0$, the middle Kramers doublet has an isotropic g value of 4.29 [22-23].

The EPR spectrum of compound $[\text{Mn}(\text{L}^1)\text{N}_3] \cdot \text{H}_2\text{O}$ (**9**) at 298 K in polycrystalline state exhibited a broad signal with a g value at 2.106 with no hyperfine splittings. However, the solution spectrum in DMF at 77 K (Fig. 4.3), displayed a central hyperfine sextet with g_{iso} 2.002. The observance of hyperfine sextet is as expected due to the interaction of the unpaired electron with the Mn(II) nucleus of spin $I = 5/2$, resulting in $2nI + 1$ lines. Thus the six lines observed corresponds to $m_s = +5/2, +1/2, \dots, -5/2$ with $\Delta m_l = 0$.

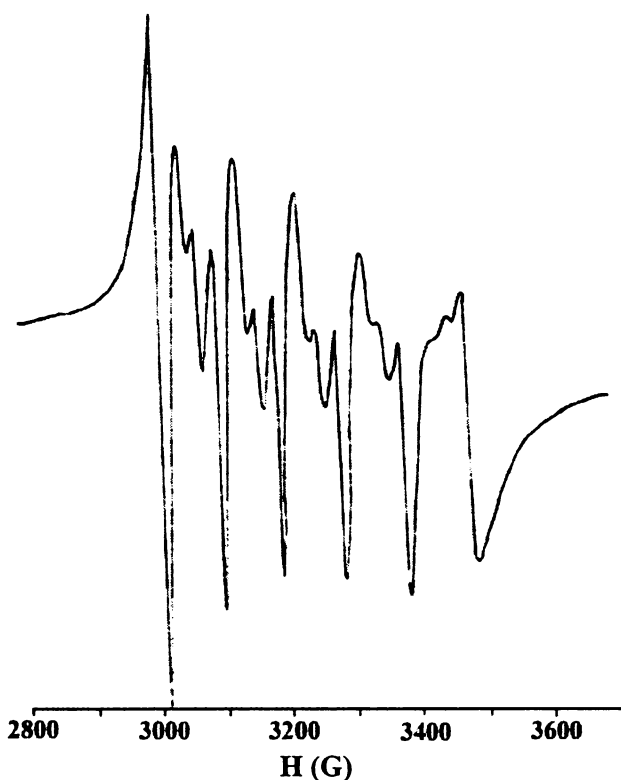


Fig. 4.3. EPR spectrum of $[\text{Mn}(\text{L}^1)\text{N}_3] \cdot \text{H}_2\text{O}$ in DMF at 77 K

A pair of low intensity lines is found in between each of the two main hyperfine lines. These are the forbidden lines corresponding to $\Delta m_l = \pm 1$,

transitions arising due to the nuclear quadrupole effect as the nuclear spin quantum number I is greater than 1. Thus the general selection rule for the transition, $\Delta m_s = \pm 1$, $\Delta m_l = 0$ is violated. The coupling constant A_{iso} , for the central sextet hyperfine lines is found to be 96 G.

The tetrahedral compound $[\text{Mn}(\text{L}^1)\text{NCS}] \cdot 1.5\text{H}_2\text{O}$ (**10**), exhibited a broad signal centered on $g_{iso}=2.012$ in polycrystalline state at 298 K. The frozen solution spectrum (Fig. 4.4) of the compound in DMF, displayed two g values, $g_1=1.998$ and $g_2=5.077$. Only the high field signal exhibited hyperfine splittings with a coupling constant of 93 G.

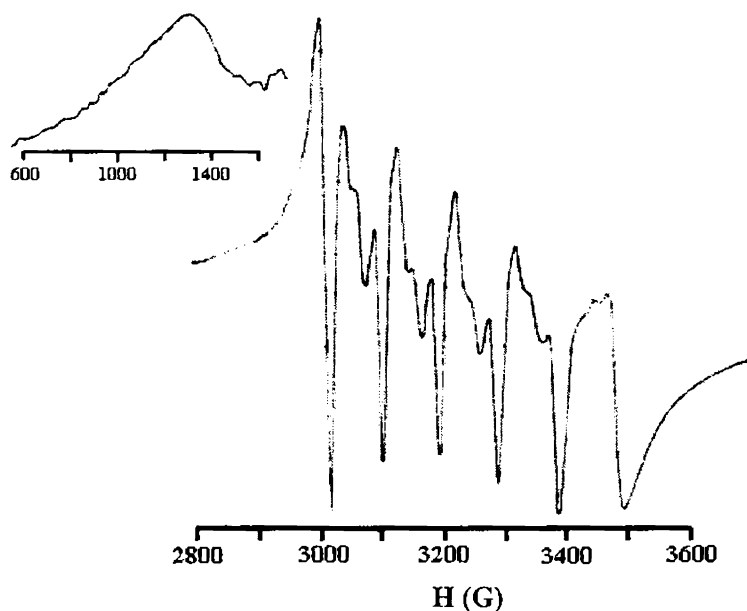


Fig. 4.4. EPR spectrum of $[\text{Mn}(\text{L}^1)\text{NCS}] \cdot 1.5\text{H}_2\text{O}$ (**10**) in DMF at 77 K

A broad isotropic signal with $g = 2.005$ was found for the compound $[\text{Mn}(\text{L}^1)_2] \cdot \text{H}_2\text{O}$ (**11**) in polycrystalline state at 298 K. The frozen solution EPR spectrum (Fig. 4.5) in DMF shows three g values $g_1=1.987$, $g_2=2.867$, $g_3=4.893$. The expected hyperfine sextet is found only for the signal in the high

field region. The coupling constant A_{iso} is found to be 92 G for the high field signal.

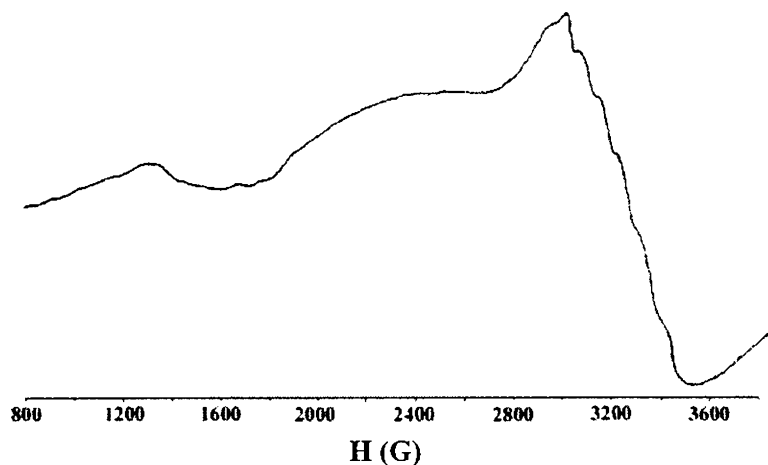


Fig. 4.5. EPR spectrum of $[\text{Mn}(\text{L}^1)_2] \cdot \text{H}_2\text{O}$ (**11**) in DMF at 77 K

The azido $[\text{Mn}(\text{L}^3)\text{N}_3] \cdot \text{H}_2\text{O}$ (**12**) and the thiocyanato $[\text{Mn}(\text{L}^3)\text{NCS}] \cdot \text{H}_2\text{O}$ (**13**) compounds of the ligand HL^3 exhibit the same EPR spectral features as that of the corresponding compound analogues of HL^1 . But the thiocyanato compound exhibited only one signal for the spectrum recorded in DMF at 77 K. The central hyperfine sextet was observed at 1.999 and 1.996 respectively for **12** and **13** for the frozen solution spectra (Figs. 4.6 and 4.7). The hyperfine coupling constants were also found to be in the same range as reported above. However, the spectrum at polycrystalline state of the azido compound, displayed three g values viz. $g_1 = 6.280$, $g_2 = 3.17$, $g_3 = 2.302$ with no hyperfine splittings.

The octahedral compound $[\text{Mn}(\text{L}^3)_2]$ (**14**) of HL^3 , displayed a broad isotropic signal for the spectrum recorded in polycrystalline state at 298 K, $g_{iso} \approx 1.990$. Compared to the above-discussed six-coordinate compound **11**, the present compound featured only two g values viz. 1.981 and 5.26 for the frozen spectrum (Fig. 4.8) in DMF. The A_{iso} value calculated for the hyperfine sextet in the high field region is 80 G.

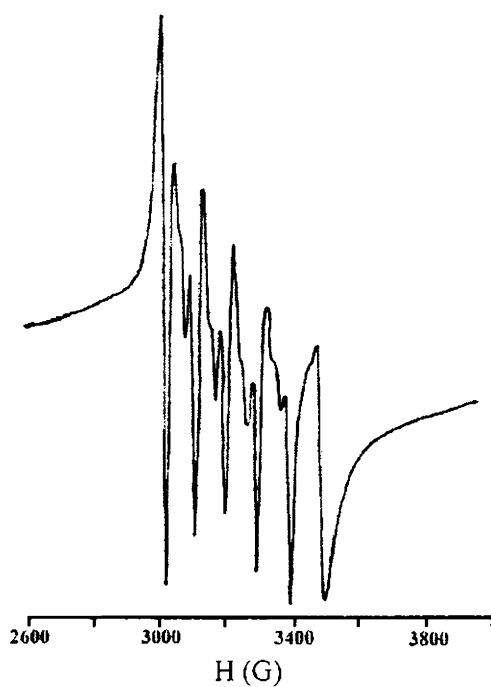


Fig. 4.6. EPR spectrum of $[\text{Mn}(\text{L}^3)\text{N}_3]\cdot\text{H}_2\text{O}$ (**12**) in DMF at 77 K

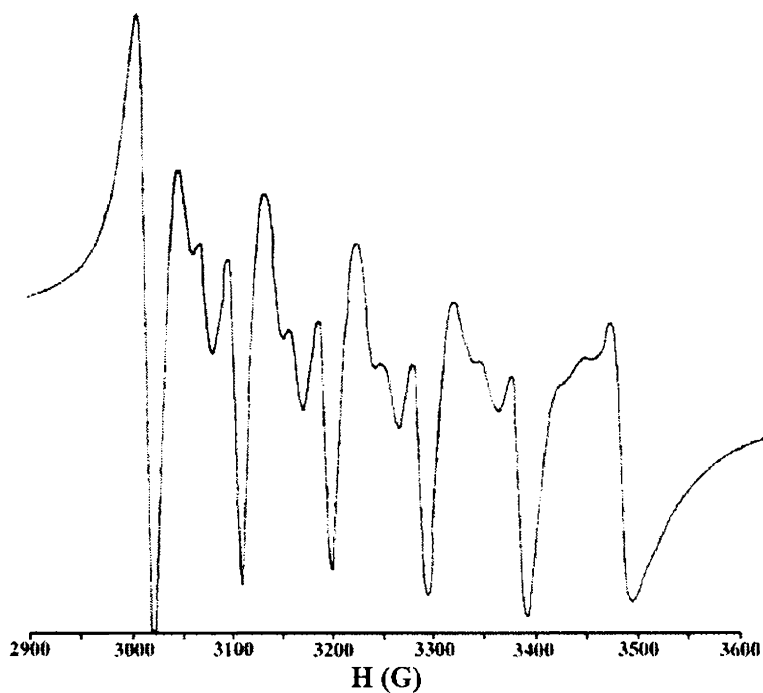


Fig. 4.7. EPR spectrum of $[\text{Mn}(\text{L}^3)\text{NCS}]\cdot\text{H}_2\text{O}$ (**13**) in DMF at 77 K

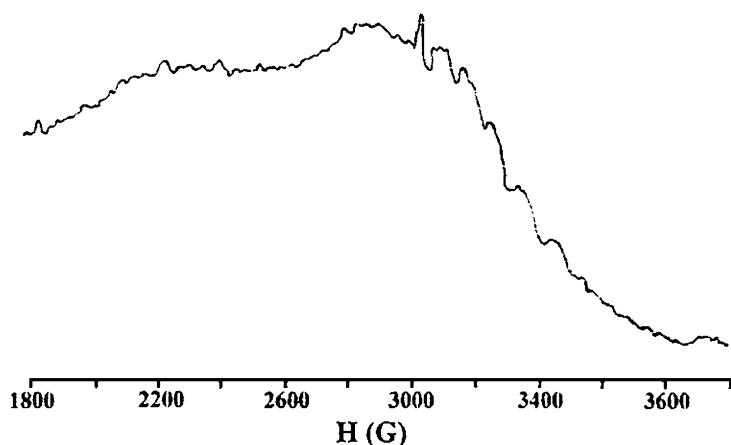


Fig. 4.8. EPR spectrum of $[\text{Mn}(\text{L}^3)_2]$ (**14**) in DMF at 77 K

4.3.2b IR spectral studies

A comparison of the IR spectra of the ligands and the complexes revealed significant variations in the characteristic bands due to coordination with the central metal ion. It was found that absorption bands attributed to $\nu(\text{C}=\text{O})$ and $\nu(\text{N}-\text{H})$ in the free ligands, disappeared in the complexes, due to coordination through enolate oxygen. The shifting of the azomethine ($\text{C}=\text{N}$) band to a lower frequency is attributed to the conjugation of the p-orbital on the double bond with the d-orbital on the metal ion with reduction of the force constant.

The broad band observed at 3420 cm^{-1} evidences the presence of lattice water in compound $[\text{Mn}(\text{L}^1)\text{N}_3]\cdot\text{H}_2\text{O}$ (**9**). The band at 1589 cm^{-1} is assigned to the $-\text{C}=\text{N}-\text{N}=\text{C}-$ moiety, newly formed as a result of deprotonation of the ligand for coordination. The azomethine band suffered a negative shift and is observed at 1556 cm^{-1} . The sharp bands viewed at 1506 and 1457 cm^{-1} are due to the aromatic ring vibrations. The antisymmetric sharp band characteristic of azido group appears at 2071 cm^{-1} . The absence of splitting in this band, confirms that the azido group is nonbridging in nature. A new band observed at 1367 cm^{-1} , is assigned to the $\nu(\text{C}-\text{O})$ stretch.

Compound $[\text{Mn}(\text{L}^1)\text{NCS}] \cdot 1.5\text{H}_2\text{O}$ (**10**) consisting of isothiocyanato group, shows the presence of lattice water by the appearance of a broad band at 3416 cm^{-1} (Fig. 4.9). The azomethine band is shifted to 1556 cm^{-1} due to binding with the metal ion. The newly formed $-\text{C}=\text{N}-$ bond is viewed at 1602 cm^{-1} . The aromatic ring vibrations are found in the usual range. The band observed at 1372 cm^{-1} is assigned to the amide III band. Coordination of isothiocyanato group through nitrogen atom is evidenced by the appearance of the band at 2062 cm^{-1} , since the characteristic bands formed due to sulfur coordination are observed at 2150 cm^{-1} [24].

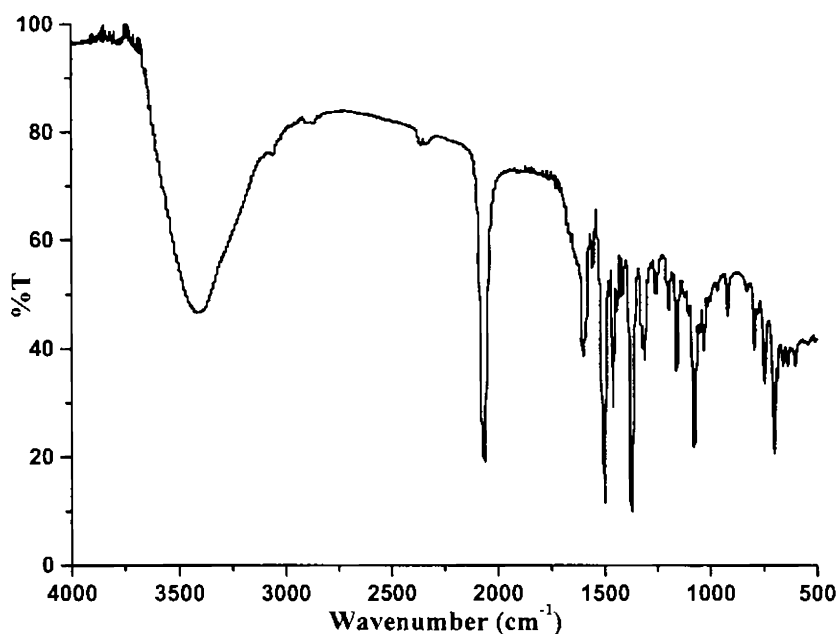


Fig. 4.9. IR spectrum of compound $[\text{Mn}(\text{L}^1)\text{NCS}] \cdot 1.5\text{H}_2\text{O}$

The IR spectrum of compound $[\text{Mn}(\text{L}^1)_2] \cdot \text{H}_2\text{O}$ (**11**), shows a sharp band at 1579 cm^{-1} corresponding to the $-\text{C}=\text{N}-\text{N}=\text{C}-$ moiety. The azomethine band is observed at 1544 cm^{-1} . The band obtained at 1363 cm^{-1} is due to the enolate oxygen formed by deprotonation. The aromatic ring vibrations occur at 1498 and 1458 cm^{-1} . Compound $[\text{Mn}(\text{L}^3)\text{N}_3] \cdot \text{H}_2\text{O}$ (**12**) consisting of the azido group shows

the characteristic antisymmetric vibration of azido moiety at 2073 cm^{-1} . Here also, the band is not split. The other vibrations are found in the usual range, with bands due to enolic stretch at 1367 and azomethine at 1561 cm^{-1} (Fig. 4.10).

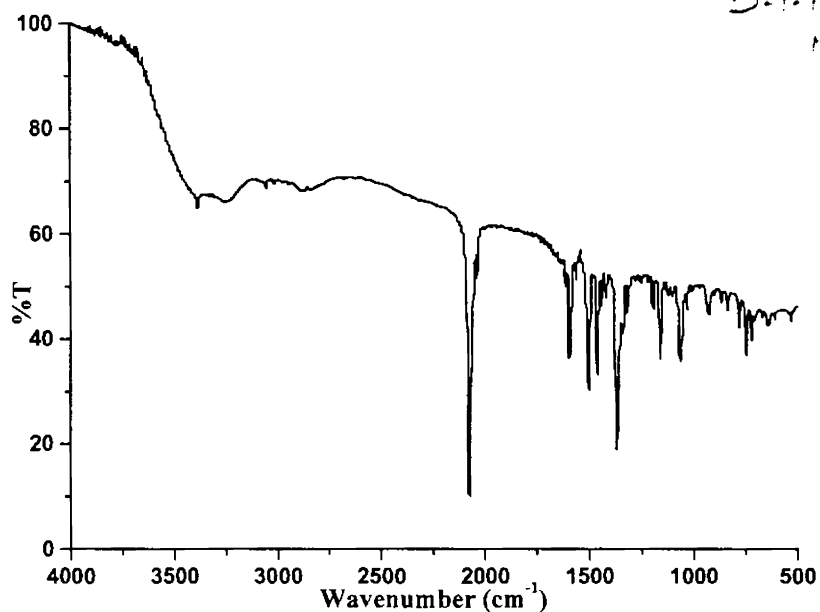


Fig. 4.10. IR spectrum of compound $[\text{Mn}(\text{L}^3)\text{N}_3]\cdot\text{H}_2\text{O}$

The IR spectrum of compound $\text{Mn}(\text{L}^3)\text{NCS}\cdot\text{H}_2\text{O}$ (**13**), (Fig.4.11) shows the presence of lattice water as a broad band at 3392 cm^{-1} . The band due to isothiocyanato group is assigned at 2081 cm^{-1} , exhibiting coordination *via* nitrogen atom. The $\nu(\text{C}-\text{O})$ is observed at 1364 and the band due to $-\text{C}=\text{N}-\text{N}=\text{C}-$ moiety at 1601 cm^{-1} . The octahedral compound $\text{Mn}(\text{L}^3)_2$ (**14**), displayed its $-\text{C}=\text{N}-\text{N}=\text{C}-$ band at 1592 cm^{-1} . The band due to enolic stretch was observed at 1362 cm^{-1} . The azomethine band due to coordination with the $\text{Mn}(\text{II})$ is shifted to 1540 cm^{-1} . The characteristic ring vibrations were seen in the usual region.

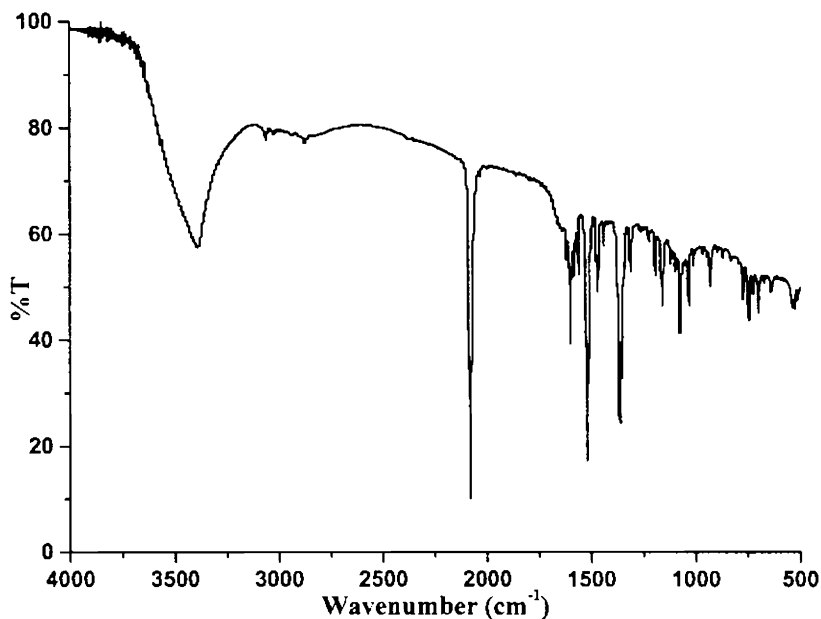
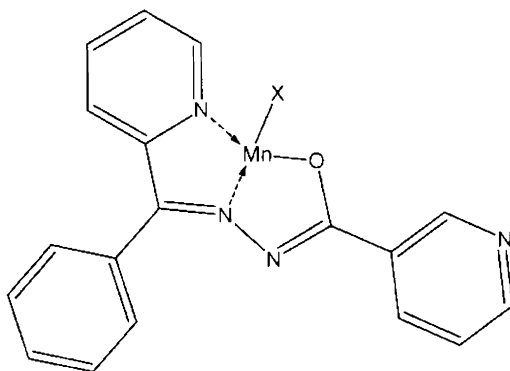


Fig. 4.11. IR spectrum of compound $[\text{Mn}(\text{L}^3)\text{NCS}] \cdot \text{H}_2\text{O}$

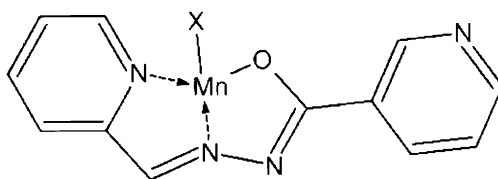
4.3.2c Electronic spectral studies

The ground state of tetrahedral and high-spin octahedral Mn(II) complex is ${}^6A_{1g}$. As there are no other terms of sextet spin multiplicity, spin allowed d-d transitions are not expected. However, some forbidden transitions occur such as ${}^6A_{1g} \rightarrow {}^4A_{1g}(G), {}^4E_g(G), {}^6A_{1g} \rightarrow {}^4E_g(D), {}^6A_{1g} \rightarrow {}^4T_{1g}(G), {}^4T_{2g}(G)$. Also for octahedral complexes, transitions are Laporte forbidden. Thus doubly forbidden transitions are extremely weak. In the present compounds, d-d bands could not be identified due to their low intensity. All the compounds possessed high intense bands in the region $26670 - 23530 \text{ cm}^{-1}$. The absorption bands found for the complexes under study are listed in Table 4.4.

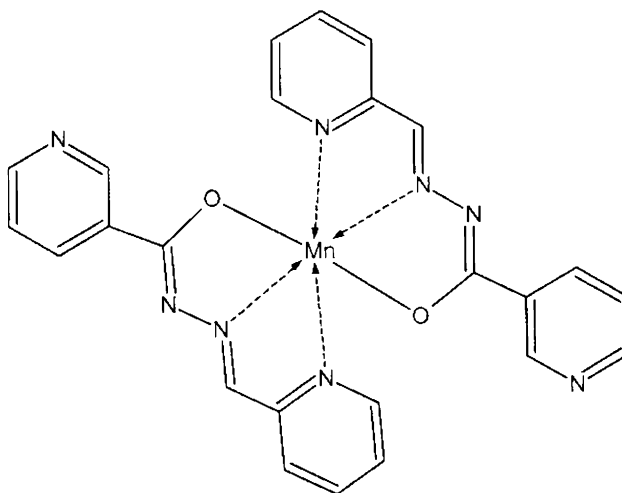
Based on the elemental analyses and spectral studies following tentative structures were assigned for the complexes.



Compounds **9** and **10** (X = N₃, NCS)



Compounds **12** and **13** (X = N₃, NCS)



Compound **14**

Table 4.1
Crystal data and structure refinement of $[\text{Mn}(\text{L}^1)_2]$

Parameters	$[\text{Mn}(\text{L}^1)_2]$
Empirical formula	$\text{C}_{36}\text{H}_{26}\text{MnN}_8\text{O}_2$
Formula weight	657.59
Crystal colour	Wine Red
Crystal habit	Diamond
Crystal system	Monoclinic
Space group	$P2_1$
Unit cell dimensions	
a (Å)	9.5454(9)
b (Å)	10.3236(10)
c (Å)	16.6630(16)
α (°)	90.00
β (°)	100.962(2)
γ (°)	90.00
Volume V (Å ³). Z	1612.1(3), 2
Calculated density (ρ) (Mg m ⁻³)	1.355
Absorption coefficient μ (mm ⁻¹)	0.456
$F(000)$	678
Crystal size (mm)	0.28 x 0.12 x 0.07
θ range for data collection	2.17 - 28.30
Index ranges	$-12 \leq h \leq 11$, $-13 \leq k \leq 11$, $-20 \leq l \leq 22$
Reflections collected / unique	9625 / 5974 [R(int) = 0.0203]
Refinement method	Full-matrix least-squares on F^2
Data / restraints / parameters	5974 / 1 / 421
Goodness-of-fit on F^2	1.062
Final R indices [$I > 2\sigma(I)$]	R1 = 0.0506, wR2 = 0.1240
R indices (all data)	R1 = 0.0570, wR2 = 0.1277

Table. 4.2

Selected bond lengths (Å) and bond angles (°) of $[\text{Mn}(\text{L}^1)_2]$

Bonds	
Mn1–O2	2.1141(19)
Mn1–O1	2.136(2)
Mn1–N2	2.202(2)
Mn1–N6	2.219(2)
Mn1–N5	2.273(2)
Mn1–N1	2.297(3)
C13–N3	1.337(4)
N2–N3	1.376(3)
C13–O1	1.267(3)
C6–N2	1.293(4)
Bond angles	
O2–Mn1–O1	103.76(9)
O2–Mn1–N2	120.55(8)
O1–Mn1–N2	72.16(8)
O2–Mn1–N6	71.81(7)
O1–Mn1–N6	114.60(8)
N2–Mn1–N6	165.21(8)
O2–Mn1–N5	142.21(8)
O1–Mn1–N5	88.42(9)
N2–Mn1–N5	97.21(9)
N6–Mn1–N5	70.61(8)
O2–Mn1–N1	93.77(9)
O1–Mn1–N1	143.59(8)
N2–Mn1–N1	71.44(8)
N6–Mn1–N1	101.06(8)
N5–Mn1–N1	97.02(9)
C6–N2–N3	119.8(2)
O1–C13–N3	127.1(3)
N2–C6–C5	114.4(2)

Table. 4.3

C-H--- π interaction parameters of the compound [Mn(L¹)₂]

X-H---Cg(J)	H---Cg (Å)	X-H---Cg (°)	X---Cg (Å)
C(9)–H(9)---Cg(6) ^a	2.98	161	3.8651
C(19)–H(19)---Cg(1) ^b	2.72	110	3.1599
C(27)–H(27)---Cg(2) ^c	2.71	139	3.4734

Equivalent position code: a = x, 1+y, z; b = x, y, z; c = -x, 1/2+y, -z
 Cg(1) = Mn1, O1, C13, N3, N2; Cg(2) = Mn1, O2, C31, N7, N6 and
 Cg(6) = N4, C15, C14, C18, C17, C16

Table. 4.4

Electronic spectral data for Mn(II) complexes

Compounds	n→ π^* (cm ⁻¹)	π → π^* (cm ⁻¹)
HL ¹	31340	37040
[Mn(L ¹)N ₃]·H ₂ O (9)	32470 (sh)	37310
[Mn(L ¹)NCS]·1.5H ₂ O (10)	32050	37740
[Mn(L ¹) ₂]·H ₂ O (11)	32260	35710
HL ³	31440	33780
[Mn(L ³)N ₃]·H ₂ O (12)	33110	38020
[Mn(L ³)NCS]·H ₂ O (13)	32570	37730
[Mn(L ³) ₂] (14)	33000	37590

References

1. P. D. W. Boyd, Q. Li, J. B. Vincent, K. Folting, R. H. -Chang, W. E. Streib, J. B. Huffman, G. Christou, D. N. Hendrickson, *J. Am. Chem. Soc.* 110 (1988) 8537.
2. K. Fegy, D. Luneau, E. Belorizky, M. Novac, J. -L. Tholence, C. Paulsen, T. Ohm, P. Rey, *Inorg. Chem.* 37 (1998) 4524.
3. M. W. Wemple, L. H.- Tsai, W. E. Streib, D. N. Hendrickson, G. Christou, *J. Chem. Soc. Chem. Commun.* (1994) 1031.
4. K. Weighardt, *Angew. Chem., Int. Ed. Engl.* 28 (1989) 1153.
5. V. K. Yachandra, *Chem. Rev.* 96 (1996) 2927.
6. M. Yagi, M. Kaneko, *Chem. Rev.* 101 (2001) 21.
7. G. C. Dismukes, *Chem. Rev.* 96 (1996) 2909.
8. C. Tommos, G. T. Babcock, *Acc. Chem. Res.* 31 (1998) 18.
9. A. Zouni, H. T. Witt, J. Kern, P. Formme, N. Kraub, W. Saenger, P. Orth, *Nature* 409 (2001) 739.
10. C. M. Armstrong, P. V. Bernhardt, P. Chin, D. R. Richardson, *Eur. J. Inorg. Chem.* (2003) 1145.
11. Y. J. Jang, Uk Lee, B. K. Koo, *Bull. Korean Chem. Soc.* 26 (2005) 925.
12. R. C. Maurya, P. Patel, D. Sutradhar, *Synth. React. Inorg. Met.-Org. Chem.* 33 (2003) 1857.
13. P. V. Bernhardt, J. Mattsson, D. R. Richardson, *Inorg. Chem.* 45 (2006) 752.
14. P. Cheng, D. Liao, S. Yan, Z. Jiang, G. Wang, *Polyhedron* 14 (1995) 2355.
15. M. R. Bermejo, M. Fondo, A. M. Gonzalez, O. L. Hoyos, A. Sousa, C. A. McAuliffe, W. Hussain, R. Pritchard, V. M. Novotorsev, *J. Chem. Soc. Dalton Trans.* (1999) 2211.
16. S. Naskar, S. Biswas, D. Mishra, B. Adhikary, L. R. Falvello, T. Soler, C. H. Schwalbe, S. K. Chattopadhyay, *Inorg. Chim. Acta* 357 (2004) 4257.
17. N. Nawar, N. M. Hosny, *Chem. Pharm. Bull.* 47 (1999) 944.

18. A. El. Mottaleb, M. Ramadan, I. M. El-Mehasseb, *Transition Met. Chem.* 23 (1998) 183.
19. M. Carcelli, P. Mazza, C. Pelizzi, G. Pelizzi, F. Zani, *J. Inorg. Biochem.* 57 (1995) 43.
20. R. Luck, R. Stosser, O. G. Poluektov, O. Ya. Grinberg, S. Ya. Lebedev, G. M. Woltermann, J. R. Wasson, *Inorg. Chem.* 12 (1973) 2366.
21. E. Meirovitch, R. Poupko, *J. Phys. Chem.* 82 (1978) 1920.
22. B. S. Garg, M. R. P. Kurup, S. K. Jain, Y. K. Bhoon, *Transition Met. Chem.*, 13 (1988) 92.
23. K. B. Pandeya, R. Singh, P. Mathur, R. P. Singh, *Transition Met. Chem.* 11 (1986) 347.
24. K. Nakamoto in *Infrared and Raman Spectra of Inorganic and Coordination Compounds*, 4th ed., John Wiley & Sons, New York, 1986.

Vanadium complexes of 2-benzoylpyridine heteroaroylhydrazones: Syntheses, structural and spectral investigations

The study of the biochemical role of vanadium has become recently a hot topic of bioinorganic chemistry particularly due to the presence of this element in significant amounts in some organisms and its involvement in both promotory and inhibitory enzymatic processes in biological systems [1, 2]. The revelation, that the vanadium coordination compounds play an important role in nitrogen activation, fixation and other biologically important reactions [3, 4] have stimulated the interest in the stereochemistry and reactivity of its coordination compounds that contain the diazo and hydrazido group because they may provide some understanding of the mechanism of metalloenzymatic reduction of dinitrogen.

Constituting 0.015% of earth's crust, vanadium is about as abundant as zinc. Vanadium is actually the second most abundant transition metal in sea water. The concentration of vanadium in sea water is comparatively high, which contains vanadate(V), in the form of contact ion pairs $\text{Na}^+\text{H}_2\text{VO}_4^-$ [5]. Cationic V^{V} species such as VO^{3+} or VO_2^+ are stable in solution around pH 7 only when coordinated to sufficiently strong ligands, which prevent precipitation of hydroxides. The same is true for VO^{2+} , the predominant species under anaerobic physiological conditions. Vanadate is a well-established inhibitor for phosphate metabolizing enzymes, e.g. phosphatases, kinases and ribonucleases. But can also stimulate specific enzymes such as phosphomutases and isomerases [6]. Medicinal applications of vanadium compounds have focused on their *in vitro* and *in vivo* activity in the treatment of insulin deficiency, type 1 diabetes and insulin tolerance, type 2 diabetes. The effects caused by vanadium compounds are

usually referred to as insulin-mimetic effect. They encompass the stimulation of glucose intake into cells and thus lowering of the blood glucose level. For various groups of vanadium compounds, anticarcinogenic potency towards experimentally induced tumors has been noted. These compounds encompass organic vanadium compounds, particularly vanadocene dichloride [Cp_2VCl_2], which is active against animal tumors such as the Ehrlich ascites tumor and certain types of leukemia, with an activity comparable to cis platin.

In haloperoxidase enzymes, vanadium(V) has been found to be present as a mononuclear unit in the resting state. Synthetic reactions between $[\text{VO}(\text{acac})_2]$ and dibasic tridentate ligands have yielded dinuclear structures [7, 8], however use of a sterically demanding monobasic tridentate ligand has yielded a mononuclear species with a VN_2O_3 core which is proposed as a model for the transition state analog-RNase inhibitor [9]. Involvement of vanadate at the catalytic site of ribonuclease T1 through *ca.* eleven hydrogen bonds is an interesting crystal feature and needs further study to clarify the role of such a structure in its biological activity [10].

All this clearly indicates the need for the development of small molecular vanadium analogues to understand more clearly the role of vanadium in its various oxidation states relevant to biological processes.

5.1. Stereochemistry

Vanadium exists in a plethora of oxidation states; easily switching between the oxidation states IV and V, along with III are the oxidation states of naturally occurring vanadium compounds. Complexes of vanadium usually adopt five-coordinate square pyramidal or six-coordinate distorted octahedral or trigonal bipyramidal geometries. However, the usual geometries are square pyramid and octahedron, which suggest that electronic and steric requirements preclude the achievement of the trigonal bipyramidal stereochemistry.

5.2. Experimental

5.2.1 Materials

2-Benzoylpyridine (Sigma Aldrich), nicotinoylhydrazide (Sigma Aldrich), 4-hydroxybenzhydrazide (Fluka), VO(acac)₂ (Merck) and dimethylformamide were used as received. When the solvent used was ethyl alcohol, it was repeatedly distilled before use.

5.2.2 Syntheses of ligands

Preparation of the ligands HL¹ and H₂L² were done as described previously in Chapter 2.

5.2.3 Preparation of oxovanadium(IV) and (V) complexes

[VO(L¹)OCH₃]-0.14 H₂O (15): HL¹ (0.302 g, 1 mmol) was dissolved in methanol and refluxed with a solution of VO(acac)₂ (0.265 g, 1 mmol) in dimethylformamide for 6 hours. Reddish orange crystalline product separated out, which was filtered, washed with methanol, followed by ether and dried over P₄O₁₀ *in vacuo*. Yield: 0.27 g (68.8%). Elemental Anal. Found (Calcd.) (%): C, 56.05 (56.72); H, 3.46 (4.09); N, 13.98 (13.93).

[VO(HL²)(μ₂-O)]₂ (16): To the ligand solution H₂L² (0.317 g, 1 mmol) in DMF-methanol mixture, metal salt VO(acac)₂ (0.265 g, 1 mmol) dissolved in dimethylformamide, was added and refluxed for 6 hours. The resulting deep brown solution was concentrated to half its volume and kept for evaporation. Reddish brown needle like product separated out, which was filtered, washed by ether and dried over P₄O₁₀ *in vacuo*. Yield: 0.20 g (51%). Light yellow block shaped crystals suitable for diffraction were grown from a solution of the compound in methanol-DMF mixture. Elemental Anal. Found (Calcd.) (%): C, 57.05 (57.15); H, 3.46 (3.53); N, 10.66 (10.52).

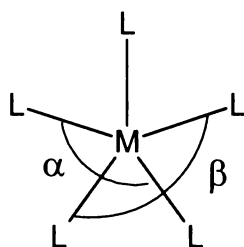
5.3. Results and discussion

When salts of V(V) or V(IV) in aerobic condition are treated with dibasic tridentate ligands, dioxovanadium complexes are possible products. Monobasic tridentate ligands favor formation of neutral mononuclear dioxovanadium(V) complexes provided dimerisation is prevented on steric grounds [9]. Here in the present case, reaction of equimolar ratios of the tridentate ligands and the metal salt yielded mononuclear oxovanadium(IV) (15) with HL^1 and dimeric oxovanadium(V) (16) compound with H_2L^2 . The compound (15) due to aerial oxidation, oxidized to dioxovanadium compound during crystal formation.

5.3.1 Crystal structures of $[VO_2(L^1)]$ and $[VO(HL^2)(\mu_2-O)]_2 \cdot 2H_2O$

$[VO_2(L^1)]$: Yellow block shaped crystals suitable for X-ray diffraction were grown from a solution of the compound (15) in a mixture of methanol and DMF (1:1 v/v). The compound crystallized into a monoclinic lattice with $P2_1/c$ symmetry. The crystal data and structural refinement parameters are given in Table 5.1. The ligand deprotonates and acts as a tridentate chelating species forming two five membered chelate rings. The oxygen atoms satisfy the other two sites of the square pyramid (Fig. 5.1). Thus the compound exists in the VO_2^+ state. Comparing the bond angles, it is evident that the geometry is considerably distorted, with the axial site taken up by one of the terminal oxo atom O(2) of the VO_2 core. The $V=O_{\text{apical}}$ distance 1.606(2) is not exceptional [11-12]. The C(13)-O(1) bond length due to deprotonation extends to 1.307(3) Å in the complex from 1.2158(15) Å in the ligand, making the V(1)-O(1) distance, 1.969(2) Å. The V(1)=O(3) distance corresponds to 1.6495(19) Å. The selected bond lengths and bond angles are presented in Table 5.2. The trans angles O(3)-V(1)-N(2) $148.27(10)^\circ$ and O(1)-V(1)-N(1) $145.99(8)^\circ$ are reasonably compressed. As a result, the basal plane constituted by atoms O(3), O(1), N(1) and N(2) deviates significantly from planarity with the central vanadium atom shifted by 0.7041 Å from this plane towards the apical oxygen atom O(2).

Trigonal bipyramidal geometries are actually rare for five coordinated vanadium compounds which usually tend to adopt a more or less distorted square pyramidal configuration. The extent to which either geometry is acquired can be quantified by the trigonality index τ [$\tau = (\alpha - \beta)/60$], which determines the in-plane angular distortion (Scheme 5.1). While $\tau = 0$ for an ideal square pyramidal geometry, $\tau = 1$ for the ideal trigonal bipyramidal geometry [13]. The τ parameter calculated for the vanadate complex 0.038 [$\alpha = \text{O}(3)\text{-V}(1)\text{-N}(2)$, 148.27 and $\beta = \text{N}(1)\text{-V}(1)\text{-O}(1)$, 145.99] indicates that the coordination geometry around the vanadium atom is distorted square pyramid.



Scheme 5.1.

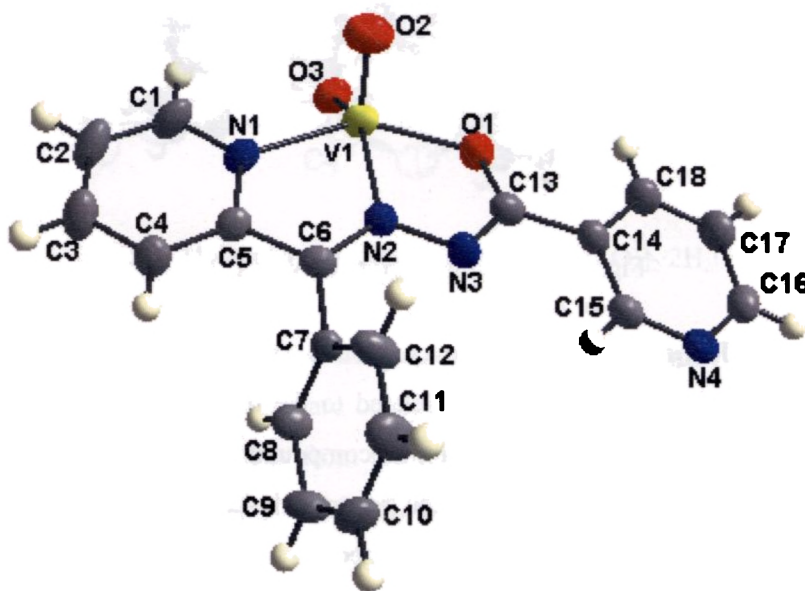


Fig. 5.1. Molecular structure of $[\text{VO}_2(\text{L}^1)]$

The packing of the molecules (Fig. 5.2) is such that the adjacent molecules in a set acquire an offset fashion, such that the VO_2^+ moieties of two molecules point in opposite directions. No classic hydrogen bonds are observed and the Cg–Cg interactions viewed are weak due to the comparatively higher distance of 4.00 Å. There exists a $\text{V}(1)\text{--Cg}(2)^i$ ring metal interaction at a metal centroid distance of 3.899 Å [$\text{Cg}(2)$: V(1), N(1), C(5), C(6), N(2); $i = 1-x, 1-y, 1-z$]. A weak $\text{C}\text{--H}\text{---}\pi$ interaction is found between $\text{C}(8)\text{--H}(8)\text{---Cg}(4)^{ii}$ at $d_{\text{C}(8)\text{---Cg}(4)} = 3.483$ Å [$\text{Cg}(4)$: N(4), C(15), C(14), C(18), C(17), C(16); $ii = 1+x, y, z$]. Other two interactions viewed are $\text{V}(1)\text{--O}(3)\text{---Cg}(1)^{iii}$ [$\text{Cg}(1)$: V(1), O(1), C(13), N(3), N(2); $d_{\text{V}(1)\text{---Cg}(1)} = 4.0495(12)$; $iii = 1-x, 1-y, 1-z$] and $\text{V}(1)\text{--O}(3)\text{---Cg}(2)^{iii}$ [$d_{\text{V}(1)\text{---Cg}(2)} = 3.8989(12)$].

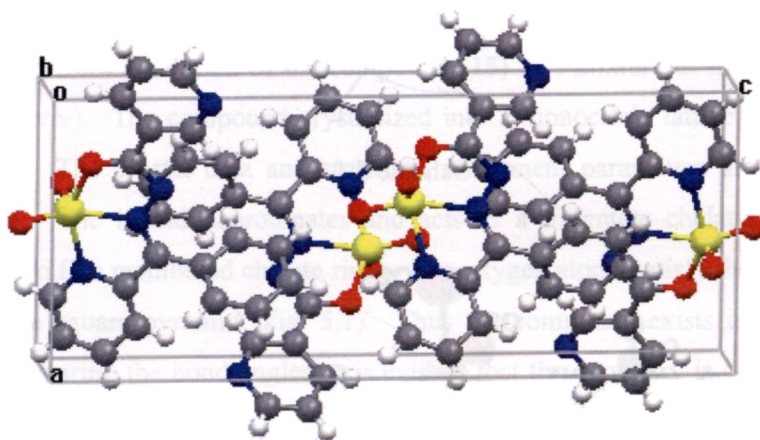


Fig. 5.2. Packing diagram of $\text{VO}_2(\text{L}^1)$

$[\text{VO}(\text{HL}^2)(\mu_2\text{-O})]_2 \cdot 2\text{H}_2\text{O}$: The compound crystallized into a dimer in which the one half of the molecule is related to the other half by an inversion centre [symmetry code: $2-x, -y, -z$]. A similar compound with a thiosemicarbazone derived from 2-benzoylpyridine has been reported [14]. The centrosymmetric dimer is formed *via* the bridging oxygens connecting two vanadium atoms. Hence the vanadium atom adopts a distorted octahedral geometry (Fig. 5.3). For dimeric vanadium chelates with an oxo bridging core, five configurations are possible in

accordance with the orientation of the vanadyl groups with respect to the plane defined by the vanadium centers and the bridging oxygen atoms [15]. The configurations are *syn*-orthogonal, *anti*-orthogonal, *syn*-coplanar, *anti*-coplanar and twist. The present compound with the inversion centre, reveals that the disposition of the oxovanadium groups is *anti*-coplanar, a configuration usually found in dimeric oxovanadium compounds [16, 17]. The crystal data and structural refinement parameters are given in Table 5.1.

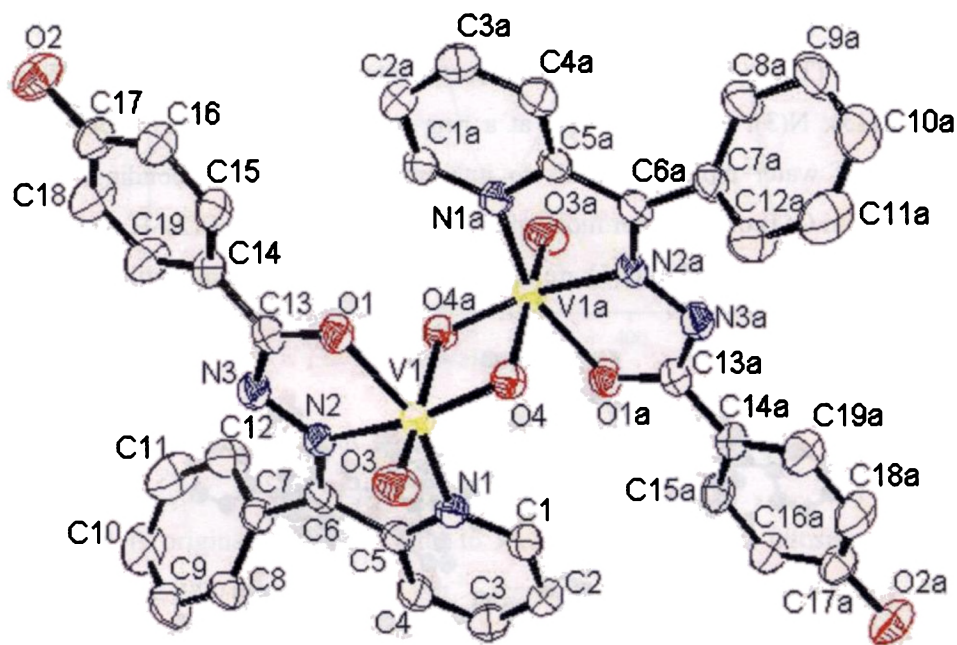


Fig. 5.3. Molecular structure of $[\text{VO}(\text{HL}^2)(\mu_2\text{-O})]_2 \cdot 2\text{H}_2\text{O}$

The atoms O3, N2 and the bridging oxygen atoms constitute the equatorial plane, while the axial positions are occupied by the pyridyl nitrogen and enolic oxygen. Prominent deviations from the regular octahedron is evident from the bond angles O(1)–V(1)–N(1) 146.59(8), O(4)–V(1)–N(2) 152.75(10). The two five membered rings [Cg(2): V(1)–N(1)–C(5)–C(6)–N(2) and Cg(1): V(1)–O(1)–C(13)–N(3)–N(2)] formed as a result of chelation exist with a dihedral angle of 6.38°. The planar central plane V(1)–O(4)–V(1A)–O(4A) consisting the inversion

center, makes dihedral angles of 88.55° and 85.40° with the chelate rings Cg(2) and Cg(1). The dihedral angle between the pyridyl ring and the phenyl ring bearing the hydroxyl substituent O(2)–H is $18.12(1)$. The C(15)–H forms an intramolecular hydrogen bond with O(1). The torsional angle 174.85° , perceived by N(2)–N(3)–C(6)–C(5) reveals the *trans* nature of C(6)–N(2) bond. Thus the ligand has undergone a rotation around the C(6)–N(2) bond for complex formation. The selected bond lengths and bond angles are depicted in Table 5.2.

The packing in the unit cell (Fig. 5.4) is stabilized by short ring interactions (Table 5.3.) and by a ring metal interaction between Cg(2) [V(1), O(1), C(13), N(3), N(2)] and V(1) at a ring metal distance of 3.962 \AA . The presence of water molecules leads to intermolecular hydrogen bonding. The oxygen atom O(5) of the water molecule is hydrogen bonded to O(2)–H. Also the hydrogen atoms attached to O(5) are involved in hydrogen bonding with O(4) and O(3).

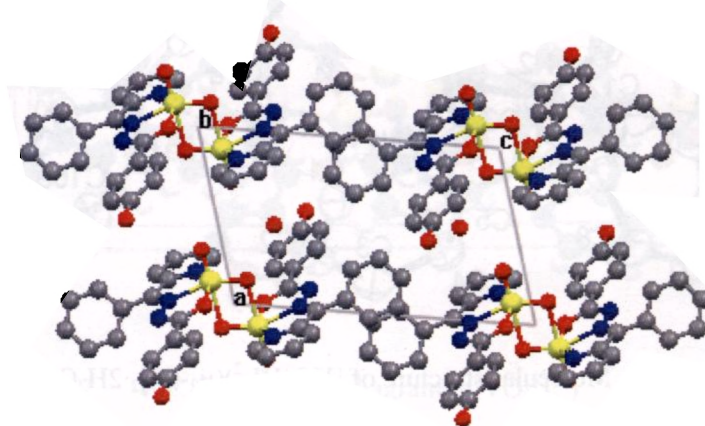


Fig. 5.4. Packing diagram of $[\text{VO}(\text{HL}^2)(\mu_2\text{-O})]_2\cdot\text{H}_2\text{O}$

5.3.2 Spectral characteristics of oxovanadium complexes

5.3.2a Electronic spectral studies

For the oxovanadium(V) complex, no d-d bands are expected as there are no d electrons. In compound **15**, a shoulder at 22570 cm^{-1} can be assigned to the

d-d transition (Fig. 5.5). Both the vanadium complexes display intense electronic spectral bands with shoulders in the near-UV region.

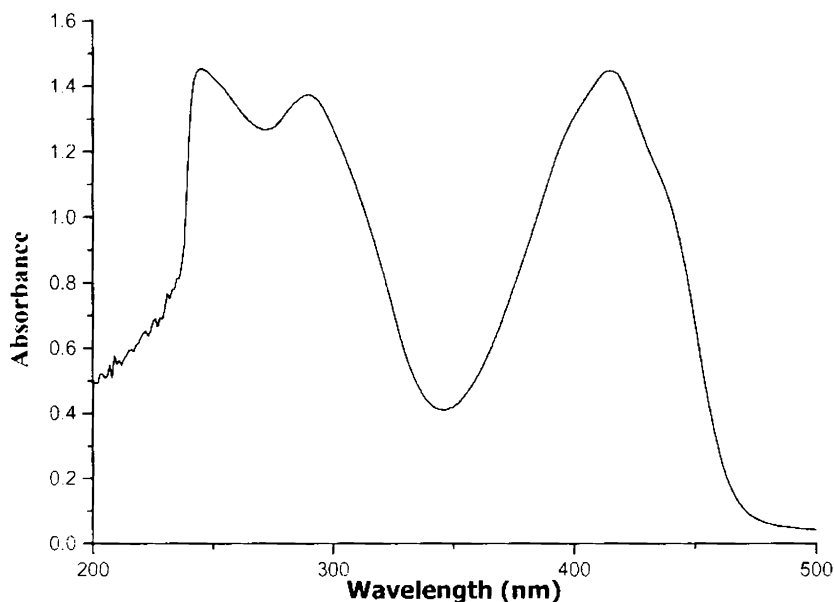


Fig. 5.5. Electronic spectrum of $[\text{VO}(\text{L}^1)\text{OCH}_3]$ complex

This band is originating from ligand to metal charge transfer transition. The values are 24090 and 23800 cm^{-1} respectively for $[\text{VO}(\text{L}^1)\text{OCH}_3]$ and $[\text{VO}(\text{HL}^2)(\mu_2\text{-O})_2]$. The other bands observed at 31740 (sh) and 34600 cm^{-1} for **15** and 32250 and 34600 cm^{-1} for **16** corresponds to intraligand transitions.

5.3.2b Electron paramagnetic resonance studies

EPR spectroscopy examines the transitions between electron spin states separated by the presence of an external magnetic field. Values of g in vanadyl EPR spectra are typically less than the free electron value, usually *ca.* 1.95. For the case of vanadium(IV), the nuclear spin of ^{51}V is $I = 7/2$, so the states are split into $2I+1 = 8$ different energy states each, separated by the hyperfine coupling constant, A . As 99% of vanadium is ^{51}V , there are no additional isotopes with nuclear spin to complicate the spectrum. Superhyperfine coupling occurs due to

nearby nuclei, such as ^{14}N . For the vanadium(IV) species, usually superhyperfine coupling is not resolved in a typical X-band EPR spectrum, as the electron is residing in a σ -non-bonding orbital that points away from the ligands in the equatorial (xy) plane. EPR transitions are electronic in nature, and their selection rules can be expressed as $\Delta m_s = \pm 1$, $\Delta m_l = 0$. For a vanadium(IV) complex, this gives rise to an eight-line spectrum.

The EPR spectrum of the compound **15** was recorded in DMF solution at 77 K. The absence of a forbidden $\Delta m_s = \pm 2$ transition, at half the field of the allowed $\Delta m_s = \pm 1$, transition excludes the possibility for the dimeric species which would also split the resonant absorptions into 15 lines [$2nI+1$; $n = 2$; $I = 7/2$]. In DMF solution at 77 K (Fig. 5.6), the compound displayed an axial spectrum. The g values calculated are $g_{\parallel} = 1.937$ and $g_{\perp} = 2.008$. The corresponding coupling constants are found to be 197.1 and 62.5 Gauss respectively.

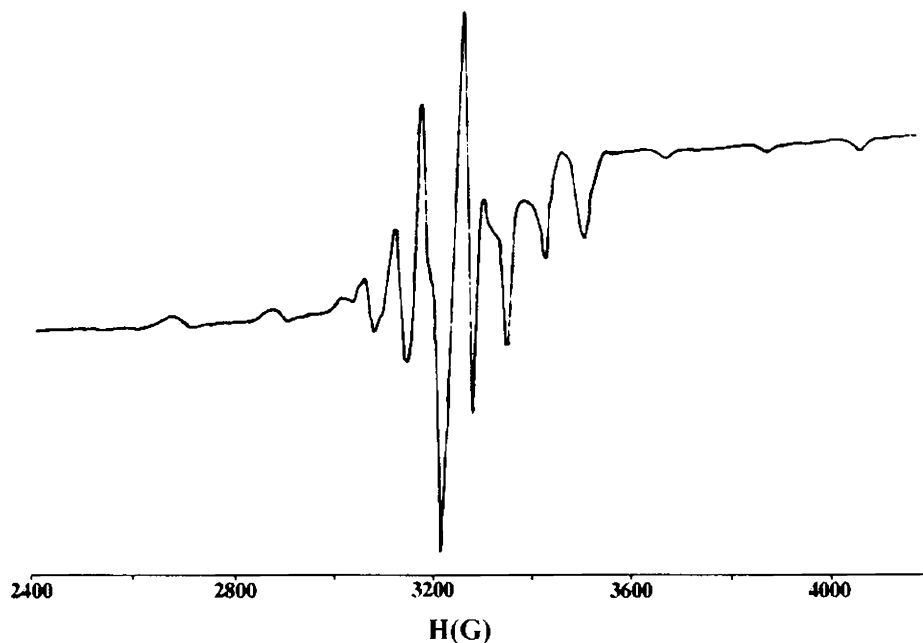


Fig. 5.6. EPR spectrum of compound **15** in DMF solution at 77 K.

5.3.2c IR spectral studies

The IR spectra of the complexes display characteristic variations when compared to that of the ligand, upon complexation. However, complete assignment is difficult due to crowding of peaks. So the assignments done are tentative. In compound **15**, a medium intensity band observed with splittings at 1597 cm^{-1} is due to newly formed $-\text{C}=\text{N}=\text{N}=\text{C}-$ moiety. The shifting of the $\text{C}=\text{N}_{\text{azo}}$ band, due to complexation is comparatively less when compared to that of the ligand and is found at 1580 cm^{-1} . A strong band observed at 1368 cm^{-1} is assigned to the amide III band. Strong bands are observed in the range $1510 - 1420\text{ cm}^{-1}$. These are attributed to the aromatic ring vibrations. The band at 939 cm^{-1} is assigned to $\nu(\text{V}=\text{O})$.

In the compound **16**, the $-\text{C}=\text{N}=\text{N}=\text{C}-$ moiety is observed as a medium band at 1650 cm^{-1} . In the present compound, the band corresponding to the azomethine bond found to be shifted to higher frequency. The band was viewed as a strong band at 1607 cm^{-1} . Such shifting of the $\text{C}=\text{N}$ band to higher frequencies are reported [18, 19]. The amide III band is assigned for the band at 1365 cm^{-1} [20-22]. The phenolic $\text{C}-\text{O}$ stretch is observed at 1332 cm^{-1} . The $-\text{OH}$ stretching frequency is attributed to the band at 3407 cm^{-1} . The dimeric compound **16** exhibits the $\nu(\text{V}=\text{O})$ band at 934 and the $\nu[\text{V}-(\mu\text{-O})-\text{V}]$ band at 898 cm^{-1} [23].

Table. 5.1
Crystal data and structure refinement for VO_2L^1 and $[\text{VO}(\text{HL}^2)(\mu_2\text{-O})]_2 \cdot 2\text{H}_2\text{O}$

Parameters	VO_2L^1	$[\text{VO}(\text{HL}^2)(\mu_2\text{-O})]_2 \cdot 2\text{H}_2\text{O}$
Empirical formula	$\text{C}_{18}\text{H}_{13}\text{N}_4\text{O}_7\text{V}$	$\text{C}_{38}\text{H}_{32}\text{N}_6\text{O}_{10}\text{V}_2$
Formula weight	384.26	834.58
Crystal system	Monoclinic	Triclinic
Space group	$P2_1/c$	$P\bar{1}$
Unit cell dimensions		
a (Å)	8.6580(6)	8.246(5)
b (Å)	8.9000(7)	8.468(5)
c (Å)	21.105(3)	13.793(8)
α (°)	90.00	85.537(9)
β (°)	91.163(8)	74.352(8)
γ (°)	90.00	83.260(9)
Volume V (Å ³), Z	1625.9(3), 4	919.9(9), 1
Calculated density (ρ) (Mg m ⁻³)	1.570	1.506
Absorption coefficient μ (mm ⁻¹)	0.637	0.576
F (000)	784	428
Crystal size (mm)	0.35 x 0.20 x 0.15	0.28 x 0.14 x 0.08
θ range for data collection	1.93-24.98	1.54 - 28.24
Index ranges	-10 ≤ h ≤ 10, 0 ≤ k ≤ 10, -25 ≤ l ≤ 0	-10 ≤ h ≤ 10, -10 ≤ k ≤ 10, -18 ≤ l ≤ 17
Reflections collected / unique	2947 / 2862 [R(int) = 0.0206]	6801 / 3801 [R(int) = 0.0342]
Refinement method	Full-matrix least-squares on F^2	Full-matrix least-squares on F^2
Data / restraints / parameters	2862 / 0 / 235	3801 / 0 / 317
Goodness-of-fit on F^2	1.041	0.956
Final R indices [$I > 2\sigma(I)$]	R1 = 0.0384, wR2 = 0.0828	R1 = 0.0487, wR2 = 0.1101
R indices (all data)	R1 = 0.0766, wR2 = 0.0925	R1 = 0.0687, wR2 = 0.1213

Table. 5.2
Selected bond lengths (Å) and bond angles (°) of vanadium compounds

Bonds	VO ₂ L ¹	[VO(HL ²)(μ ₂ -O)] ₂ ·2H ₂ O
V1-O2	1.606(2)	-
V1-O4	-	1.673(2)
V1-O3	1.6495(19)	1.610(2)
V1-O1	1.969(2)	1.955(2)
V1-N1	2.109(2)	2.134(2)
V1-N2	2.127(2)	2.119(2)
O1-C13	1.307(3)	1.316(3)
C6-N2	1.292(3)	1.298(3)
N2-N3	1.381(3)	1.381(3)
C13-N3	1.315(3)	1.316(3)
Bond angles		
O2-V1-O3	107.33(11)	-
O3-V1-O4	-	105.52(10)
O2-V1-O1	99.97(11)	-
O4-V1-O1	-	106.26(8)
O3-V1-O1	105.11(9)	99.31(11)
O2-V1-N1	96.59(11)	-
O4-V1-N1	-	99.26(9)
O3-V1-N1	97.89(10)	94.14(10)
O1-V1-N1	145.99(8)	146.59(8)
O2-V1-N2	103.93(10)	-
O4-V1-N2	-	152.75(10)
O3-V1-N2	148.27(10)	101.11(10)
O1-V1-N2	74.28(8)	74.58(7)
N1-V1-N2	73.00(8)	72.87(8)
C6-N2-N3	120.3(2)	120.9(2)
N2-N3-C13	107.4(2)	108.1(2)
N3-C13-O1	124.3(3)	123.0(2)
C5-C6-N2	112.4(2)	111.8(2)
N3-C13-C14	117.3(2)	118.1(2)

Table. 5.3
H-bonding and π - π interaction parameters of $[\text{VO}(\text{HL}^2)(\mu_2\text{-O})]_2 \cdot 2\text{H}_2\text{O}$

H-bonding

Donor---H---A	D-H (Å)	H---A (Å)	D---A (Å)	D-H-A (°)
C15-H---O1	0.890	2.553	2.841	99.62
O2-H---O5	0.813	1.889	2.701	178.09
O5-H---O4	0.793	2.076	2.866	173.08
O5-H---O3	0.800	1.977	2.776	176.86

 π - π interactions

Cg(I)-Res(1)---Cg(J)	Cg-Cg (Å)	α (°)	β (°)
Cg(2)-[1]--- Cg(1) ^a	2.6323	85.39	55.46
Cg(3)-[1]--- Cg(1) ^a	2.6956	88.55	57.36
Cg(1)-[1]--- Cg(4) ^a	3.8959	86.34	28.41

Equivalent position code

a = x, y, z

Cg(1) = V1, O4, V1A, O4A

Cg(2) = V1, O1, C13, N3, N2

Cg(3) = V1, N1, C5, C6, N2

Cg(4) = N1, C1, C2, C3, C4, C5

References

1. D. Rehder, *Angew. Chem. Int. Ed. Engl.* 30 (1991) 148.
2. A. Butler, J. V. Walker, *Chem. Rev.* 93 (1993) 1937.
3. A. Butler, C. J. Carrano, *Coord. Chem. Rev.* 109 (1991) 61.
4. I. Cavaco, J. C. Pessoa, M. Duarte, R. D. Gillard, P. Matias, *Chem. Commun.* (1996) 1365.
5. A. Butler, *Science* 281 (1998) 207.
6. G. L. Mendz, *Arch. Biochem. Biophys.* 291 (1991) 201.
7. A. Syamal, K. S. Kale, *Inorg. Chem.* 18 (1979) 992.
8. C. J. Carrano, C. M. Nunn, R. Quan, J. A. Bonadies, V. L. Pecoraro, *Inorg. Chem.* 29 (1990) 944.
9. L. M. Mokry, C. J. Carrano, *Inorg. Chem.* 32 (1993) 6119.
10. D. Kostrewa, H. W. Choe, U. Heinmann, W. Saenger, *Biochemistry* 28 (1989) 7592.
11. S. Samanta, D. Ghosh, S. Mukhopadhyay, A. Endo, T. J. R. Weakley, M. Chaudhury, *Inorg. Chem.* 42 (2003) 1508.
12. M. R. Maurya, A. Kumar, A. R. Bhat, A. Azam, C. Bader, D. Rehder, *Inorg. Chem.* 45 (2006) 1260.
13. A. W. Addison, T. N. Rao, J. Reedijk, J. van Rijn, G. C. Verschoor, *J. Chem. Soc. Dalton Trans.* (1984) 1349.
14. A. Sreekanth, H.-K. Fun, R. P. John, M. R. P. Kurup, S. Chantrapromma, *Acta Cryst. E* 62 (2006) 1919.
15. W. Plass, *Angew. Chem., Int. Ed. Engl.* 35 (1996) 627.
16. T. Carofiglio, E. Solari, C. Floriani, A. Chiesi-Villa, C. Rizzoli, *Polyhedron* 15 (1996) 4435.
17. J. Salta, J. Zubieta, *Inorg. Chim. Acta* 257 (1997) 83.
18. D. Demertzi, D. Nicholls, *Inorg. Chim. Acta* 73 (1983) 37.
19. C. N. Elgy, D. Nicholls, *J. Inorg. Chem. Nuclear Chem.* 43 (1981) 2025.
20. P. K. Singh, D. N. Kumar, *Spectrochim. Acta* 64A (2006) 853.

21. V. R. Rao, K. G. Reddy, U. V. Sessaiah, *Transition Met. Chem.* 18 (1993) 258.
22. S. Srinivasan, J. Annaraj, P. R. Athappan, *J. Inorg. Biochem.* 99 (2005) 876.
23. M.R. Maurya, S. Khurana, C. Schulzke, D. Rehder, *Eur. J. Inorg. Chem.* (2001) 779.

Syntheses, structural and spectral studies of Ni(II) and Pd(II) complexes of heteroaroylhydrazone ligands

For the present day medicine and chemical investigations, metal chelation is a very important process. Presence of vacant sites around the metal center is a criterion for understanding the role played by the metal to be biologically effective. Since the recognition that the trace presence of Ni is essential for bacteria, plants, animals and humans, [1] nickel has been chosen for study, as many nickel complexes are coordinatively unsaturated, can behave as Lewis acids. The redox chemistry of nickel has received considerable attention in the last few years due to its essential role in bioinorganic chemistry and several enzymes [2, 3]. Morrow and Kolasa reported the cleavage of plasmid DNA by square planar nickel-salen [bis-(salicylidene)ethylenediamine] in the presence of either magnesium monoperoxyphthalic acid (MPPA) or iodosylbenzene [4]. The observation of different oxidation states for nickel during the catalytic cycle, has spurred a great interest in the investigation of the electronic and structural factors that contribute to stabilize a particular oxidation state for the nickel center. Several factors have been recognized to be particularly important in the stabilization of the +3 and +1 oxidation states, namely coordination number, geometry, type of donor atom and electronic characteristics of the ligand.

Ni(II) complexes of aroylhydrazones have been studied extensively [5-14]. Ivanovic et al. [15] have studied the denticities of bis(acylhydrazone) with Ni(II) ion. Because of steric requirements [16] and due to a lower electron density in $d_{x^2-y^2}$ than in d_{xy} orbital of Ni(II) ion [15] tetracoordination of

bis(acylhydrazone) ligand involves the coordination of one hydrazide NH group accompanied by deprotonation. The same group reported the first tridentate coordination of bis(acylhydrazone)-2, 6-diacetylpyridine in which the Ni(II) metal center attained a distorted octahedral geometry [17]. Schiff bases of Pd(II) complexes have also considerably gained attraction owing to their applications in the field of catalysis [18-21].

6.1. Stereochemistry

The most stable oxidation state found for both Ni and Pd is II. In the divalent state nickel exhibits wide and interesting variety of coordination numbers and stereochemistries whereas palladium has a strong preference for the square planar geometry.

6.2. Experimental

6.2.1. Materials

2-Benzoylpyridine (Sigma Aldrich), pyridine-2-carbaldehyde (Sigma Aldrich), nicotinoylhydrazide (Sigma Aldrich), 4-hydroxybenzhydrazide (Fluka), Ni(II) acetate (CDH) and Pd(II) chloride (SD Fine) were used as received. The solvent used, ethanol was distilled before use.

6.2.2. Syntheses of ligands

Ligands HL¹, H₂L² and HL³ were synthesized as described in previously in Chapter 2.

6.2.3 Preparation of Ni(II) complexes

[Ni(L¹)₂].H₂O (17): To a solution of the ligand HL¹ (0.302 g, 1 mmol) in ethanol, Ni(OAc)₂.H₂O (0.248 g, 1 mmol) dissolved in ethanol was added and refluxed for 4 hours. The deep brown solution obtained was kept for slow evaporation. The brown precipitate obtained was filtered, washed with ether and

dried over P_4O_{10} *in vacuo*. Yield: 0.679 g (52%). Elemental Anal. Found (Calcd.) (%): C, 63.68 (63.65); H, 3.54 (4.15); N, 16.31 (16.49).

[Ni(L³)₂·H₂O (18): Compound **18** was prepared by the same procedure as that of compound **17**. HL³ (0.262 g, 1 mmol) was used instead of HL¹. Yield: 0.630 g (63%). Elemental Anal. Found (Calcd.) (%): C, 54.79 (54.68); H, 2.77 (3.82); N, 20.89 (21.26).

6.2.4. Preparation of Pd(II) complexes

[Pd(HL¹)Cl₂] (19): A solution of PdCl₂ (0.177 g, 1 mmol) in DMF was added to the ligand HL¹ (0.302 g, 1 mmol) in ethanol by stirring. A yellow product formed immediately upon addition of metal salt, stirring was continued for 3 hours. The precipitate was filtered, washed with ethanol, followed by ether and dried over P_4O_{10} *in vacuo*. Yield: 0.190 g (75%). Elemental Anal. Found (Calcd.) (%): C, 44.66 (45.07); H, 2.81 (2.94); N, 11.60 (11.68).

[Pd(HL²)(Cl)(H₂O)]₂ (20): To a solution of the ligand H₂L² (0.317 g, 1 mmol) in DMF-ethanol (1:1 v/v) mixture, PdCl₂ (0.177 g, 1 mmol) in DMF was added. The orange colored solution obtained was stirred for 5 hours. The orange product formed was filtered, washed with ethanol, followed by ether and dried over P_4O_{10} *in vacuo*. Yield: 0.333 g (69.9%). Elemental Anal. Found (Calcd.) (%): C, 47.89 (47.92); H, 3.22 (3.39); N, 8.82 (8.82).

[Pd(HL³)Cl₂]·2H₂O (21): PdCl₂ (0.177 g, 1 mmol) in DMF solution was added to HL³ (0.262 g, 1 mmol) dissolved in ethanol. The resulting solution was stirred for 6 hours. The dark green product obtained was filtered, washed with ethanol, followed by ether and dried over P_4O_{10} *in vacuo*. Yield: 0.241 g (54.9%). Elemental Anal. Found (Calcd.) (%): C, 32.36 (32.79); H, 2.90 (3.21); N, 12.49 (12.75).

6.3. Results and discussion

Reaction of equimolar ratios of the ligand and the metal salt yielded compounds of stoichiometry $[ML_2]$ for nickel and of $[M(HL)Cl_2]$ for compounds **19** and **21** of palladium. Elemental analyses suggested a neutral form of the ligand in palladium compounds **19** and **21**. Compound **20** showed a stoichiometry of $[M(HL)(Cl)(H_2O)]_2$. The Ni(II) compounds are found to be paramagnetic with magnetic moment values in the range of 2.5 - 2.9 BM consistent with two unpaired electrons. The magnetic susceptibility measurements of the Pd(II) complexes revealed that the compounds **19** and **21** are diamagnetic, but the compound **20** showed a magnetic moment of 2.69 BM corresponding to a d^8 system with two unpaired electrons. So a six coordinate geometry is suggested for the compound. Pd(II) complexes generally have square planar geometry around the palladium atom, and six-coordinate complexes of Pd(II) are very rare, but has been reported with crystal structure evidences [22, 23]. The conductivity measurements showed that all the compounds are non-electrolyte in nature.

6.3.1 Crystal structures of $[Ni(L^1)_2]$ and $[Ni(L^3)_2] \cdot H_2O$

$[Ni(L^1)_2]$: Single crystals suitable for X-ray diffraction were grown from a DMF/ethanol mixture (1:1 v/v) of the compound by slow evaporation. The compound crystallizes into a monoclinic lattice with $P2_1$ space group. The structural refinement parameters are given in Table. 6.1. Unit cell comprises of two molecules. The compound adopts a distorted octahedral geometry with six sites occupied by two molecules of the tridentate ligand (Fig. 6.1). The distortion is imposed by the rigidity of the newly formed chelate rings. Four nitrogens and two oxygens of two HL^1 ligands surround the Ni atom. For complexation, the ligand acquires a *trans* configuration with respect to C=N bond, thereby forming two five membered chelate rings. As described in Chapter 2, out of the four possible conformations of the enolic form, the one adopted here is the *EZ* conformer, i.e. *E* with respect to the C6–N2 bond and *Z* with respect to C13–N3

bond. Only the coordination of azomethine nitrogens to the Ni atom approaches a regular *trans* angle of 180° , N6–Ni–N2 $175.45(10)$.

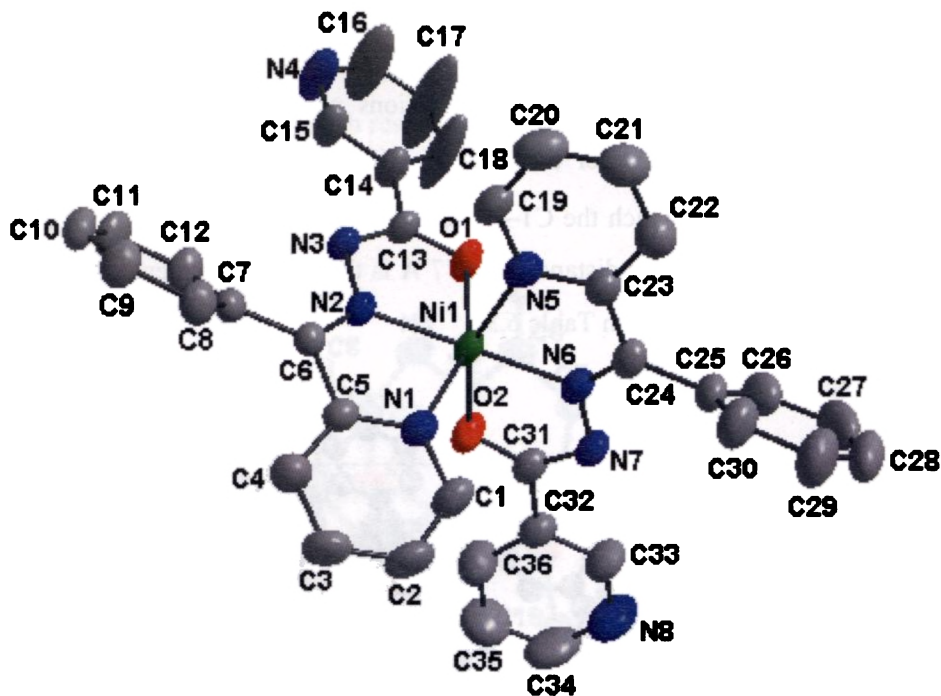


Fig. 6.1. Molecular structure of the compound $\text{Ni}(\text{L}^1)_2$. Hydrogen atoms are omitted for clarity

The bond lengths and bond angles given in Table 6.2 suggest that for the first ligand the three coordinating centers are in one plane and for the second ligand one of the nitrogen atom is in the plane of the first ligand while the other two coordinating sites are in other plane. This implies that the ligands bind the metal ion meridionally. Least square analysis shows that the basal plane defined by the atoms O2, N5, N6 and N2 with Ni atom slightly deviated by 0.0204 \AA . This is further supported by the dihedral angle separation of 1.10° between the planes constituted by the atoms N5, C23, C24, N6, Ni1 and O2, C31, N7, N6, Ni1 respectively. Coordination *via* enolic oxygen atom is evident from the change in C–O bond length of $1.2158(15)$ in ligand to $1.270(3) \text{ \AA}$ in complex and the IR

spectroscopic data also supports this. The variations in bond lengths C6(24)–N2(6), N2(6)–N3(7) and C13(31)–N3(7) upon complexation are less pronounced.

The basic unit of the crystal packing consists of two molecules and this unit repeats one dimensionally in the lattice. The packing of molecules is shown in Fig. 6.2. The π – π intermolecular interactions observed are weak as they correspond to a distance greater than 3.8 Å. However, there are appreciable C–H... π interactions, in which the C1–H...Cg(2) [Cg(2): Ni1, O2, C31, N7, N6] interaction, found at a H...Cg distance of 2.77 Å is the most prominent. A list of C–H... π interactions is given in Table 6.3.

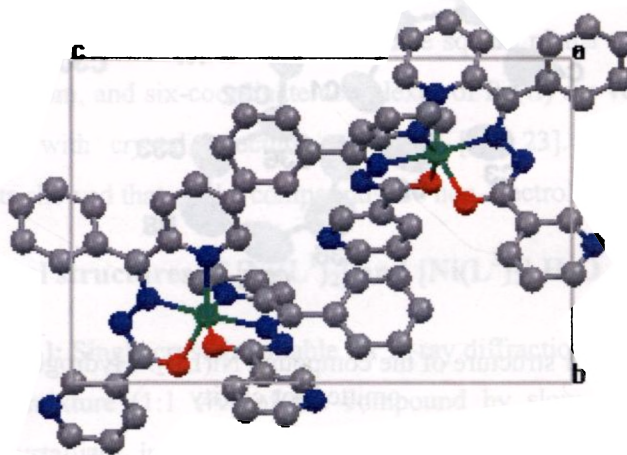


Fig. 6.2. Packing diagram of Ni(L¹)₂. Hydrogen atoms are omitted for clarity

Ni(L³)₂·H₂O: Suitable reddish brown crystals for structural analysis were grown from a solution of the compound in a mixture of DMF and ethanol (1:1 v/v). A depiction of the complex along with numbering scheme is given in Fig. 6.3. The bonding pattern is similar to that observed in case of compound 17. The structural refinement parameters are given in Table 6.1. The triclinic lattice with space group symmetry $P\bar{1}$ consists of one water molecule. The Ni(II) ion remains fixed in the center of a distorted octahedron formed by two ligands. The bond

lengths and bond angles are given in Table 6.2. The four chelate rings around the metal center enable this fitting. Here also the two ligands bind the metal ion in an meridional manner so as to minimize the repulsion. The *trans* nature of the C6–N2 bond in the ligand is maintained as such in the present compound facilitating the chelation, whereas in compound 17, the ligand undergoes a transformation from *cis* to *trans* geometry with respect to the C6–N2 bond for complexation.

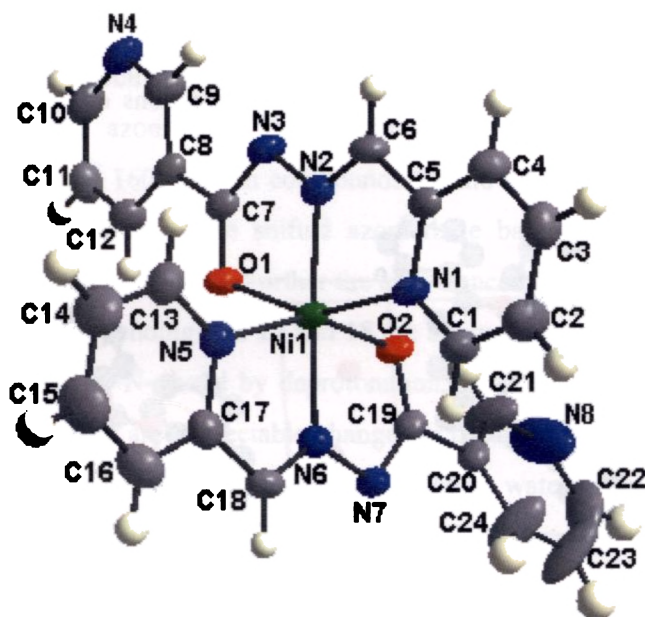


Fig. 6.3. Molecular structure of the compound $\text{Ni}(\text{L}^3)_2 \cdot \text{H}_2\text{O}$. The water molecule is omitted for clarity

The observed torsion angle of 179.48° for C5–C6–N2–N3 supports this *trans* configuration along the C6–N2 bond. For the formation of the chelate ring Ni–N2–C6–C5–N1, the ligand itself adjusts its geometry to *cis* form along the C5–C6 bond, as viewed from the torsion angle of -0.80° for N1–C5–C6–N2. Thus the coordinated enolate form of the ligand reveals an *EE* conformation along the N2–N3 and C6–N2 bonds. The equatorial plane constituted by atoms N1, N2, O1 and N6 forms a dihedral angle separation of 88.36° and 89.65° with the axial

planes N5–C17–C18–N6–Ni1 and N6–N7–C19–O2–Ni1 respectively. This suggests a meridional coordination mode of ligands around the metal ion. The Ni–N_{imine} and Ni–O_{amide} distances are comparable with those observed in other octahedral Ni(II) complexes with aroylhydrazones [24, 25].

The unit cell consists of two molecules, which forms the repeating unit in crystal packing with Ni atoms arranged in a zig-zag manner. The packing diagram of the compound is given in Fig. 6.4. From the packing diagram, the perpendicular plane between the ligands is evident. The intermolecular hydrogen bonds observed are weak. A list of C–H--- π interactions of the compound are given in Table 6.4.

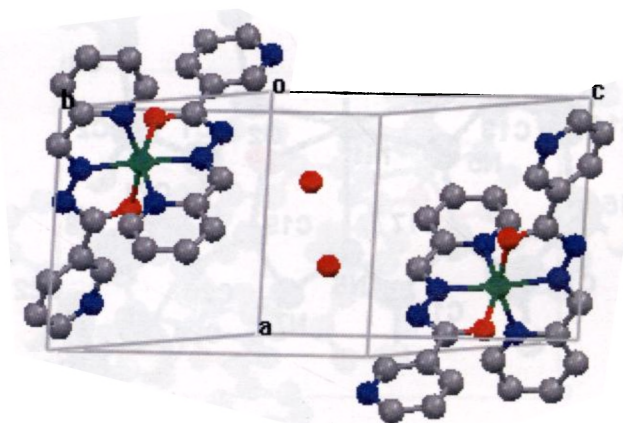


Fig. 6.4. Packing diagram of Ni(L³)₂·H₂O

6.3.2 Spectral characteristics of nickel complexes

6.3.2a Electronic spectral studies

For an octahedral nickel(II) complex, three absorptions are expected *viz.* ν_1 (8000 – 13000 cm⁻¹) for ${}^3A_{2g} \rightarrow {}^3T_{2g}$, ν_2 (15000 - 19000 cm⁻¹) corresponding to ${}^3A_{2g} \rightarrow {}^3T_{1g}$ (F) and ν_3 (25000 – 30000 cm⁻¹) assigned to ${}^3A_{2g} \rightarrow {}^3T_{1g}$ (P). In the present case, the compound **17** exhibited a single broad d-d band at 12020 cm⁻¹, which corresponds to the ${}^3A_{2g} \rightarrow {}^3T_{2g}$. This broad band and the charge transfer

band observed at 25510 cm^{-1} may have masked the other two d-d bands. The ligand-based transitions were shifted upon complexation. They were observed as a shoulder and as a sharp peak at 32460 and 39680 cm^{-1} respectively. In compound **18**, d-d bands were found at 11760 and as a shoulder at 24150 cm^{-1} . The $L \rightarrow Ni$ charge transfer band was viewed at 25770 cm^{-1} . The compound reveals $n \rightarrow \pi^*$ transition at 34360 cm^{-1} and $\pi \rightarrow \pi^*$ transition at 37730 cm^{-1} .

6.3.2b IR spectral studies

In the IR spectra of the complexes, it is found that the carbonyl band disappears and the azomethine band shifts due to coordination. The bands obtained at 1593 and 1603 cm^{-1} in compounds **17** and **18** respectively, are due to the $-C=N-N=C-$ moiety. The shifted azomethine bands are correspondingly assigned at 1566 and 1573 cm^{-1} . Further the appearance of two new bands at 1363 and 1356 cm^{-1} correspondingly in **17** and **18** are assigned for C-O band [26]. The formation of new $-C=N-$ bond by deprotonation, is confirmed by single crystal X-ray studies, as there are appreciable changes in the bond length of this bond in ligand to the metal complexes. The presence of lattice water gives broad bands in the region 3420 cm^{-1} in both the complexes.

6.3.3 Spectral characteristics of palladium complexes

6.3.3a Electronic spectral studies

The electronic spectra of the palladium compounds were recorded in DMF solution. The d-d bands observed were considerably weak. The electronic spectral assignments of the complexes are listed in Table 6.5.

6.3.3b ^1H NMR spectral studies

In compound $[\text{Pd}(\text{HL}^1)\text{Cl}_2]$, coordination of the ligand in the neutral form was evidenced by the appearance of the signal at 14.77 ppm corresponding to the N-H proton (Fig. 6.5). Two doublet of doublets observed at 8.64 and 8.72 ppm are assigned for the α protons of the pyridyl ring and nicotinoyl ring, i.e. C(1)-H

and C(16)–H. A comparison with the ligand spectrum, suggests that the shifting of the signal observed at 8.64 ppm corresponding to C(1)–H, is not much profound. But the IR spectrum of the compound, suggested the coordination of pyridyl nitrogen N1 to the metal center, as evident from the M–N_{py} band appeared at 270 cm⁻¹. The proton C(15)–H with no adjacent protons was observed at 9.24 ppm. The doublet observed at 8.25 ppm is assigned for the C(18)–H proton. The coordination of azomethine nitrogen was supported by the signal observed at 8.25 ppm as a doublet of triplet which corresponds to C(8)–H and C(12)–H protons of the phenyl ring. The higher δ values of these protons are attributed to a decrease in electron density in the ring as a result of the coordination of azomethine nitrogen. So the compound could be probably five coordinate.

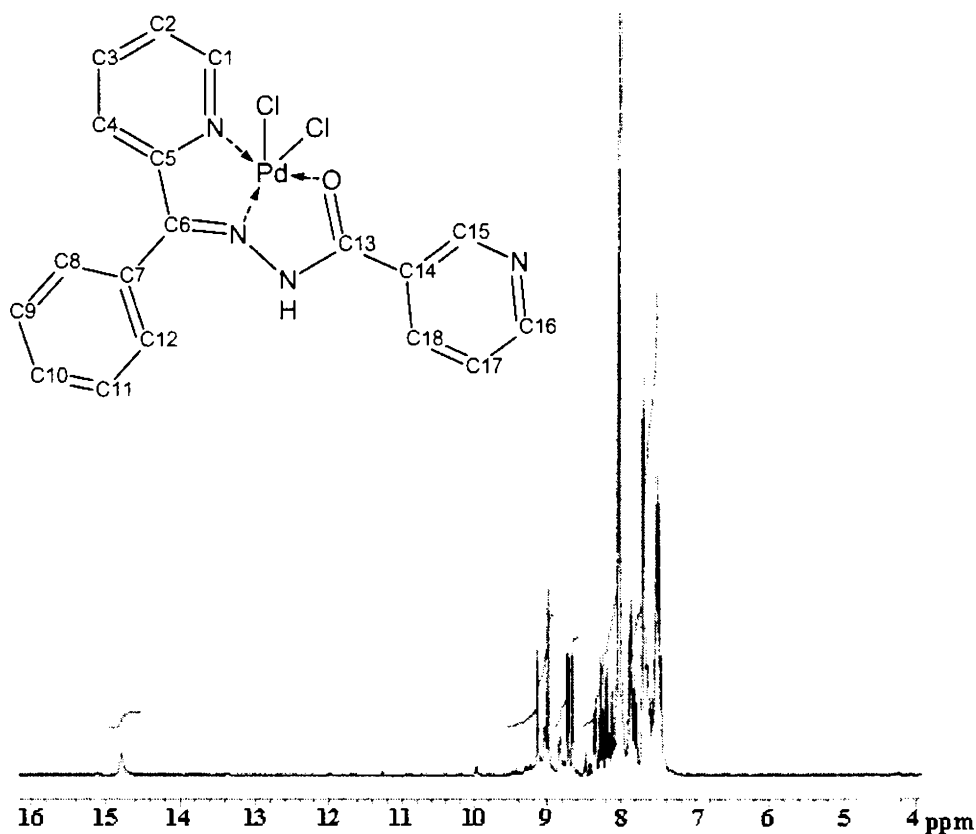


Fig. 6.5. ¹H NMR spectrum of compound Pd(HL)Cl₂ (19)

Elemental analysis of the compound $[\text{Pd}(\text{HL}^2)(\text{Cl})(\text{H}_2\text{O})]_2$ suggested a deprotonated ligand, implying coordination of the ligand in enolate form with Pd(II) ion. This was in fact supported by the disappearance of the N-H peak in the ^1H NMR spectrum. The proton corresponding to -OH group of the phenyl ring is found to resonate at 10.47 ppm (Fig. 6.6). The shifting of C(1)-H proton due to coordination of N(1) of pyridyl ring, was prominent as is suggested by the observance of the signal at 8.62 ppm as a doublet of doublet due to coupling with C(2)-H and C(3)-H. The C(8)-H and C(12)-H protons are observed at 8.2 ppm, due to a decrease in electron density in ring, suggesting the coordination of azomethine nitrogen. The meta protons C(9)-H and C(11)-H is assigned for the multiplet observed at 6.82 ppm. C(4)-H proton was found to resonate at 7.41 ppm. The assignment of remaining protons was difficult as they resonated as a multiplet observed at 7.64 - 7.84 ppm.

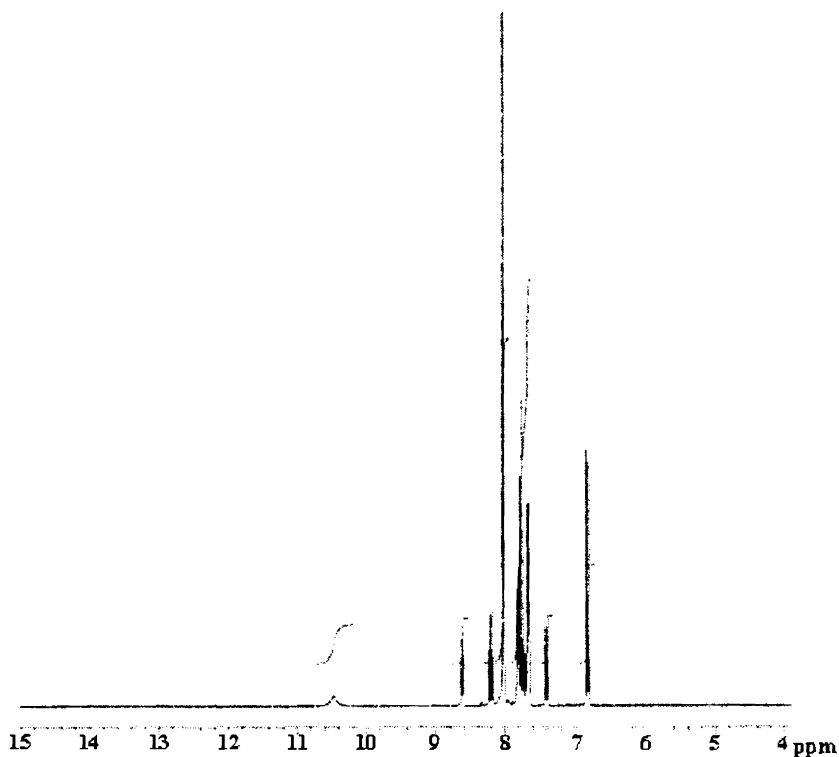


Fig. 6.6. ^1H NMR spectrum of compound $[\text{Pd}(\text{HL}^2)(\text{Cl})(\text{H}_2\text{O})]_2$ (**20**)

Coordination of the ligand in neutral form in compound $[\text{Pd}(\text{HL}^3)\text{Cl}_2]\cdot 2\text{H}_2\text{O}$, was evidenced by the signal at 14.26 ppm corresponding to N–H proton. Aldehydic proton was found to resonate at 11.6 ppm. The α protons on pyridyl and nicotinoyl rings viz. C(1)–H and C(10)–H was found as doublet of doublets at 8.77 and 8.92 ppm respectively. The shifting of C(1)–H proton was profound when compared to that of the free ligand. This shifting may be due to the decrease in electron density in the aryl ring as a result of coordination of pyridyl nitrogen N(1), to the metal center. The C(12)–H proton is assigned at 8.63 ppm. The multiplet observed at 9.11 ppm corresponds to that of C(3)–H. This shift can be explained by the *para* positioned coordinated pyridyl nitrogen. The C(4)–H proton was found to resonate at 8.42 ppm as a multiplet. The multiplet observed at 8.0 - 7.6 ppm corresponds to two protons C(2)–H and C(11)–H.

6.3.3c IR spectral studies

The IR spectra of Pd complexes were found to be interesting. In compound $[\text{Pd}(\text{HL}^1)\text{Cl}_2]$, the frequency of the $-\text{C}=\text{O}$ bond is shifted when compared to that of the ligand. Accurate assignment is difficult as a broad band with splittings were observed at $1670 - 1500 \text{ cm}^{-1}$. The usual ring vibrations and the azomethine band are found in this region. However, elemental analysis and ^1H NMR suggested a nondeprotonated ligand. So as the frequency of the bond shifted to lower frequency, it is assumed that the carbonyl oxygen forms a coordinate bond with Pd(II). Such coordination is confirmed by single crystal XRD studies in our similar Cd(II) octahedral complex with the ligand HL^3 [27]. It should be noted that in the referred Cd(II) complex also, the shift of the coordinated $-\text{C}=\text{O}$ bond is not so profound. Conductivity studies indicate the complex to be non-electrolyte in nature. An accurate assignment of the shift of the azomethine band cannot be carried out as the signal observed at $1670\text{-}1500 \text{ cm}^{-1}$, is a combination band consisting of $\nu(\text{C}=\text{N})$, the N–H bending and C–N stretching vibrations of the C–N–H group. Coordination of N_{py} to palladium metal center is

visible from the observance of a band at 270 cm^{-1} . The magnetic studies also reveal the diamagnetic nature of the complex.

In the $[\text{Pd}(\text{HL}^2)(\text{Cl})(\text{H}_2\text{O})_2]$ complex, the ligand is found to be deprotonated, as confirmed by the disappearance of the amide I band (Fig. 6.7). The band appeared at 1605 cm^{-1} corresponds to the $-\text{C}=\text{N}-\text{N}=\text{C}-$ moiety. Shifting of azomethine band is not so profound. Coordination of enolate oxygen to the metal center is observed as a band at 1365 cm^{-1} . The presence of $-\text{OH}$ group gives a band at 3430 cm^{-1} . The $\text{Pd}-\text{N}_{\text{px}}$ and $\text{Pd}-\text{Cl}$ bands are found at 250 and 324 cm^{-1} respectively. So a six coordinate octahedral complex is suggested based on the magnetic susceptibility measurements and spectral studies (Fig. 6.8).

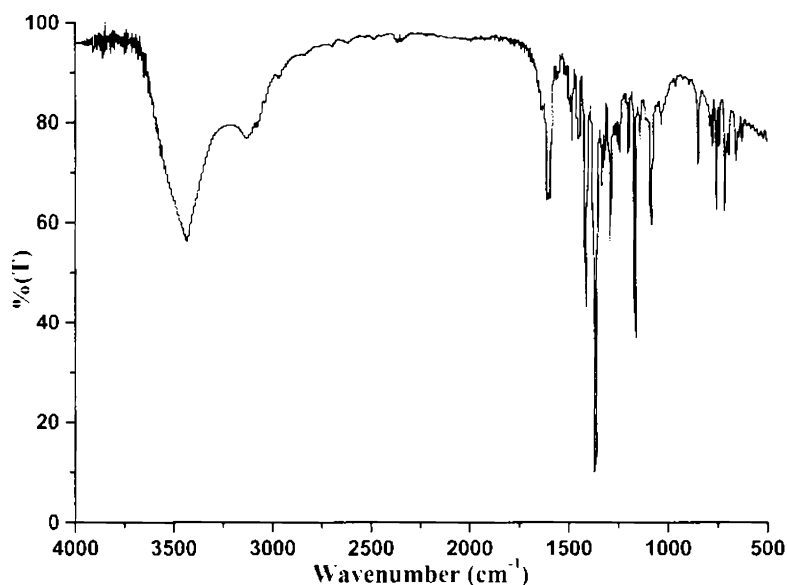


Fig. 6.7. IR spectrum of $[\text{Pd}(\text{HL}^2)(\text{Cl})(\text{H}_2\text{O})_2]$

The IR spectrum of the third Pd complex is found to be a little confusing. A sharp band is found at 1697 cm^{-1} . The $-\text{C}=\text{O}$ band in the free ligand, is viewed at 1669 cm^{-1} . This means that the band has been blue shifted. Such a shift may be due to the electronic changes occurring in the molecule as a whole due to complexation. A medium band viewed at 1607 cm^{-1} is assigned to the azomethine

bond. Such a positive shift of the coordinated azomethine bond to higher frequencies has been reported earlier [28]. A sharp band observed at 1543 cm^{-1} may be due amide II. The presence of a broad band at 3450 cm^{-1} and the band viewed at 3270 cm^{-1} are assigned to the lattice water and the -N-H vibration consistent with the elemental analysis. The Pd-N_{py} and Pd-Cl bands could not be assigned due to poor quality of far IR spectrum. The magnetic susceptibility measurement also supported the diamagnetic nature of the four-coordinated complex.

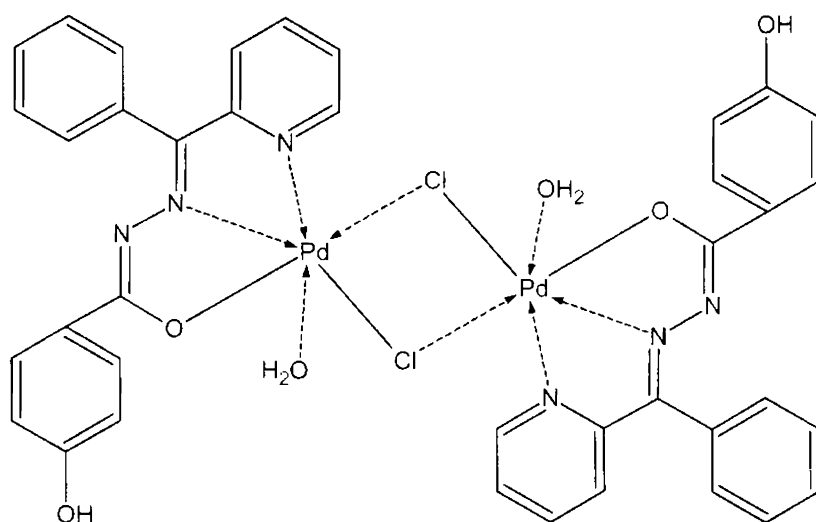


Fig. 6.8. Tentative structure of $[\text{Pd}(\text{HL}^2)(\text{Cl})(\text{H}_2\text{O})]_2$

Table 6.1.
Crystal Data and Structure Refinement for the Ni(II) complexes

	(NiL ¹) ₂	(NiL ³) ₂ ·H ₂ O
Empirical formula	C ₃₆ H ₂₆ N ₈ NiO ₂	C ₂₄ H ₁₈ N ₈ NiO ₃
Formula weight	661.36	525.17
Temperature	273(2) K	273(2) K
Color	Wine red	Wine red
Nature	Blocks	Plates
Wavelength	0.71073 Å	0.71073 Å
Crystal system	Monoclinic	Triclinic
Space group	<i>P</i> 2 ₁	<i>P</i> $\bar{1}$
Unit cell dimensions	a = 9.245(3) Å b = 10.520(3) Å c = 16.798(5) Å α = 90.00° β = 103.137(5)° γ = 90.00°	a = 8.7980(16) Å b = 11.054(2) Å c = 12.962(2) Å α = 92.261° β = 106.933(3)° γ = 105.840(3)°
Volume, Z	1591.1(8) Å ³ , 2	1150.5(4) Å ³ , 2
Calculated density	1.380 Mg/m ³	1.516 Mg/m ³
Absorption coefficient	0.656 mm ⁻¹	0.889 mm ⁻¹
F (000)	684	540
Crystal size	0.34x 0.28x 0.22 mm	0.24 x 0.12 x 0.06 mm
θ range for data collection	2.26-28.33°	1.66-25.00°
Index ranges	-7 ≤ h ≤ 12, -12 ≤ k ≤ 14, -22 ≤ l ≤ 21	-10 ≤ h ≤ 10, -10 ≤ k ≤ 13, -14 ≤ l ≤ 15
Reflections collected / unique	9441 / 6676 [R(int) = 0.0200]	5636 / 3941 [R(int) = 0.0208]
Refinement method	Full-matrix least- squares on <i>F</i> ²	Full-matrix least- squares on <i>F</i> ²
Data / restraints / parameters	6676 / 1 / 424	3941 / 0 / 325
Goodness-of-fit on <i>F</i> ²	0.993	1.095
Final R indices [I > 2σ(I)]	R1 = 0.0429, wR ₂ = 0.1038	R1 = 0.0529, wR ₂ = 0.1364
R indices (all data)	R1 = 0.0487, wR ₂ = 0.1072	R1 = 0.0679, wR ₂ = 0.1659
Largest diff. peak and hole	0.655 and -0.232	0.572 and -0.416

Table 6.2.

Selected bond lengths (Å) and bond angles (°) for Ni(II) complexes

Bonds	(NiL ¹) ₂	(NiL ³) ₂ ·H ₂ O
N2-C6	1.292(3)	1.264(5)
N2-N3	1.384(3)	1.373(5)
N3-C7	-	1.334(5)
N3-C13	1.329(4)	-
O1-C7	-	1.264(5)
O1-C13	1.270(3)	-
Ni1-N2	1.997(2)	1.980(3)
Ni1-N6	1.996(2)	1.983(3)
Ni1-O1	2.061(2)	2.121(3)
Ni1-O2	2.101(2)	2.095(3)
Ni1-N1	2.091(2)	2.117(4)
Ni1-N5	2.130(3)	2.113(4)
Bond angles		
C6-N2-N3	121.7(2)	121.3(3)
C7-N3-N2	-	108.3(3)
O1-C13-N3	126.9(3)	-
O1-C7-N3	-	126.9(4)
O1-C13-C14	117.8(3)	-
O1-C7-C8	-	119.0(4)
N3-C13-C14	115.2(2)	-
N3-C7-C8	-	114.1(4)
N1-C5-C6	115.9(2)	114.5(4)
N2-Ni1-N6	175.45(10)	174.75(14)
N2-Ni1-O1	76.49(13)	77.68(9)
N2-Ni1-O2	106.53(9)	103.53
N2-Ni1-N5	99.03(9)	101.93(14)
O2-Ni1-N5	154.44(9)	154.53(13)
N2-Ni1-N1	77.54(9)	78.11(14)
N5-Ni1-N1	96.41(10)	91.98(14)
N2-Ni1-O1	77.68(9)	76.49(13)
O2-Ni1-O1	94.63(10)	92.79(12)
N5-Ni1-O1	90.99(10)	92.42(13)
N1-Ni1-O1	154.96(9)	154.58(12)

Table 6.3.
C-H... π interactions of [Ni(L¹)₂]

X-H(I)---Cg(J)	H---Cg (Å)	X---Cg (Å)	X-H---Cg (°)
C(1)–H(1)[1]---Cg(2) ^a	2.77	3.1105	103
C(9)–H(9)[1]---Cg(1) ^b	2.80	3.5818	142
C(16)–H(16)[1]---Cg(9) ^c	2.84	3.6381	145
C(19)–H(19)[1]---Cg(1) ^a	2.95	3.2631	101

Equivalent position code

a = x, y, z, b = 1-x, -1/2+y, 1-z, c = 2-x, 1/2+y, 1-z

Cg(2) = Ni(1), O(2), C(31), N(7), N(6); Cg(1) = Ni(1), O(1), C(13), N(3), N(2);

Cg(9) = C(7), C(8), C(9), C(10), C(11), C(12)

Table 6.4.
C-H... π interactions of [Ni(L³)₂]·H₂O

Cg(I)Res(I)---Cg(J)	Cg-Cg (Å)	α (°)	β (°)
Cg(5) [1] -> Cg(6) ^a	3.6159	1.68	20.02
Cg(6) [1] -> Cg(6) ^b	3.6043	0.00	21.17
Cg(4) [1] -> Cg(4) ^c	3.9244	0.00	31.88

a = 1+x, y, z, b = -x, 2-y, 1-z, c = -x, 2-y, -z

Cg(5) = N(1), C(1), C(2), C(3), C(4), C(5); Cg(6) = N(4), C(9), C(8), C(12), C(11), C(10); Cg(4) = Ni(1), N(5), C(17), C(18), N(6)

Table 6.5.
Electronic spectral assignments of the palladium(II) compounds in (cm⁻¹)

Compounds	Ligand transitions	d-d	CT
HL ¹	31340, 37040	-	-
Pd(HL ¹)Cl ₂	30670, 34600	14140, 18310	22990, 21460 (sh)
H ₂ L ²	30580, 35460	-	-
Pd(HL ²)Cl·H ₂ O	31850 (sh), 37170	12410, 17010	21190, 22520
HL ³	31440, 33780	-	-
Pd(HL ³)Cl ₂ ·2H ₂ O	31150, 35560, 37730 (sh)	15920	22075 (sh), 23580

References

1. M. A. Halcrow, G. Cristou, *Chem. Rev.* 94 (1994) 2421.
2. A. F. Kolodziej, *Prog. Inorg. Chem.* 41 (1994) 493.
3. D. X. West, H. Gebremedhin, R. J. Butcher, J. P. Jasinski, A. E. Liberta, *Polyhedron* 12 (1993) 2489.
4. J. R. Morrow, K. A. Kolasa, *Inorg. Chim. Acta* 195 (1992) 245.
5. Z. H. Chohan, H. Pervez, S. Kausar, C. T. Supuran, *Synth. React. Inorg. Met.-Org. Chem.* 32 (2002) 529.
6. F. H. Urena, N. A. I. Cabeza, M. N. M. Carretero, A. L. P. Chamorro, *Acta Chim. Slov.* 47 (2000) 481.
7. A. Bacchi, M. Carcelli, P. Pelagitti, C. Pelizzi, G. Pelizzi, C. Salati, P. Sgarabotto, *Inorg. Chim. Acta* 295 (1999) 171.
8. P. K. Singh, D. N. Kumar, *Spectrochim. Acta* 64A (2006) 853.
9. S. Chandra, U. Kumar, *Spectrochim. Acta* 61A (2005) 219.
10. N. Nawar, N. M. Hosny, *Chem. Pharm. Bull.* 47 (1999) 944.
11. R. C. Maurya, P. Patel, D. Sutradhar, *Synth. React. Inorg. Met.-Org. Chem.* 33 (2003) 1857.
12. Y. J. Jang, U. Lee, B. K. Koo, *Bull. Korean Chem. Soc.* 26 (2005) 925.
13. S. S. Tandon, S. Chander, L. K. Thompson, *Inorg. Chim. Acta* 300-302 (2000) 683.
14. M. Shakir, S. Parveen, N. Begum, Y. Azim, *Transition Met. Chem.* 29 (2004) 916.
15. I. Ivanovic-Burmazovic, A. Bacchi, G. Pellizzi, V. M. Leovac, K. Andjelkovic, *Polyhedron* 18 (1998) 119.
16. K. Andjelkovic, I. Ivanovic, S. R. Niketic, B. V. Prelesnik, V. M. Leovac, *Polyhedron* 16 (1997) 4221.
17. G. Pellizzi, A. Bacchi, I. Ivanovic-Burmazovic, M. Gruden, K. Andjelkovic, *Inorg. Chem. Comm.* 4 (2001) 311.

18. P. Pelagatti, M. Carcelli, C. Pelizzi, M. Costa, *Inorg. Chim. Acta* 342 (2003) 323.
19. T. Mino, T. Ogawa, M. Yamashita, *J. Org. Met. Chem.* 665 (2003) 122.
20. S. D. Perera, B. L. Shaw, M. T. Pett, *Inorg. Chim. Acta* 236 (1995) 7.
21. J. F. Hartwig, *Angew. Chem. Int. Ed.* 37 (1998) 2090.
22. N. Takeda, D. Shimizu, N. Tokitoh, *Inorg. Chem.* 44 (2005) 8561.
23. A. L. Hector, W. Levason, M. Webster, *Inorg. Chim. Acta* 343 (2003) 90.
24. C. M. Armstrong, P. V. Bernhardt, P. Chin, D. R. Richardson, *Eur. J. Inorg Chem.* (2003) 1145.
25. P. V. Bernhardt, J. Mattsson, D. R. Richardson, *Inorg. Chem.* 45 (2006) 752.
26. M. F. Iskander, T. E. Khalil, R. Werner, W. Haase, I. Svoboda, H. Fuess, *Polyhedron* 19 (2000) 1181.
27. See Chapter 7 of this thesis.
28. D. Demertzi, D. Nicholls, *Inorg. Chim. Acta* 73 (1983) 37.

Investigations on the structural and spectral aspects of Zn(II) and Cd(II) complexes of nicotinoylhydrazone

Zinc with atomic number 30, atomic weight 65.39 and with the usual and most stable oxidation state II is an essential element in all-living systems and plays a structural role in many proteins and enzymes. Many proteins have been found to have a zinc-containing motif that serves to bind DNA embedded in their structure. In the relevance of zinc to Diabetes Mellitus (DM), zinc is known to be present in insulin, coordinated by three nitrogen atoms from histidines and three water molecules in an irregular octahedral environment, which is also believed to have a functional structure. Zinc containing carboxylate bridged complexes [1, 2] have varied structural motifs in hydrolytic metalloenzymes, such as phosphatases and aminopeptidases. The catalytic role of Zn comprises Lewis acid activation of the substrate, generation of a reactive nucleophile (Zn-OH) and stabilization of the leaving group [3]. There are several reports in literature based on the Zn(II) complexes of aroylhydrazones [4-8].

Cadmium is an extremely toxic element that is naturally present in the environment and also as a result of human activities. Analysis of biosystems with cadmium ion becomes a problem of particular importance in view of the established toxic influence of this metal, associated with Hg and Pb to the group of the most toxic environmental pollutants [9-11]. Its toxicity derives from the fact that it is rapidly localized intracellularly, mainly in the liver and then bound to metallothionein forming a complex that is slowly transferred to the blood stream to be deposited in the kidneys. This metal competes with Zn and blocks active sites of metal-enzymes and as a relatively soft acid it can dislodge Zn(II) in

cysteine-coordinated zinc compounds or Ca(II) ions in bone cells. The development of chelating agents is essential for the treatment of cadmium intoxication. Several transition metal complexes including some cadmium complexes containing different types of hydrazone ligands have been reported [12-15]. Though cadmium has been known as a toxic metal and is often associated with mercury and lead as one of the biologically harmful metal ions, the cadmium(II) ion has recently been found to serve as the catalytic center in a newly discovered carbonic anhydrase [16].

7.1. Stereochemistry

Zn(II) and Cd(II) systems with d^{10} configuration usually forms six coordinate and four coordinate structures. In the present study, the synthesized Zn(II) complexes exhibit both the geometries whereas the Cd(II) systems are found to have octahedral geometry.

7.2. Experimental

7.2.1. Materials

2-Benzoylpyridine (Sigma Aldrich), pyridine-2-carbaldehyde (Sigma Aldrich), nicotinoylhydrazide (Sigma Aldrich), $\text{Zn}(\text{CH}_3\text{COO})_2 \cdot 2\text{H}_2\text{O}$ (S. D. Fine), ZnBr_2 (Riedel-de-Haen), $\text{Cd}(\text{CH}_3\text{COO})_2 \cdot 2\text{H}_2\text{O}$ (Qualigens), and $\text{CdCl}_2 \cdot 2.5\text{H}_2\text{O}$ (CDH) used as received. The solvent used, ethanol was distilled before use.

7.2.2. Syntheses of ligands

Ligands HL^1 and HL^3 were synthesized as described previously in Chapter 2.

7.2.3 Preparation of Zn(II) complexes

$[\text{Zn}(\text{L}^1)\text{Cl}] \cdot \text{H}_2\text{O}$ (22): To a solution of the ligand (0.302 g, 1 mmol) in ethanol, ZnCl_2 (0.136 g, 1 mmol) dissolved in ethanol was added. The resulting yellow colored solution was stirred for 6 hours. The solution was then left

overnight for slow evaporation. The shining yellow solid deposited was filtered, washed with ethanol, followed by ether and dried over P_4O_{10} *in vacuo*. Yield: 0.683 g (68.3%). Elemental Anal. Found (Calcd.) (%): C, 52.04 (51.45); H, 4.01 (3.60); N, 12.71 (13.33).

[Zn(L¹)Br]·0.5H₂O (23): Compound **23** was prepared by the same procedure as that of compound **22**. ZnBr₂ (0.225 g, 1 mmol) was used instead of ZnCl₂. Yield: 0.237 g (52%). Elemental Anal. Found (Calcd.) (%): C, 47.53 (47.45); H, 3.58 (3.10); N, 11.67 (12.30).

[Zn(L¹)NCS]·0.5H₂O (24): Zn(II) acetate (0.219 g, 1 mmol) dissolved in ethanol was added to a solution of the ligand HL¹ (0.302 g, 1 mmol) in ethanol by stirring. To the resulting yellow solution, aqueous solution of KNCS (0.971 g, 1 mmol) was added and the stirring was continued for 6 hours. The solution was then left overnight for slow evaporation. Yellow product formed was filtered, washed with water, followed by ethanol and ether and dried over P_4O_{10} *in vacuo*. Yield: 0.245 g (56.4%). Elemental Anal. Found (Calcd.) (%): C, 52.22 (52.61); H, 3.25 (3.25); N, 15.81 (16.14).

[Zn(L¹)₂]·0.5H₂O (25): To a solution of the ligand HL¹ (0.302 g, 1 mmol) in ethanol, Zn(II) acetate (0.109 g, 0.5 mmol) in ethanol was added and stirred for 3 hours. The yellow crystalline solid deposited was separated, washed with ethanol, followed by ether and dried over P_4O_{10} *in vacuo*. Yield: 0.496 g (73.2%). Elemental Anal. Found (Calcd.) (%): C, 63.82 (63.86); H, 3.93 (4.02); N, 16.68 (16.55).

[Zn(L³)₂]·2H₂O (26): Zn(II) acetate (0.109 g, 0.5 mmol) in ethanol was added to an ethanolic solution of the ligand HL³ (0.262 g, 1 mmol) and stirred for 6 hours. The resulting yellow turbid solution was left overnight to obtain a yellow product. The product was filtered, washed with ethanol followed by ether and dried over P_4O_{10} *in vacuo*. Yield: 0.320 g (57.9%). Elemental Anal. Found (Calcd.) (%): C, 52.89 (52.23); H, 3.42 (4.02); N, 19.9 (20.30).

7.2.4 Preparation of Cd(II) complexes

[Cd(L¹)₂] (27): To an ethanolic solution of ligand HL¹ (0.302 g, 1 mmol), Cd(CH₃COO)₂·2H₂O (0.133 g, 0.5 mmol) dissolved in ethanol was added by stirring. The stirring was continued for 5 hours. The resulting bright yellow solution was left overnight to obtain shining yellow crystals. The crystals were separated and washed with ether and dried over P₄O₁₀ *in vacuo*. Yield: 0.503 g (70.3%). Elemental Anal. Found (Calcd.) (%): C, 60.40 (60.47); H, 3.59 (3.66); N, 15.89 (15.67).

[Cd(HL³)Cl₂]_n·nH₂O (28): CdCl₂·2.5H₂O (0.228 g, 1 mmol) was dissolved in ethanol and added to ligand HL³ (0.262 g, 1 mmol) dissolved in ethanol by stirring. The stirring was continued for 3 hours. The pale yellow product obtained was collected, filtered, washed with ethanol followed by ether and dried over P₄O₁₀ *in vacuo*. Yield: 0.296 g (69.3%). Elemental Anal. Found (Calcd.) (%): C, 33.79 (33.71); H, 2.68 (2.83); N, 13.08 (13.10).

[Cd(HL³)Br₂]·H₂O (29): Compound 29 was prepared by the same procedure as that of compound 28. CdBr₂·4H₂O (0.344 g, 1 mmol) was used instead of CdCl₂·2.5H₂O. Yield: 0.347 g (67.1%). Elemental Anal. Found (Calcd.) (%): C, 28.09 (27.91); H, 2.21 (2.34); N, 10.85 (10.85).

7.3. Results and discussion

Reaction of equimolar ratios of the ligand and the metal salt yielded metal complexes in which the ligand to metal ratio is 1:1. In all Zn(II) complexes, the ligands are coordinated in enolate form. However in Cd(II) complexes, HL¹ is coordinated in enolate form whereas HL³ existed in neutral form. Formation of [M(L)₂] complexes was straightforward by reaction of 2:1 ratios of the ligand and the metal salt. All the Zn(II) complexes and the Cd(II) complex, [Cd(L¹)₂] was found to be colored yellow. The other two Cd(II) complexes were found to be colorless. The compounds are less soluble in organic solvents such as ethanol, methanol and chloroform, but more soluble in solvents like DMSO and DMF.

7.3.1 Crystal structure of $[\text{Zn}(\text{L}^1)_2]$

$[\text{Zn}(\text{L}^1)_2]$: Crystals of $[\text{Zn}(\text{L}^1)_2]$, suitable for X-ray analysis were obtained from a solution of the compound dissolved in 1:1 solution of ethanol and DMF. The selected crystal was pale yellow in color and block shaped of dimensions 0.30 x 0.25 x 0.25 mm³. The structural refinement parameters are given in Table 7.1. As evident from the structure (Fig. 7.1), the two terdentate ligands are coordinated to the metal in the anionic form. The bond length C(13)–O(1) (1.263(6) Å) observed, supports this coordination. The ligands as found in the other similar structures of $[\text{Cu}(\text{L}^1)_2]$, $[\text{Ni}(\text{L}^1)_2]$ and $[\text{Mn}(\text{L}^1)_2]$, coordinates to zinc through the enolate oxygen, azomethine nitrogen and pyridine nitrogen, thereby forming four five membered chelate rings.

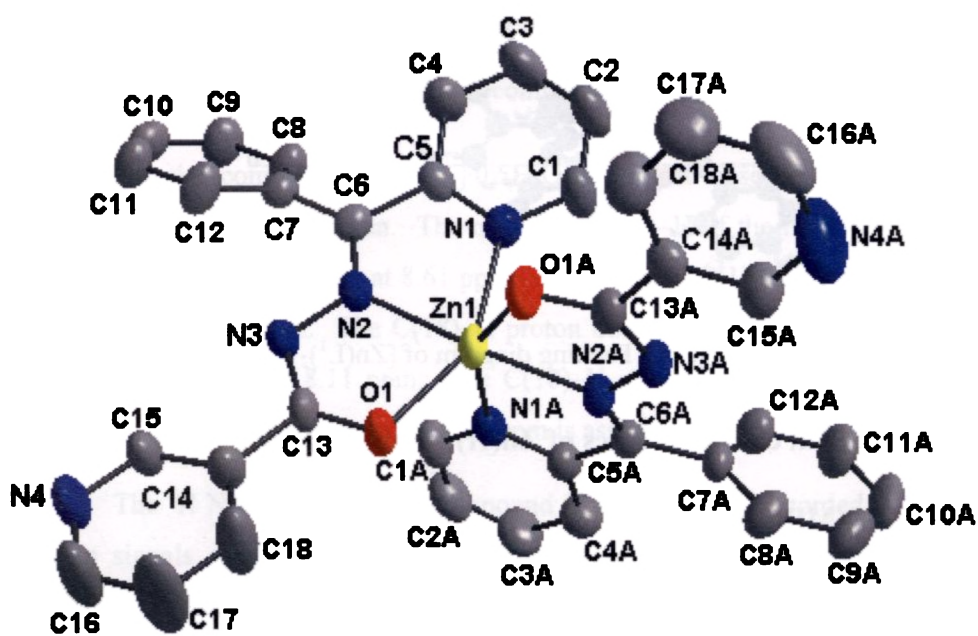


Fig. 7.1. Molecular structure of $[\text{Zn}(\text{L}^1)_2]$. Hydrogen atoms are omitted for clarity

The list of bond distances and bond angles quoted in Table 7.2 indicates relevant departures from the ideal octahedral values. Table 7.3 lists the deviations

from the three least-square coordination planes around the metal center. It is seen that the plane comprised of atoms N(1), O(1), O(1A), N(1A) were close to planarity compared to others, the largest deviation from the mean least square plane through them being 0.59 Å and Zn being displaced by 0.0009 Å. The packing diagram of the compound is given in Fig. 7.2. Four C–H--- π interactions are seen which are listed in Table 7.4. The π - π interactions observed are weak, as they are found at distances greater than 3.9 Å.

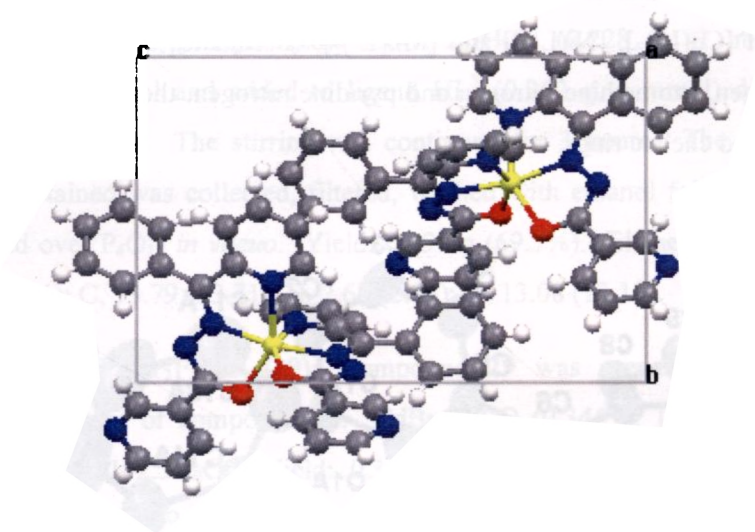


Fig. 7.2. Packing diagram of $[\text{Zn}(\text{L}^1)_2]$

7.3.2 Spectral characteristics of Zn(II) complexes

7.3.2a ^1H NMR spectral studies

The ^1H NMR spectrum of compound $[\text{Zn}(\text{L}^1)\text{Cl}]\cdot\text{H}_2\text{O}$ recorded in CDCl_3 displayed a singlet at 9.33 ppm corresponding to one proton which is assigned to C(15)–H proton. The multiplet observed at 8.87 ppm corresponding to two protons are that of C(1)–H and C(16)–H protons. The assignment of remaining protons are difficult as they are found as a multiplet at 7.79 - 7.08 ppm. In the compound $[\text{Zn}(\text{L}^1)\text{NCS}]\cdot 0.5\text{H}_2\text{O}$, the C(15)–H proton adjacent to pyridyl nitrogen

and carbonyl group is observed at 9.13 ppm (Fig. 7.3). The α protons of the pyridyl ring, C(1)-H and nicotinoyl ring, C(16)-H integrated as two protons, for the multiplet observed at 8.63 ppm. The signal at 8.28 ppm corresponding to one proton is assigned for the C(18)-H proton.

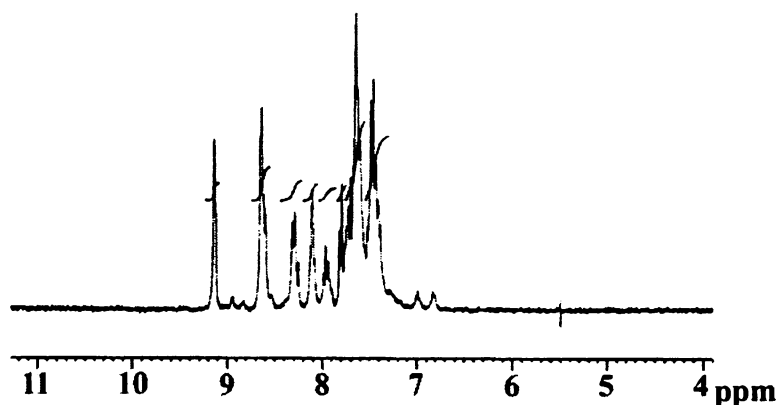


Fig. 7.3. ^1H NMR spectrum of compound $[\text{Zn}(\text{L}^1)\text{NCS}] \cdot 0.5\text{H}_2\text{O}$

For the compound $[\text{Zn}(\text{L}^1)_2] \cdot 0.5\text{H}_2\text{O}$, a singlet observed at 9.12 ppm corresponds to C(15)-H proton. The α proton, C(16)-H of the nicotinoyl ring is found as a doublet of doublet at 8.61 ppm. The α proton C(1)-H, of pyridine ring is observed at 8.25 ppm. The C(18)-H proton due to coupling with C(17)-H is viewed as a doublet at 8.11 ppm. The C(10)-H proton resonates as a triplet at 7.95 ppm. The doublet observed at 7.81 ppm is assigned to C(4)-H proton.

The ^1H NMR spectrum of compound $[\text{Zn}(\text{L}^3)_2] \cdot 2\text{H}_2\text{O}$, recorded in DMSO has no signals corresponding to N-H proton (Fig. 7.4). This implies that the ligand is coordinated in enolate form. The α proton C(9)-H, with no neighboring protons is observed at 9.27 ppm. The singlet at 8.81 ppm corresponds to the aldehydic proton C(6)-H. The C(10)-H proton resonates as a doublet of doublet at 8.64 ppm. The signal at 8.36 ppm is assigned for the C(1)-H proton. The multiplet observed at 8.02 ppm corresponds to the C(3)-H and C(12)-H protons. The C(4)-H proton resonates as a doublet at 7.81 ppm.

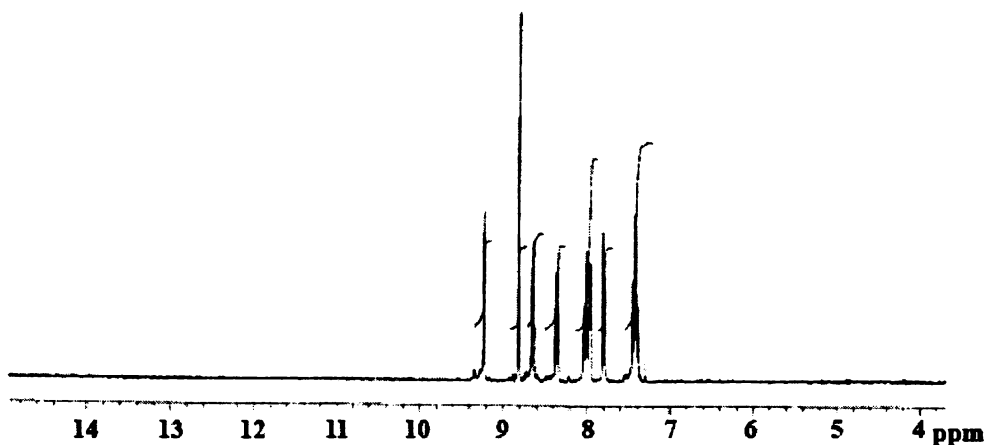


Fig. 7.4. ^1H NMR spectrum of compound $[\text{Zn}(\text{L}^3)_2]\cdot 2\text{H}_2\text{O}$

7.3.2b Electronic spectral studies

For zinc(II) systems no d-d transitions are expected since the d shell is completely filled. All the zinc complexes were found to be yellow in color. This color arises due to charge transfer transitions. Table 7.5 lists the various ligand and charge transfer transitions in the zinc(II) complexes.

7.3.2c IR spectral studies

The elemental analyses of the Zn(II) complexes suggested an enolate coordination of the ligands in all the zinc(II) complexes. IR spectral analysis also supports this observance. The azomethine bands were shifted as a result of coordination and the newly formed C=N band is observed at a higher frequency than that of the azomethine band. The bands observed at $1355\text{--}1375\text{ cm}^{-1}$ correspond to that of the C–O bond. The compound $[\text{Zn}(\text{L}^1)\text{NCS}]\cdot 0.5\text{H}_2\text{O}$ (**24**) displays a band at 2066 cm^{-1} corresponding to that of $\nu(\text{NCS})$ band. This indicates coordination of isothiocyanato group through nitrogen atom to the metal center. The IR spectral data of the Zn(II) complexes are listed in Table 7.6.

7.3.3 Crystal structures of $[\text{Cd}(\text{L}^1)_2]$ and $[\text{Cd}(\text{HL}^3)\text{Cl}_2]_n \cdot n\text{H}_2\text{O}$

$[\text{Cd}(\text{L}^1)_2]$: Diamond shaped light yellow crystals suitable for diffraction were obtained from a 1:1 mixture of ethanol and DMF. The crystal system is orthorhombic with $Fdd2$ space group. The structural refinement parameters are given in Table 7.7. The number of molecules per unit cell is eight. The ligand coordinates to the Cd(II) center in the enolate form, forming two five membered chelate rings, $\text{Cd}(1)\text{--O}(1)\text{--C}(13)\text{--N}(3)\text{--N}(2)$ and $\text{Cd}(1)\text{--N}(1)\text{--C}(5)\text{--C}(6)\text{--N}(2)$ (Fig. 7.5). The mode of coordination is meridional binding through the NNO donor atoms. The distorted octahedral geometry around the metal center is well evident from the departure of bond angles from the ideal octahedral values. The selected bond lengths and bond angles are listed in Table 7.8. A comparison of the bond lengths of $[\text{Cd}(\text{L}^1)_2]$ with that of $[\text{Zn}(\text{L}^1)_2]$ shows that the metal-donor bond lengths in the Cd(II) complex are nearly the same, whereas there are variations in these bond lengths in case of Zn(II) complex. Packing diagram of the compound is given in Fig. 7.6.

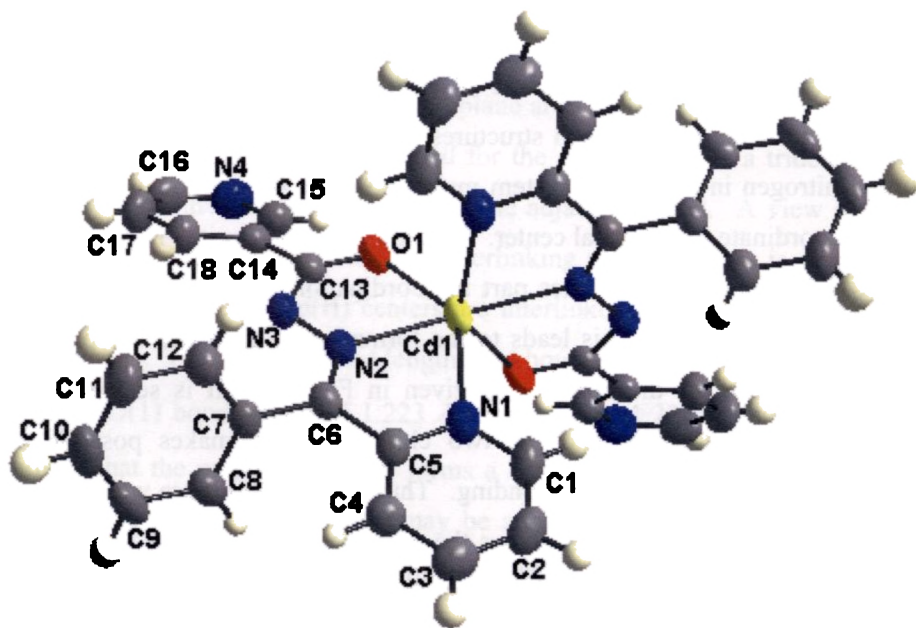


Fig. 7.5. Molecular structure of $[\text{Cd}(\text{L}^1)_2]$

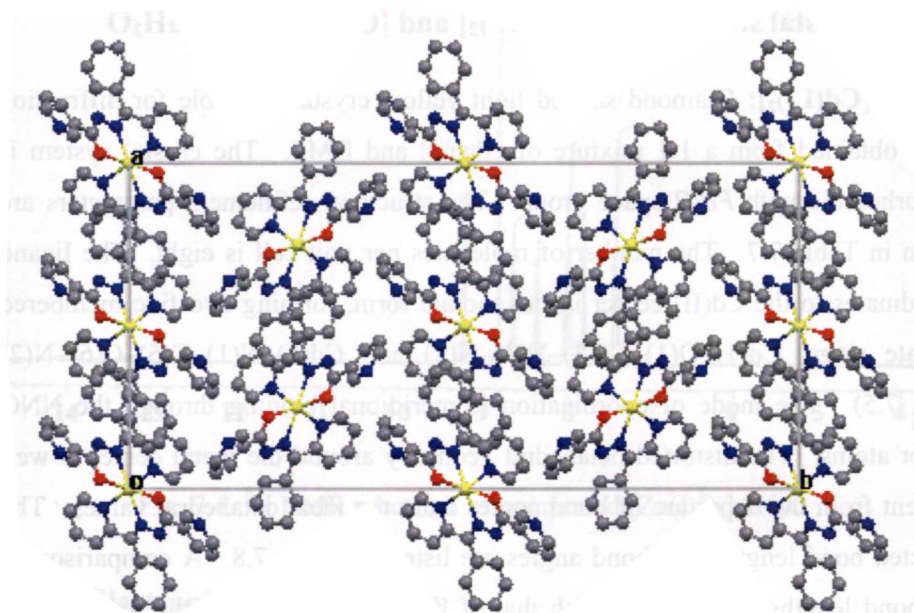


Fig. 7.6. Packing diagram of the compound $[\text{Cd}(\text{L}^1)_2]$

$[\text{Cd}(\text{HL}^3)\text{Cl}_2]_n \cdot n\text{H}_2\text{O}$: Colorless single crystals suitable for X-ray diffraction analysis were obtained from the solution of the complex in DMF-ethanol mixture. The crystal structure of $[\text{Cd}(\text{HL}^3)\text{Cl}_2]_n \cdot n\text{H}_2\text{O}$ appeared to be different from all the other crystal structures described earlier. The presence of nicotinoyl nitrogen in the ligand system makes possible an additional donor site, which can coordinate to the metal center. This nitrogen (N4) as it is far away from the usual NNO donor core, it takes part in coordination by binding itself to the neighboring Cd(II) center. This leads to the formation of a polymeric complex. The crystal structure of the complex is given in Fig. 7.7. It is seen that the presence of water molecule and the two chlorine atoms makes possible an extensive intermolecular hydrogen bonding. Thus the molecules are well packed. The presence of two chloride ions shows the existence of the neutral form of the ligand. Single crystal X-ray diffraction study provided a clear picture of the coordination mode of the ligand. The structural refinement parameters are given in Table 7.9.

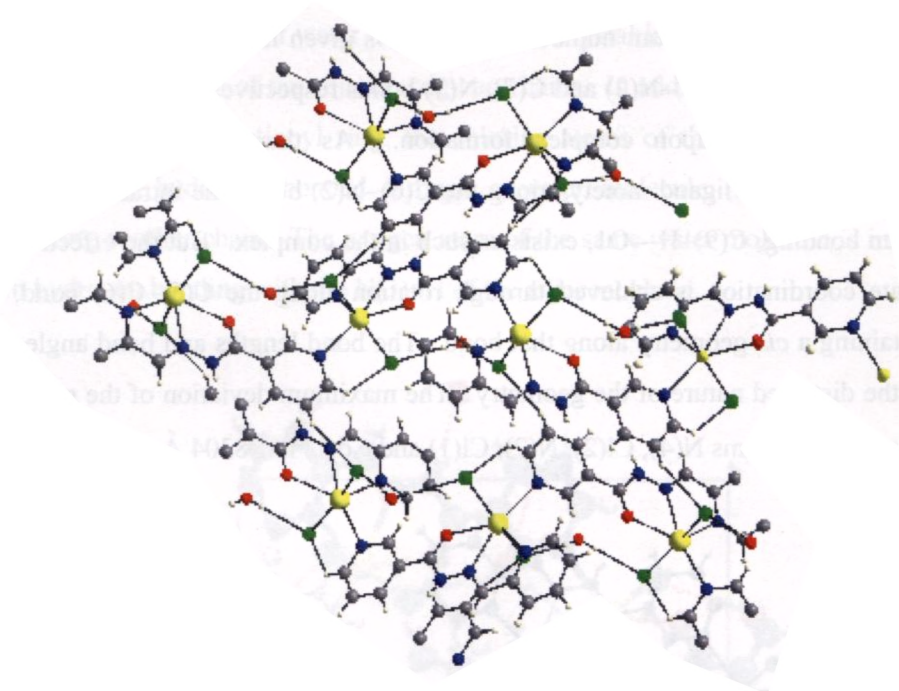


Fig. 7.7. Crystal structure of $[\text{Cd}(\text{HL}^3)\text{Cl}_2]_n \cdot n\text{H}_2\text{O}$ with intermolecular hydrogen bonding

The geometry of the central Cd(II) ion is best described as a six coordinate distorted octahedron. The coordination plane around the Cd(II) ion is surrounded by N_3OC_2 core. The ligand employed for the construction is a tridentate NNO donor. So the third nitrogen donor is of the adjacent ligand. A view of the 1D polymeric chain formed as a result of interlinking nictinoyl rings is given in Fig. 7.8. Thus two adjacent Cd(II) centers are interlinked by the bridging nictinoyl nitrogen N(4). The selected bond lengths and bond angles are listed in Table 7.10. The C(7)–O(1) bond length of 1.223 Å compared to 1.227 Å in the free ligand confirms that the carbonyl oxygen forms a coordinate bond with the Cd(II) ion. The decrease in this bond length, may be attributed to the loss of lone pair on oxygen atom upon coordination, which imparts a partial positive nature for the C(7)–O(1) bond. The chloride ligands are *trans* positioned with respect to the metal ion [Cl(1)–Cd(1)–Cl(2) 158.34° (3)] so as to minimize the lone pair repulsion. The crystal structure of one independent molecule of

$[\text{Cd}(\text{L}^3)\text{Cl}_2]_n \cdot n\text{H}_2\text{O}$ with atom numbering scheme is given in Fig. 7.9. The *trans* and *cis* nature of the C(6)–N(2) and C(7)–N(3) bonds respectively of the ligand is maintained as such upon complex formation. As there is no change in configuration of the ligand moiety, along the C(6)–N(2) bond, the intramolecular hydrogen bonding, C(9)–H---O1, exists as such in the complex. But the effective tridentate coordination is achieved through rotation along the C(5)–C(6) bond, thus attaining a *cis* geometry along that bond. The bond lengths and bond angles reveal the distorted nature of the geometry. The maximum deviation of the plane described by the atoms N(4), Cl(2), N(2), Cl(1) and Cd(1) is 1.8304 Å.

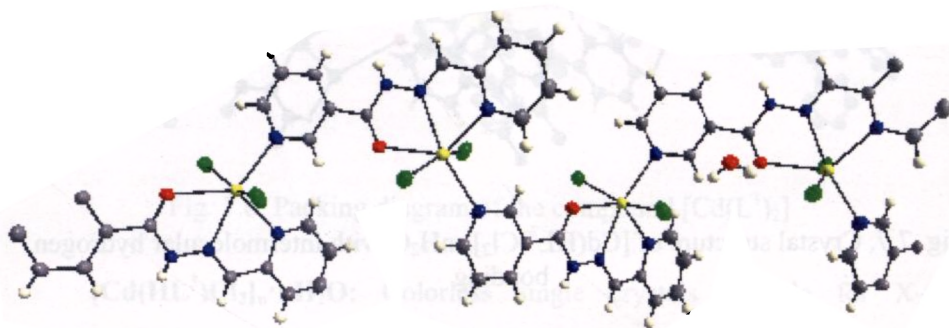


Fig. 7.8. 1D polymeric chain of $[\text{Cd}(\text{HL}^3)\text{Cl}_2]_n \cdot n\text{H}_2\text{O}$

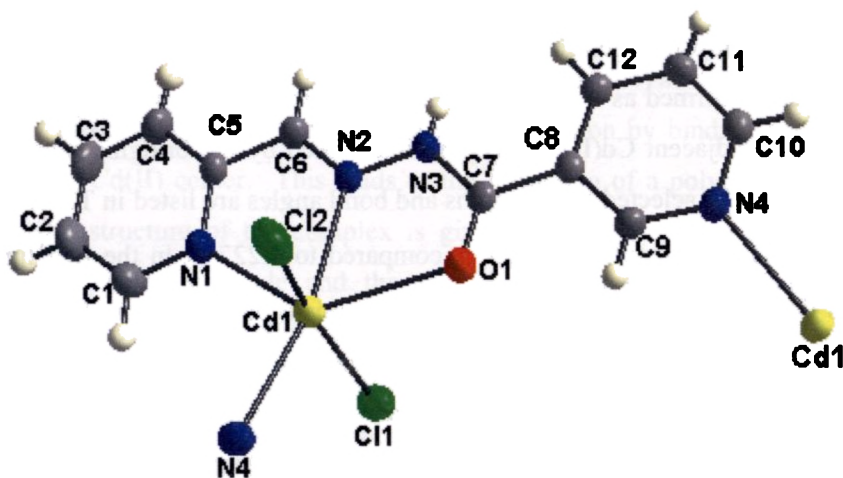


Fig. 7.9. Molecular structure of $[\text{Cd}(\text{HL}^3)\text{Cl}_2]_n \cdot n\text{H}_2\text{O}$ with atom numbering scheme

The presence of water molecule in the crystal lattice plays a major role in the interconnection of the adjacent zig-zag chains. In addition to the chain formed by the bridging nicotinoyl ring, the chlorine atoms of the nearby cadmium(II) centers are hydrogen bonded through a water molecule (Fig. 7.10), thereby creating another chain. The oxygen atom of the same water molecule is involved in hydrogen bonding with the N(3)–H of the adjacent chain.

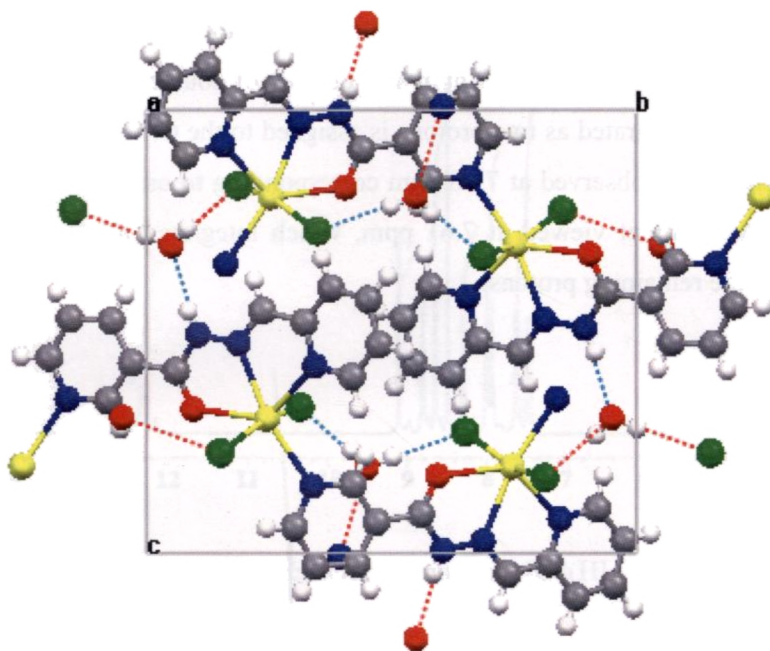


Fig. 7.10. Packing diagram of of $[\text{Cd}(\text{HL}^3)\text{Cl}_2]_n \cdot n\text{H}_2\text{O}$ with hydrogen bonding

The other intermolecular interactions involve $\text{C}(11)\text{--H}\cdots\text{Cl}(2)^i$ [$d_{\text{C}(11)\text{--Cl}(2)}$ 3.505(3) Å; $i = 1-x, -y, 1-z$] and $\text{C}(12)\text{--H}\cdots\text{O}(5)^{ii}$ [$d_{\text{C}(12)\text{--O}(5)}$ 3.329(4) Å; $ii = 1/2+x, 1/2-y, -1/2+z$]. Hence a wide network of interconnected chains is formed in the lattice. In the 1D chain, a distance of 7.958 Å separates the Cd centers, whereas the Cd–Cd distance between the adjacent chains is a little less than the above value, 7.536 Å. The π – π interactions observed are at distances greater than 3.5 Å.

7.3.4 Spectral characteristics of Cd(II) complexes

7.3.4a ^1H NMR spectral studies

^1H NMR spectra of all the Cd(II) compounds were recorded in DMSO solution. The compound $[\text{Cd}(\text{L}^1)_2]$ (**27**) displayed a signal at 9.10 ppm (Fig. 7.11) corresponding to one proton, which is assigned for the C(15)–H proton with no neighboring protons. The coordination of the ligand in enolate form is evidenced by the absence of the signal corresponding to N–H proton. The C(16)–H proton resonated as a single proton at 8.59 ppm as a doublet of doublet. The multiplet at 8.24 ppm which integrated as two protons is assigned to the C(1)–H and C(18)–H protons. The triplet observed at 7.96 ppm corresponding to one proton is that of C(10)–H. A multiplet viewed at 7.61 ppm, which integrated as six protons is assigned for the remaining protons.

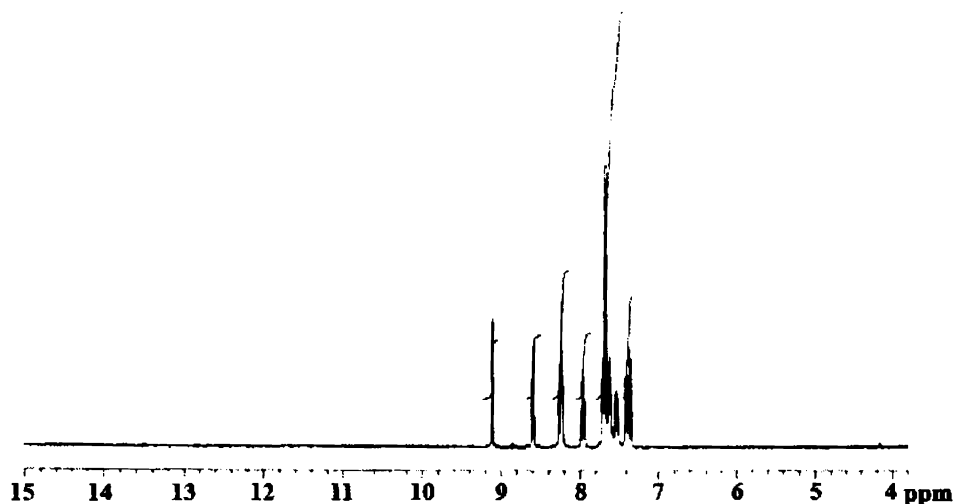


Fig. 7.11. ^1H NMR spectrum of compound $[\text{Cd}(\text{L}^1)_2]$

The coordination of the ligand HL^3 , in neutral form in the compound $[\text{Cd}(\text{HL}^3)\text{Cl}_2]_n \cdot n\text{H}_2\text{O}$ is evidenced by the singlet corresponding to one proton observed at 8.49 ppm. This is due to N–H proton. The aldehyde proton C(6)–H

resonates at 12.33 ppm (Fig. 7.12). The two doublets integrated as two protons at 8.79 and 8.64 ppm corresponds to α protons in the nicotinoyl ring and pyridyl rings, *viz.* C(10)-H and C(1)-H respectively. The C(12)-H proton *para* positioned to pyridyl nitrogen and adjacent to the carbonyl group is observed as a doublet at 8.31 ppm. The multiplet at 7.96 ppm integrated as two protons is assigned to C(3)-H and C(4)-H. The C(2)-H and C(11)-H protons are observed at 7.55 ppm as a multiplet.

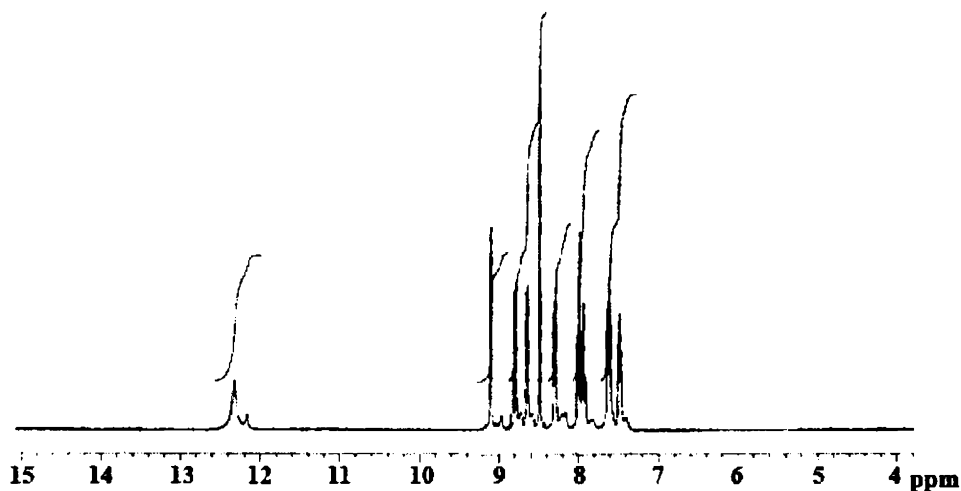


Fig. 7.12. ^1H NMR spectrum of compound $[\text{Cd}(\text{HL}^3)\text{Cl}_2]_n \cdot n\text{H}_2\text{O}$

The ^1H NMR spectrum of compound $[\text{Cd}(\text{HL}^3)\text{Br}_2] \cdot \text{H}_2\text{O}$ is similar in features to the $[\text{Cd}(\text{HL}^3)\text{Cl}_2]_n \cdot n\text{H}_2\text{O}$ compound. Here also the N-H proton resonated at 8.49 ppm as a singlet. The C(9)-H proton is observed at 9.10 ppm (Fig. 7.13). The aldehyde proton is observed at 12.41 ppm. The doublet viewed at 8.85 ppm is assigned for the C(10)-H proton. The α proton C(1)-H, adjacent to the pyridyl nitrogen resonated as a doublet at 8.65 ppm. The doublet which integrated as one proton at 8.30 ppm corresponds to C(12)-H proton.

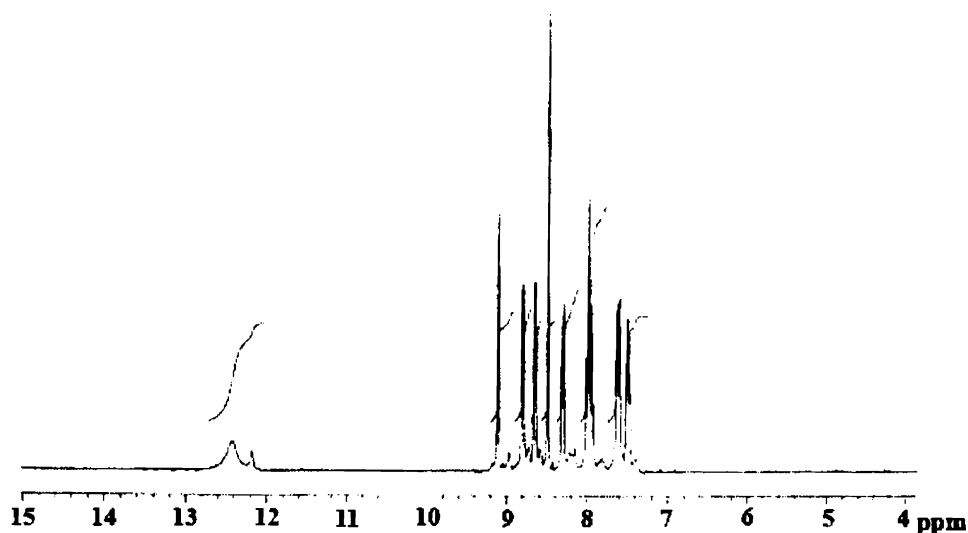


Fig. 7.13. ^1H NMR spectrum of compound $[\text{Cd}(\text{HL}^3)\text{Br}_2]\cdot\text{H}_2\text{O}$

7.3.4b Electronic spectral studies

For the Cd(II) complexes also, no d-d transitions are expected. The ligand and the charge transfer transitions found are listed in Table 7.11.

7.3.4c IR spectral studies

The crystal structure of the polymeric Cd(II) complex $[\text{Cd}(\text{HL}^3)\text{Cl}_2]_n\cdot n\text{H}_2\text{O}$ evidenced the coordination of the ligand in neutral form. The bromo complex $[\text{Cd}(\text{HL}^3)\text{Br}_2]\cdot\text{H}_2\text{O}$, also displayed similar IR spectral features to that of $[\text{Cd}(\text{HL}^3)\text{Cl}_2]_n\cdot n\text{H}_2\text{O}$. So possibly the bromo complex also could be polymeric with bridging nicotinoyl rings. Unfortunately single crystals suitable for diffraction were not obtained. The azomethine bands were found to have a positive shift. The shift of the coordinated carbonyl groups in $[\text{Cd}(\text{HL}^3)\text{Cl}_2]_n\cdot n\text{H}_2\text{O}$ and $[\text{Cd}(\text{HL}^3)\text{Br}_2]\cdot\text{H}_2\text{O}$ were not so profound. The IR spectral data of the Cd(II) complexes are given in Table 7.12.

Table 7.1.
Crystal data and structure refinement for the $[\text{Zn}(\text{L}^1)_2]$ complex

Parameters	$\text{Zn}(\text{L}^1)_2$
Empirical formula	$\text{C}_{36}\text{H}_{26}\text{N}_8\text{ZnO}_2$
Formula weight	668.02
Temperature	293(2) K
Color	Pale yellow
Nature	Blocks
Wavelength	0.71073 Å
Crystal system	Monoclinic
Space group	$P2_1$
Unit cell dimensions	$a = 9.3980(8)$ Å $b = 10.3990(19)$ Å $c = 16.7450(16)$ Å $\alpha = 90.00^\circ$ $\beta = 101.846(7)^\circ$ $\gamma = 90.00^\circ$
Volume, Z	$1601.6(4)$ Å ³ , 2
Calculated density	1.385 Mg/m ³
Absorption coefficient	0.813 mm ⁻¹
F (000)	688
Crystal size	0.30x 0.25x 0.25 mm
θ range for data collection	1.24 - 24.97°
Index ranges	$-10 \leq h \leq 11$, $-12 \leq k \leq 0$, $-19 \leq l \leq 0$
Reflections collected / unique	3073/2970 [R(int) = 0.0190]
Refinement method	Full-matrix least-squares on F^2
Data / restraints / parameters	2970 / 1 / 424
Goodness-of-fit on F^2	1.041
Final R indices [$I > 2\sigma(I)$]	$R1 = 0.0407$, $wR2 = 0.1047$
R indices (all data)	$R1 = 0.0666$, $wR2 = 0.1143$

Table 7.2.
Selected bond lengths (Å) and bond angles (°) for Zn(II) complex

Bonds		Bond angles	
N2–C6	1.293(7)	C6–N2–N3	121.2(4)
N2–N3	1.375(6)	O1–C13–N3	127.1(5)
N3–C13	1.346(7)	O1–C13–C14	117.8(5)
O1–C13	1.263(6)	N3–C13–C14	115.0(4)
Zn1–N2	2.095(4)	N1–C5–C6	115.9(5)
Zn1–N2A	2.075(4)	N2A–Zn1–N2	169.05(18)
Zn1–O1	2.071(4)	N2–Zn1–O1	75.61(17)
Zn1–O1A	2.100(4)	O1–Zn1–N2A	112.76(17)
Zn1–N1	2.194(5)	N2–Zn1–N1A	98.59(17)
Zn1–N1A	2.237(5)	O1A–Zn1–N1A	149.93(16)
		N2–Zn1–N1	74.19(17)
		N1A–Zn1–N1	96.27(19)
		N2–Zn1–O1	75.61(17)
		O1A–Zn1–O1	98.05(18)
		N1A–Zn1–O1	92.6(2)
		N1–Zn1–O1	149.46(17)

Table 7.3.
Deviations of atoms from least-square planes

In the coordination polyhedron	
N2, N1, O1A, O2A, Zn1	N2, 0.4886; N1, -0.3916; O1A, -0.3809; O2A, 0.2839; Zn1, -0.7906
N1A, N2A, O1A, O2A, Zn1	N1A, 0.3906; N2A, -0.5102; O1A, -0.2776; O2A, 0.3972; Zn1, 0.7497
N1, O1A, O2A, N1A, Zn1	N1, 0.5561; O1A, 0.5626; O2A, -0.5901; N1A, -0.5286; Zn1, -0.0009
In the ligands	
N1, C1, C2, C3, C4, C5	max. dev. -0.0096 for C4
C7, C8, C9, C10, C11, C12	max. dev. -0.0100 for C7
C14, C15, N4, C16, C17, C18	max. dev. 0.0109 for C17
N1A, C1A, C2A, C3A, C4A, C5A	max. dev. -0.0130 for C3A
C7A, C8A, C9A, C10A, C11A, C12A	max. dev. -0.0093 for C8A
C14, C15, N4, C16, C17, C18	max. dev. 0.0197 for C16A

Table 7.4.
C-H--- π interactions of [(ZnL¹)₂]

X-H(I)---Cg(J)	H--Cg (Å)	X--Cg (Å)	X-H--Cg (°)
C(1)–H(1)[1]---Cg(2) ^a	2.77	3.1435	105
C(1A)–H(1A) [1]---Cg(1) ^d	2.99	3.3556	105
C(9)–H(9)[1]---Cg(1) ^b	2.73	3.5111	142
C(16)–H(16)[1]---Cg(9) ^c	2.90	3.6949	144

Equivalent position code

a – x, y, z; b = 1-x, -1/2+y, 1-z; c – 2-x, 1/2+y, 1-z

Cg(1) – Zn(1), O(1A), C(13), N(3), N(2); Cg(2) = Zn(1), O(2A), C(13A), N(3A), N(2A); Cg(9) = C(7), C(8), C(9), C(10), C(11), C(12)

Table 7.5.
Electronic spectral data (cm⁻¹) of zinc(II) complexes

Compounds	n → π^*	$\pi \rightarrow \pi^*$	CT
HL ¹	31340	37040, 46510	-
[Zn(L ¹)Cl]·H ₂ O	30570	35330	25650
[Zn(L ¹)Br]·0.5H ₂ O	31250	37030	25980
[Zn(L ¹)NCS]·0.5H ₂ O	31060	36500	25640
[Zn(L ¹) ₂]·0.5H ₂ O	32890	38160	26040
HL ³	31440	33780	-
[Zn(L ³) ₂]·2H ₂ O	33330	36630	26460

Table 7.6.
IR spectral data (cm⁻¹) of zinc(II) complexes

Compounds	$\nu(\text{C}=\text{N})$	$\nu(\text{C}=\text{N}_{\text{azo}})$	$\nu(\text{C}=\text{O})/(\text{C}-\text{O})$
HL ¹	-	1579	1683
[Zn(L ¹)Cl]·H ₂ O	1615	1559	1373
[Zn(L ¹)Br]·0.5H ₂ O	1619	1555	1369
[Zn(L ¹)NCS]·0.5H ₂ O	1614	1563	1377
[Zn(L ¹) ₂]·0.5H ₂ O	1588	1561	1367
HL ³	-	1595	1669
[Zn(L ³) ₂]·2H ₂ O	1591	1563	1356

Table 7.7.
Crystal data and structure refinement for the $[\text{Cd}(\text{L}^1)_2]$ complex

Parameters	$\text{Cd}(\text{L}^1)_2$
Empirical formula	$\text{C}_{36}\text{H}_{26}\text{CdN}_8\text{O}_2$
Formula weight	715.06
Temperature	296(2) K
Color	Light yellow
Nature	Diamond
Wavelength	0.71073 Å
Crystal system	Orthorhombic
Space group	$Fdd2$
Unit cell dimensions	$a = 18.791(4)$ Å $b = 38.998(9)$ Å $c = 8.6666(19)$ Å $\alpha = 90.00^\circ$ $\beta = 90.00^\circ$ $\gamma = 90.00^\circ$
Volume, Z	$6351(2)$ Å ³ , 8
Calculated density	$1.4957(5)$ Mg/m ³
Absorption coefficient	0.735 mm ⁻¹
$F(000)$	2896
Crystal size	0.36x 0.22x 0.12 mm
θ range for data collection	2.41-28.31
Index ranges	$-24 \leq h \leq 24$, $-51 \leq k \leq 51$, $-11 \leq l \leq 11$
Reflections collected / unique	12990 / 3733 [$R(\text{int}) = 0.0184$]
Refinement method	Full-matrix least-squares on F^2
Data / restraints / parameters	3733 / 1 / 265
Goodness-of-fit on F^2	1.056
Final R indices [$>2\sigma(1)$]	$R1 = 0.0220$, $wR2 = 0.0549$
R indices (all data)	$R1 = 0.0231$, $wR2 = 0.0554$

Table 7.8.

Selected bond lengths (Å) and bond angles (°) for [Cd(L¹)₂] complex

Bonds	[Cd(L ¹) ₂]
N2–C6	1.288(2)
N2–N3	1.377(2)
N3–C13	1.329(2)
O1–C13	1.265(2)
Cd1–N2	2.2761(15)
Cd1–O1	2.2783(15)
Cd1–N1	2.4062(19)
Bond angles	
C6–N2–N3	119.30(15)
O1–C13–N3	128.48(17)
O1–C13–C14	117.45(17)
N3–C13–C14	113.93(15)
N1–C5–C6	116.29(17)
N2–Cd1–N2	159.91(8)
N2–Cd1–O1	69.73(5)
O1–Cd1–N2	124.54(5)
N2–Cd1–N1	69.41(6)
O1–Cd1–N1	138.27(6)
N2–Cd1–N1	97.12(6)
N1–Cd1–N1	98.46(10)
O1–Cd1–O1	101.55(9)
N1–Cd1–O1	94.56(6)

Table 7.9.
Crystal data and structure refinement for the $[\text{Cd}(\text{HL}^3)\text{Cl}_2]_n \cdot n\text{H}_2\text{O}$ complex

Parameters	$[\text{Cd}(\text{HL}^3)\text{Cl}_2]_n \cdot n\text{H}_2\text{O}$
Empirical formula	$\text{C}_{12}\text{H}_{12}\text{CdCl}_2\text{N}_4\text{O}_2$
Formula weight	427.56
Temperature	273(2) K
Color	Colorless
Nature	Blocks
Wavelength	0.71073 Å
Crystal system	Monoclinic
Space group	$P2_1/n$
Unit cell dimensions	$a = 7.7393(8)$ Å $b = 14.6574(15)$ Å $c = 13.1252(14)$ Å $\alpha = 90.00^\circ$ $\beta = 91.431(2)^\circ$ $\gamma = 90.00^\circ$
Volume, Z	$1488.4(3)$ Å ³ , 4
Calculated density	1.908 Mg/m ³
Absorption coefficient	1.834 mm ⁻¹
F (000)	840
Crystal size	0.38x 0.33x 0.26 mm
θ range for data collection	2.08 - 28.29°
Index ranges	$-10 \leq h \leq 8$, $-12 \leq k \leq 19$, $-16 \leq l \leq 16$
Reflections collected / unique	8603 / 3430 [R(int) = 0.0201]
Refinement method	Full-matrix least-squares on F^2
Data / restraints / parameters	3430 / 0 / 238
Goodness-of-fit on F^2	1.141
Final R indices [$I > 2\sigma(I)$]	$R1 = 0.0353$, $wR2 = 0.0778$
R indices (all data)	$R1 = 0.0400$, $wR2 = 0.0801$

Table 7.10.

Selected bond lengths (Å) and bond angles (°) of $[\text{Cd}(\text{HL}^3)\text{Cl}_2]_n \cdot n\text{H}_2\text{O}$

Bonds		Bond angles	
N2-C6	1.267(4)	C6-N2-N3	120.0(3)
N2-N3	1.367(3)	O1-C7-N3	121.7(3)
C7-N3	1.360(4)	O1-C7-C8	121.3(3)
C7-O1	1.223(3)	N3-C7-C8	117.0(2)
Cd1-N1	2.378(2)	N1-Cd1-N2	68.51(8)
Cd1-N2	2.386(2)	N1-Cd1-N4	101.23(9)
Cd1-N4	2.411(3)	N2-Cd1-N4	166.83(8)
Cd1-C11	2.4926(9)	N1-Cd1-C11	106.02(7)
Cd1-O1	2.543(2)	N2-Cd1-C11	102.47(6)
Cd1-C12	2.5439(10)	N4-Cd1-C11	88.09(7)
		N1-Cd1-O1	132.41(7)
		N2-Cd1-O1	63.90(7)
		N4-Cd1-O1	125.85(8)
		C11-Cd1-O1	84.21(6)
		N1-Cd1-C12	95.35(7)
		N2-Cd1-C12	88.43(6)
		N4-Cd1-C12	84.26(7)
		C11-Cd1-C12	158.34(3)
		O1-Cd1-C12	83.94(6)

Table 7.11.
Electronic spectral data (cm^{-1}) of Cd(II) complexes

Compounds	$n \rightarrow \pi^*$	$\pi \rightarrow \pi^*$	CT
HL ¹	31340	37040, 46510	-
[Cd(L ¹) ₂]	32890	37170	25840
HL ³	31440	33780	-
[Cd(HL ³)Cl ₂] _n ·nH ₂ O	33440	36770	25910
[Cd(HL ³)Br ₂] _n ·nH ₂ O	32900	37180	25710

Table 7.12.
IR spectral data (cm^{-1}) of Cd(II) complexes

Compounds	$\nu(\text{C}=\text{N})$	$\nu(\text{C}=\text{N}_{\text{azo}})$	$\nu(\text{C}=\text{O})/(\text{C}-\text{O})$
HL ¹	-	1579	1683
[Cd(L ¹) ₂]	1590	1556	1354
HL ³	-	1595	1669
[Cd(HL ³)Cl ₂] _n ·nH ₂ O	-	1602	1664
[Cd(HL ³)Br ₂] _n ·nH ₂ O	-	1599	1658

References

1. Z. -L. You, H. -L. Zhu, W. -S. Liu, *Z. Anorg. Allg. Chem.* 630 (2004) 1617.
2. Z. -L. You, H. -L. Zhu, *Z. Anorg. Allg. Chem.* 630 (2004) 2754.
3. A. Erxleben, J. Hermann, *J. Chem. Soc. Dalton Trans.* (2000) 569.
4. K. K. Narang, R. M. Dubey, *Indian J. Chem.* 21A (1982) 830.
5. K. K. Narang, R. A. Lal, *Transition Met. Chem.* 2 (1977) 100.
6. G. Paolucci, P. A. Vigato, G. Rosetto, U. Casellato, M. Vidali, *Inorg. Chim. Acta* 65 (1982) L71.
7. C. Lorenzini, C. Pelizzi, G. Pelizzi, G. Predieri, *J. Chem. Soc. Dalton Trans.* (1983) 721.
8. C. Pelizzi, G. Pelizzi, G. Predieri, S. Resola, *J. Chem. Soc. Dalton Trans.* (1982) 1350.
9. G. D. Munno, S. Mauro, T. Pizzino, D. Viterbo, *J. Chem. Soc. Dalton Trans.* (1993) 1113.
10. H. P. Srivastava, D. Tiwari, *J. Indian Chem. Soc.* 70 (1993) 499.
11. M. D. Walker, D. R. Williams, *J. Chem. Soc. Dalton Trans.* (1974) 1186.
12. D. G. Paschalidis, I. A. Tossidis, M. Gdaniec, *Polyhedron* 19 (2000) 1629.
13. N. R. Sangeetha, S. Pal, C. E. Anson, K. A. Powell, S. Pal, *Inorg. Chem. Commun.* 3 (2000) 415.
14. C. Pelizzi, G. Pelizzi, F. Vitali, *J. Chem. Soc. Dalton Trans.* (1987) 177.
15. M. Fondo, A. Sousa, M. R. Bermejo, A. Garcia-Deibe, A. Sousa-Pedrares, O. L. Hoyos, M. Helliwell, *Eur. J. Inorg. Chem.* (2002) 703.
16. T. W. Lane, F. M. M. Morel, *Proc. Natl. Acad. Sci. USA* 97 (2000) 4627.

Schiff bases of hydrazides containing the main linkage RCH=N-NHR, are efficient multidentate ligands in forming metal complexes of interesting structures and properties. Attaching various substituents to the central hydrazide chain enhances the denticity of ligands. The presence of heterocyclic rings in this chain, provide potential donor sites which makes possible the formation of polynuclear metal complexes. These compounds are capable of exhibiting keto-enol tautomerism. Usually, upon metal complexation the ligand adopts the enolate form, thus acting in the anionic form. But coordination in keto form is also possible.

The heterocyclic ring systems chosen include pyridyl ring and nicotinoyl ring. The nicotinoyl systems are well known for their ability to form bridged polymer complexes with intriguing structural features. For the present study, C=O substituted hydrazone systems are selected. The presence of this group and the heterocyclic rings enhances the delocalization of electron charge density and can act as multidentate chelating agents. Accordingly, three new aroylhydrazone ligands are synthesized and characterized by ^1H NMR, IR and electronic spectral studies. The ligands synthesized are

- 1) 2-Benzoylpyridine nicotinoylhydrazone (HL^1)
- 2) 2-Benzoylpyridine-4-hydroxybenzoylhydrazone (H_2L^2)
- 3) Pyridine-2-carbaldehyde nicotinoylhydrazone (HL^3)

The ligands consist of two nitrogens and one oxygen capable of coordination with the metal ion. However, in the nicotinoyl systems, there is a fourth potential donor site corresponding to that of the nicotinoyl ring nitrogen. We could successfully isolate the single crystals of all the three ligands. The first (HL^1) and third (HL^3) ligands are triclinic with $P\bar{1}$ space group whereas the second ligand (H_2L^2) is monoclinic with $P2_1/n$ space group. In the first two ligands, HL^1

and H_2L^2 the geometry is *cis* in nature along the azomethine bond, whereas in the third ligand HL^3 , the geometry is *trans*.

Eight Cu(II) compounds are synthesized and characterized by various spectroscopic techniques such as IR, electronic spectral studies and EPR. The ligands are found to coordinate in the neutral form and in enolate form. The magnetic susceptibility measurements are found to be in the range of 1.5-1.9 BM characteristic of a d^9 system with one unpaired electron. In the electronic spectral studies, the d-d transitions are found to be broad. The EPR spectra of all the Cu(II) complexes were recorded both in polycrystalline state at 298 K and at solution in DMF at 77 K. The hyperfine splittings in the spectra are well evident in the frozen solution EPR spectra. But in none of the spectra, superhyperfine splittings were visible. The g values and the various EPR spectral parameters are calculated. The g values calculated indicate that in most of the complexes except that of $[Cu(L^3)_2]$ the unpaired electron is present in the $d_{x^2-y^2}$ orbital. The EPR spectrum of $[Cu(L^3)_2]$ is reverse axial in nature, which indicated that the unpaired electron resides in d_{z^2} orbital. We could isolate the single crystals of the six coordinate Cu(II) complexes viz. $[Cu(L^1)_2]$ (monoclinic, $P2_1$), $[Cu(HL^2)_2]$ (Monoclinic, $P2_1/n$) and $[Cu(L^3)_2]$ (triclinic, $P\bar{1}$). In all the three cases the ligand coordinates in the enolate form with NNO donor atoms. The geometry is distorted octahedral. The bond angles support this. In Cu(II) complexes $[Cu(L^1)_2]$ and $[Cu(HL^2)_2]$, the ligands undergo a rotation along the azomethine band for an effective tridentate coordination. Thus the *cis* nature of the bond is transformed to *trans*. However, the third ligand maintained its *trans* geometry along the azomethine bond. So for attaining NNO coordination, the ligand undergoes a rotation along the C5-C6 bond of the ligand. The single crystal studies revealed that in the Cu(II) complexes with ligands HL^1 and H_2L^2 , there occurs an elongation along one of the axis and in the compound $[Cu(L^3)_2]$, an axial compression occurs resulting in two short bonds and four long bonds. The EPR spectral study of this compound also supports this.

Elemental analyses of the synthesized Mn(II) compounds suggested four coordinate as well as six coordinate complexes. The compounds were characterized by various spectral studies. The single crystal X-ray diffraction studies of the $[\text{Mn}(\text{L}^1)_2]$ compound, revealed a meridional coordination mode of the ligand in enolate form. The geometry is a distorted octahedron. In all the Mn(II) complexes, the ligands are coordinated in the enolate form. The IR spectral studies confirmed the presence of $-\text{NCS}$ and $-\text{N}_3$ groups in the compounds. The EPR spectral studies showed that in some compounds there is appreciable zero-field splitting. The six hyperfine splittings observed correspond to coupling of unpaired electron with that of Mn nucleus with $I=5/2$.

Two oxovanadium compounds are synthesized. Both the compounds are characterized by various spectral studies. Attempts to prepare the single crystal of the oxovanadium VO(IV) compound, resulted in a $\text{VO}_2(\text{V})$ compound due to oxidation with a distorted square pyramidal geometry. The crystal structure of the second oxovanadium compound with the ligand H_2L^2 , revealed a dioxobridged dimer with an inversion centre. The coordination core around the vanadium metal centre is a distorted octahedron. The EPR spectrum of the oxovanadium(IV) compound in solution at 77 K displayed axial features with eight hyperfine splittings.

The coordination of the ligands with Ni(II) and Pd(II) salts are studied. Single crystals of both the nickel compounds were isolated. The bonding nature of the ligands are similar to that found in case of Cu(II) and Mn(II). Both the Ni(II) compounds are found to have a distorted octahedral geometry. Magnetic susceptibility measurements indicated the presence of two unpaired electrons. In the Pd(II) complexes ligands are coordinated both in keto form and enolate form. The Pd(II) complex with the ligand H_2L^2 is paramagnetic in nature with value consistent that of two unpaired electrons which suggests a six coordinate geometry. The other two compounds are diamagnetic in nature. The binding of the ligand in neutral form is evidenced by NMR spectral studies by the observance

of the $-NH$ peak. The IR spectral studies also support this. Unfortunately single crystals suitable for X-ray diffraction study are obtained for none of the Pd(II) compounds.

Zn(II) and Cd(II) compounds are also synthesized and characterized. All the Zn(II) complexes are yellow in colour and the ligands are coordinated in the enolate form. However in Cd(II) complexes, both types of ligand coordination are observed. The single crystal X-ray diffraction studies of $[Zn(L^1)_2]$ and $[Cd(L^1)_2]$ are done. 1H NMR, IR and electronic spectral studies of the complexes are done. In the Cd(II) series, a nictinoyl bridged Cd(II) complex with the ligand, HL^3 is isolated. Single crystal X-ray diffraction studies of the compound revealed a 1D polymer, with Cd(II) centres interconnected through a nicotinoyl bridge. The chloro ligands attached to the ligand are found to be trans positioned. The geometry of the Cd(II) centre is a distorted octahedron, with the ligand binding in the neutral form through keto oxygen. The bromo analogue with the same ligand displayed similar spectral features corresponding to that of the polymeric chloro compound of Cd(II). Unfortunately single crystals of the bromo compound could not be isolated.

Metal complexes of Cu(II), Mn(II), VO(IV), VO(V), Ni(II), Pd(II), Zn(II) and Cd(II) complexes are synthesized and characterized. The coordination mode of the ligands and the structural variations occurring in the ligands upon complex formation are studied. Spectral and structural studies confirm that the ligands coordinate both in keto form as well as in the enolate form with NNO donor sites. X-ray crystallographic study, which was used as major tool in the structure determination, revealed that the configuration of the ligands vary as the substituents attached and also on the nature of the ligand so as to stabilize itself with interactions such as hydrogen bonding. For complexation, the ligands HL^1 and H_2L^2 undergo a rotation about the azomethine bond thus acquiring *trans* geometry to involve all the three donor atoms in chelation. But the third ligand maintained its geometry about the azomethine bond upon complexation. But the

effective tridentate coordination was achieved by a rotation around the C5-C6 bond of the ligand. In most of the ML_2 six coordinate O_h complexes, coordinate bonds from the imine nitrogen are found to be short compared to pyridyl nitrogen and carbonyl oxygen. This may be due to steric effects and electronic effects. The steric effects may be due to the constraints imposed on the central and $M-N_{azo}$ coordinate bond by the requirement that both oxygen and pyridyl nitrogen must also coordinate, which in effect enforces a compression of the central coordinate bond. The electronic effects relate to a preference for the metal ions for N donors rather than O donors. Also the trans influence of the oxo group on the $M-N_{py}$ may also be a reason for the greater $M-N_{py}$ bond length than the $M-N_{azo}$ bond. The formation of the polymeric Cd(II) complex confirmed the fact the nicotinoyl systems could give rise to bridged polymeric complexes due to the presence of the unhindered N-donor on the nicotinoyl ring.

Curriculum Vitae

PERSONAL PROFILE

Date of Birth 19th December 1978
Permanent address Muppathiyil
Thottakaadu P.O
Kottayam 686 039, Kerala
Ph.No. 0481- 2485054

EDUCATION

1994 SSLC
Mount Carmel GHS, Kanjikuzhy, Kottayam
(88 %)

1994-1996 Pre-Degree
BCM College, Kottayam
(70%)

1996-1999 B. Sc. Chemistry
CMS College, Kottayam
(84%)

1999-2002 M. Sc. Inorganic Chemistry
School of Chemical Sciences
Mahatma Gandhi University, Kottayam
(72%)

POSITIONS OF RESPONSIBILITY

- ❖ Member, Organizing committee, National Symposium on Current Trends in Inorganic Chemistry, CTIC-2004, Cochin University of Science and Technology
- ❖ Vice President, Research Scholar Association, Cochin University of Science and Technology, 2003

RESEARCH PUBLICATIONS/COMMUNICATED

1. Structural, antimicrobial and spectroscopic studies of copper(II) complexes of 2-benzoylpyridine N(4)-phenyl thiosemicarbazone, M. Joseph, M. Kuriakose, M. R. P. Kurup, E. Suresh, A. Kishore, S. G. Bhat, *Polyhedron* 25 (2006) 61.
2. Spectral characterization and crystal structure of 2-benzoylpyridine nicotinoyl hydrazone, M. Kuriakose, M. R. P. Kurup, E. Suresh, *Spectrochim Acta* (in press).
3. Synthesis, spectroscopic studies and crystal structures of two new vanadium complexes of 2-benzoylpyridine containing hydrazone ligands, M. Kuriakose, M. R. P. Kurup, E. Suresh, *Polyhedron* (Communicated).
4. Six coordinate Ni(II) complexes of ONN donor aroylhydrazone ligands- Synthesis, spectral studies and crystal structures, M. Kuriakose, M. R. P. Kurup, E. Suresh, *Struct. Chem.* (Communicated).